2006-11-06

Biochemical Investigations of Macular Degeneration: The Significance of Protein Oxidation including Novel Methods for Its Study

Sarah Warburton
Brigham Young University - Provo

BIOCHEMICAL INVESTIGATIONS OF MACULAR DEGENERATION: THE SIGNIFICANCE OF PROTEIN OXIDATION, INCLUDING NOVEL METHODS FOR ITS STUDY

by

Sarah Warburton

A dissertation submitted to the faculty of

Brigham Young University

In partial fulfillment of the requirements for the degree of

Doctor of Philosophy

Department of Chemistry and Biochemistry

Brigham Young University

December 2006

BRIGHAM YOUNG UNIVERSITY

GRADUATE COMMITTEE APPROVAL

of a dissertation submitted by

Sarah Warburton

This dissertation has been read by each member of the following graduate committee and by majority vote has been found to be satisfactory.

_____	_____
Date	Craig D. Thulin, Chair
_____	_____
Date	Gregory F. Burton
_____	_____
Date	Barry M. Willardson
_____	_____
Date	David V. Dearden
_____	_____
Date	Heidi Vollmer-Snarr

BRIGHAM YOUNG UNIVERSITY

As chair of the candidate's graduate committee, I have read the dissertation of Sarah Warburton in its final form and have found that (1) its format, citations, and bibliographical style are consistent and acceptable and fulfill university and department style requirements; (2) its illustrative materials including figures, tables, and charts are in place; and (3) the final manuscript is satisfactory to the graduate committee and is ready for submission to the university library.

_____ _____

Date

Craig D. Thulin
Chair, Graduate Committee

Accepted for the Department

_____

David V. Dearden
Department Graduate Coordinator
Department of Chemistry and Biochemistry

Accepted for the College

_____

Thomas W. Sederberg
Associate Dean
College of Physical and Mathematical Sciences

ABSTRACT

BIOCHEMICAL INVESTIGATIONS OF MACULAR DEGENERATION: THE SIGNIFICANCE OF PROTEIN OXIDATION, INCLUDING NOVEL METHODS FOR ITS STUDY

Sarah Warburton

Department of Chemistry and Biochemistry

Doctor of Philosophy

The retinal pigment epithelium (RPE) is a monolayer of cells located directly behind the photoreceptor cells in the retina. These cells are involved in a variety of functions that support the visual process in the eye, namely 1) they form a blood-retina barrier which separates the neural retina from the choroid's blood supply, 2) the apical processes of RPE cells diurnally phagocytose the outer segments of photoreceptor cells, and 3) they participate in the renewal of the photopigment 11-cis retinal.

Age-related macular degeneration (AMD) is the leading cause of blindness in people over the age of 50 years in North America and other developed countries. AMD involves the death of retinal pigment epithelial (RPE) cells in the macula early in the progress of the disease. Like some other postmitotic cells, the RPE accumulates autofluorescent lysosomal storage bodies (lipofuscin) during senescence. Lipofuscin is reported to begin accumulating in the human RPE around age 20 and continues to accumulate throughout an individual's life. This progressive accumulation of lipofuscin

can eventually occupy a substantial fraction of the RPE cytoplasmic volume and may lead to impairment of normal RPE functions, resulting in retinal degeneration and loss of visual function as in AMD. Another autofluorescent granule that accumulates in RPE cells and may contribute to the etiology of AMD is a complex granule exhibiting properties of both melanosomes and lipofuscin granules called melanolipofuscin (MLF). In contrast with the accumulation of LF in the RPE, MLF accumulation has been reported by Feeney-Burns to more closely reflect the onset of AMD.

Although there have been significant advances in our understanding of AMD, knowledge of the mechanisms responsible for its progression remain unclear. This dissertation details experiments that were designed to better understand the factors that may play a causal role in AMD as well as the development of methods to assist in AMD research. Specifically, the protein composition of retinal LF was assessed to elucidate its origin. These findings are reported in chapter 2. The accumulation, composition and phototoxicity of MLF were analyzed to assess MLF's origin and possible contribution to AMD. These results are reported in chapter 3. Because protein oxidation is possibly a common posttranslational modification to proteins which accumulate in lipofuscin and melanolipofuscin granules, a method for the detection and analysis of oxidized proteins was developed and is reported in chapter 4. Chapter 5 details the proteomic differences between ARPE-19 cells - the only human RPE cell line available for research - in their differentiated and undifferentiated states and compares these to the proteome of human RPE cells. These results are also compared to the phenotypic difference of these cells as observed by transmission electron microscopy.

ACKNOWLEDGEMENTS

I owe my success to all of the individuals who have supported and assisted me during my graduate studies at BYU. I would like to thank my mentor Dr. Craig Thulin for his quarky sense of humor, love for science, and for believing in me. I thank my co-workers and friends Katie, Karen, Chen, Dave, and those who directly contributed to this work Brad, Seth, Wayne, Aaron, Ryan G., Ryan H. and Hardy. I would like to thank my husband Jared for his patience, love and support of my dreams. And of course a big thanks to my parents Greg and Lynette for many, many years of encouragement, love and sacrifice. Thanks!

TABLE OF CONTENTS

LIST OF FIGURES

LIST OF TABLES

ABBREVIATIONS

1DE	one-dimensional gel electrophoresis
2DE	two-dimensional gel electrophoresis
AFM	atomic force microscopy
AGE	advanced glycation end-products
AMD	age-related macular degeneration
API	atmospheric pressure ionization
BSA	bovine serum albumin
CID	collision induced dissociation
DIF	differentiated ARPE-19 cells
DNP	2,4-dinitrophenylhydrazone
DNPH	2,4-dinitrophenylhydrazine
DTT	dithiothreitol
FBS	fetal bovine serum
FC	flow cytometry
HNE	hydroxynonenol
HRP	horse radish peroxidase
IEF	isoelectric focusing
IPG	immobilized pH gradient
LF	lipofuscin
MDA	malonyldialdehyde
MLF	melanolipofuscin

oMALDI	orthogonal matrix assisted laser desorption ionization
OPAT	oxidized protein affinity tag
PBS	phosphate buffered saline
RPE	retinal pigment epithelium
SDS	sodium dodecyl sulfate
SDS-PAGE	sodium dodecyl sulfate polyacrylamide gel electrophoresis
SEM	scanning electron microscopy
TBS-T	tris buffered saline with tween-20
TEM	transmission electron microscopy
UND	undifferentiated ARPE-19 cells

CHAPTER 1

INTRODUCTION

Retinal Pigment Epithelium (RPE)

The retinal pigment epithelium is a monolayer of cells located directly behind photoreceptor cells in the retina (Figure 1-1). During embryogenesis these cells differentiate to form a polarized epithelium. Once epithelialized, RPE cells have little or no turn over for the remainder of the organism's life.

These cells are involved in a variety of functions that support the visual process in the eye, namely 1) they form a blood-retina barrier which separates the neural retina from the choroid's blood supply, 2) the apical processes of RPE cells diurnally phagocytose the outer segments of photoreceptor cells, and 3) they participate in the renewal of the photopigment 11-cis retinal.

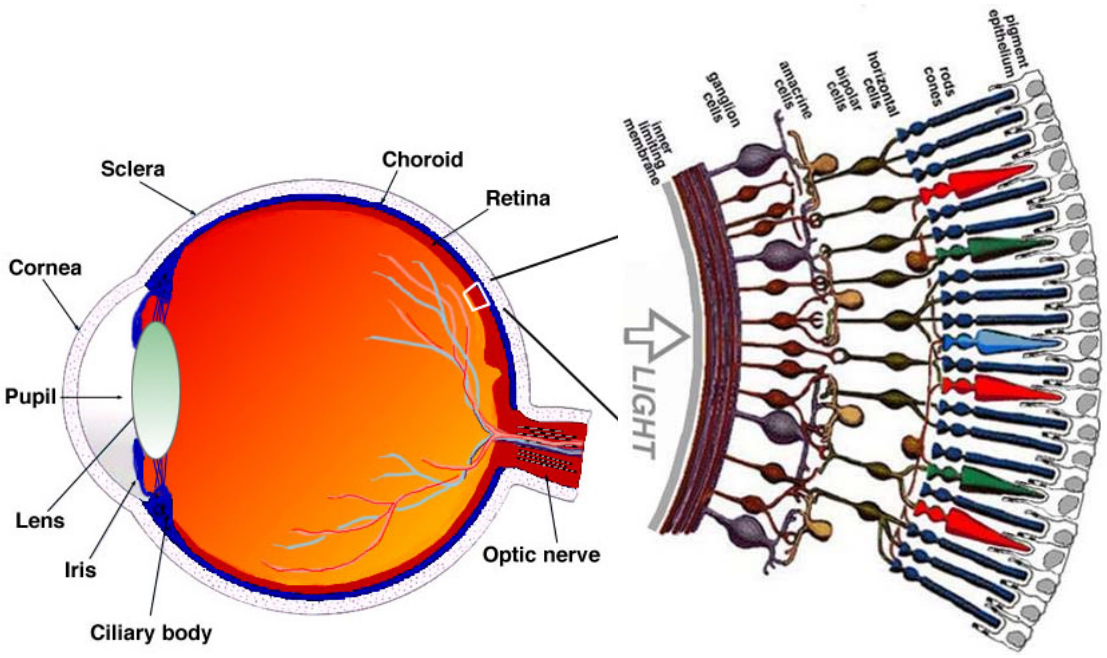

Figure 1-1. Cell layers in the retina. The retinal pigment epithelium (RPE) is located directly behind photoreceptor cells in the retina. (picture from http://webvision.med.utah.edu/sretina.html)

RPE forms a blood-retina barrier

Two sources supply blood to the mammalian retina: the central retinal artery and the choroidal blood vessels. The choroid receives the greatest blood flow (65-85%) and is vital for the maintenance of the outer retina. The remaining 20-30% flows to the retina through the central retinal artery from the optic nerve to nourish the inner retinal layers [Henkind, 1979]. Two highly selective blood-tissue barriers in the retina act to maintain a highly regulated homeostatic environment within the specialized layers of neural tissue. The outer blood-retinal barrier is established by RPE cells that lie adjacent to the outer layer of the choroid. These cells are joined together near the apical side by tight junctions, which block the free passage of water and ions. The RPE, therefore, plays a critical role in regulating the volume and composition of fluid in the subretinal space through the transport of ions, fluid and metabolites. [Steinberg and Miller, 1973; Steinberg, 1985; Bialek and Miller 1994] This regulation is accomplished by specialized transport proteins on the apical and basal surfaces of RPE cells.

RPE cells diurnally phagocytose photoreceptor outer segments

The outer segments of photoreceptor cells are composed of membranous discs that contain the visual pigment opsin, necessary for initiation of the visual transduction pathway. The photoreceptors are constantly exposed to oxygen and light, which facilitate the production of free radicals and, over time, damage the membranous discs at the distal end of each photoreceptor. Every day upwards of 100 discs at the distal end of each photoreceptor are phagocytosed by the RPE, while new discs are synthesized (Figure 1-2). The number of photoreceptors overlying each RPE cell remains nearly constant, ~45

photoreceptors per RPE cell.[Kennedy, 1995] This activity renders RPE cells the most active phagocytes in the body. A deficiency in the RPE's ability to phagocytose outer segments contributes to retinal diseases including age-related macular degeneration.[Edwards, 1977]

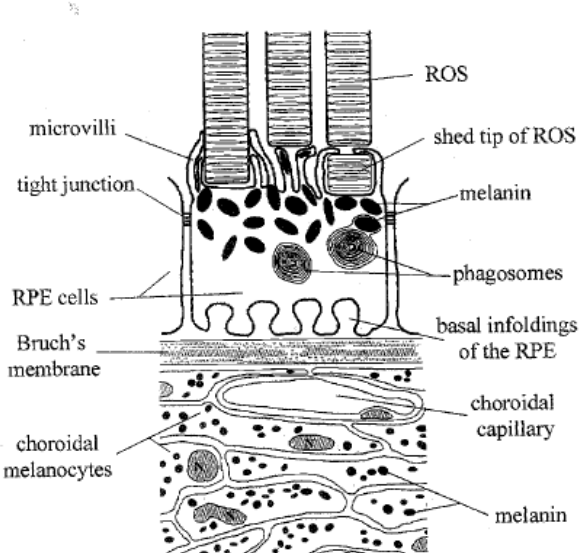

Figure 1-2. Phagocytosis of photoreceptor outer segments by the RPE. The photoreceptors are constantly exposed to oxygen and light which facilitate the production of free radicals and, over time, damage the membranous discs at the distal end of each photoreceptor. RPE cells diurnally phagocytose shed photoreceptor outer segments, while new discs are synthesized. This activity renders RPE cells the most active phagocytes in the body. Deficiency in the RPE's ability to phagocytose outer segments contributes to retinal diseases, such as age-related macular degeneration. (picture from Schraermeyer (1999) Pigment Cell Research.)

RPE cells participate in the renewal of 11-cis retinal.

The phototransduction cascade in the retina is initiated when light isomerizes 11-cis-retinal to all-trans-retinal, subsequently activating opsin. Because the turnover of 11-cis retinal during daylight hours exceeds the amount of stored vitamin A in the retina, 11-cis-retinal must be continually regenerated from all-trans-retinal. The RPE is involved in the renewal of 11-cis retinal as part of a process referred to as the visual cycle. This process begins when all-trans retinal is transported to the RPE where a series of enzymes reisomerize the molecule to 11-cis retinal (Figure 1-3). 11-cis retinal is then transported back to the photoreceptor cell and incorporated with opsin.

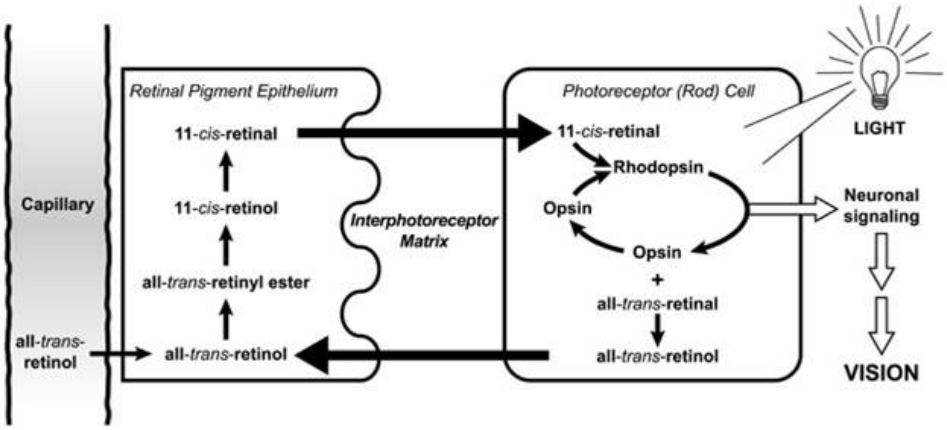

Figure 1-3. Renewal of 11-cis retinal in the visual cycle. Because the turnover of 11-cis retinal during daylight hours exceeds the amount of stored vitamin A in the retina, 11-cis-retinal must be continually regenerated from all-trans-retinal. This process begins when all-trans retinal is transported to the RPE where a series of enzymes reisomerize the molecule to 11-cis retinal. 11-cis retinal is then transported back to the photoreceptor cell and incorporated with opsin. (picture from Linus Pauling institute, Micronutrient Information Center http://lpi.oregonstate.edu/infocenter/vitamins/vitaminA/visualcycle.html)

Age-related Macular Degeneration (AMD)

Age-related macular degneration (AMD) is the leading cause of blindness in people over the age of 50 years in North America and other developed countries. [VanNewkirk, 2001; Attebo, 1996; Klein, 1995; Bressler, 1988] AMD affects 2% of individuals over 50 years of age and 30% of individuals over 75 years in the United States.[Group, 1993] AMD involves the death of retinal pigment epithelial (RPE) cells in the macula early in the progress of the disease. The macula, located in the central region of the retina, is a highly sensitive area which provides the greatest visual acuity. It is a circular area of approximately 6 mm diameter that is extremely dense in rods and cones; containing 150,000 rods per mm^2, whereas the peripheral retina has only 30,000 rods/mm^2.[Jonas, 1992]

Although increased age is the principal risk factor for AMD, studies have found several other risk factors, including cigarette smoking, high cholesterol, hypertension, cardiovascular disease, race, and family history. [Pieramici, 1998] A positive association between smoking and neovascular AMD has been suggested in both men and women, whereas an inverse association has also been found between dietary carotenoid intake and AMD. [Control, 1992; Seddon, 1996; Hung, 1997] With the exception of age, however, none of these studies has indicated a definite causal relation between a specific risk factor and AMD.

The earliest morphologic feature of AMD is the development of extracellular deposits, termed drusen, that accumulate between the basal lamina of the RPE and the collagenous layer of Bruch's membrane in the human eye. There are two phenotypes of drusen termed "hard" drusen and "soft" drusen, each observed at different stages of AMD. The first drusen deposits detected in the eye are "hard" drusen and are generally round, possess distinct borders, and are comprised of homogeneous material.

The correlation between drusen and AMD is so firmly established that many investigators and clinicians refer to the presence of "hard" drusen in the macula, in the absence of vision loss, as "early AMD." Drusen cause lateral stretching of the RPE monolayer and physical displacement of the RPE from its immediate vascular supply, the choriocapillaris.[Rones, 1937] This displacement may impede normal metabolite and waste diffusion between the choriocapillaris and the neural retina. It has also been suggested that drusen perturb photoreceptor cell function by placing pressure on rods and cones and/or by distorting photoreceptor cell alignment. Drusen appear to affect various aspects of vision prior to loss of visual acuity; these include changes in color contrast

sensitivity, macular recovery function, central visual field sensitivity, and spatiotemporal contrast sensitivity.[Midena, 1997; Tolentino, 1994; Frennesson, 1995; Midena, 1994]

Early AMD may progress into advanced AMD which has two forms: geographic atrophy (GA) or "dry" AMD and choroidal neovascularization (CNV) or "wet" AMD. GA accounts for 85-90% of all cases and is characterized by the formation of "soft" drusen between the RPE and choroid (Figure 1-4). Soft drusen are larger than hard drusen, have indistinct, sloped borders and are not usually homogeneous. Histologically, they typically contain various inclusions and spherical profiles. Visual loss associated with the appearance of soft drusen may be gradual, but results from atrophy of the RPE and the overlying photoreceptors. CNV accounts for 10-15% of AMD cases and is characterized by the growth of abnormal blood vessels either beneath the RPE or between the RPE and the retina (Figure 1-4). Only rarely do the vessels extend through the RPE and into the subretinal space. These abnormal blood vessels leak fluid and blood into the tissue at the back of the eye, resulting in disciform scarring and further cell loss. Most patients with active CNV will progress to visual acuity 6/60 or less within two years.[Landy, 2003] In either form of AMD, loss of support to the photoreceptors brings about eventual loss of vision. Currently, there is no established treatment for GA. Most current therapies and new investigational treatments are directed at CNV. In selected cases of wet macular degeneration, laser photocoagulation is effective for sealing leaking or bleeding vessels. Unfortunately, laser photocoagulation usually does not restore lost vision, but it may prevent further loss.

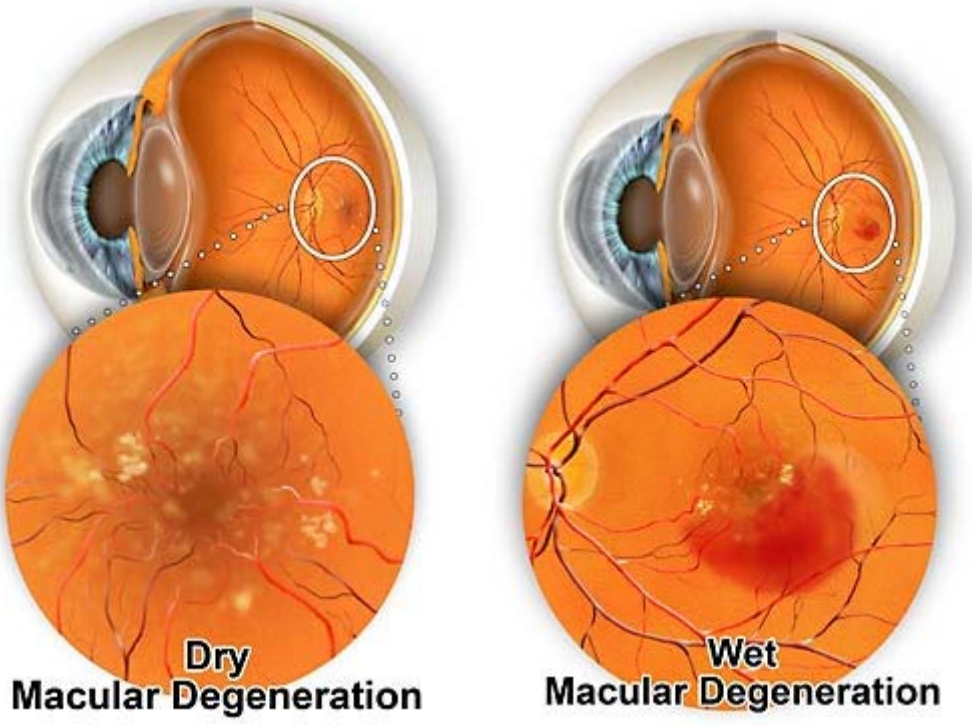

Figure 1-4. Clinical diagnosis of the dry and wet forms of age-related macular degeneration (AMD). Dry AMD is characterized by the formation of yellowish deposits in the macula, known as drusen. Wet AMD is characterized by the formation of abnormal blood vessels under the retina which leak fluid and blood into the tissue. In either form of AMD, loss of support to the photoreceptors brings about eventual loss of vision. (picture from St. Luke's Cataract & Laser Institute. Macular Degeneration–Age-Related Macular Degeneration. www.stlukeseye.com/Conditions/MacularDegeneration.asp.)

Oxidative Stress

Oxidative stress has been suggested to be a major contributing factor for retinal degeneration in AMD. The retina is exposed to a relatively high oxygen pressure that is close to that found in arterial blood. [Winkler, 1999] Both RPE and photoreceptor cells in the retina are non-replicating (post-mitotic) and must respond to a lifetime of oxidative insult, which includes light-induced oxidative stress. While there are numerous mechanisms in the retina for preventing and combating oxidative injuries, by middle-age many of these anti-oxidative mechanisms have begun to break down, which can increase

the susceptibility of the retina to accumulated damage. Ultraviolet light is largely excluded from passage to the retina by the cornea. However, visible light absorbed by photoreceptors is a significant factor in the production of reactive oxygen species that induce the molecular damage in retinal tissue which appears to contribute to the formation of AMD. To an overwhelming degree, blue wavelengths of light produce the most oxidative stress within the retina, because they are the most energetic photons to reach the retina, and are primarily responsible for exacerbating the extent of oxidative damage.

Studies have detected significant increases in oxidative modifications in individuals with AMD when compared to those without. Free radical-induced oxidation of docosahexaenoate-containing lipids generates omega-(2-carboxyethyl)pyrrole protein adducts that were found to be more abundant in ocular tissues from AMD than normal human donors.[Gu, 2003] Other oxidative protein modifications found to be more abundant in AMD patients than in normal Bruch's membrane include crosslinked species of tissue metalloproteinase inhibitor 3 and vitronectin and carboxyethyl pyrrole protein adducts.[Crabb, 2002] Carboxymethyl lysine, another oxidative modification, was also detected in drusen.[Crabb, 2002] These data support the hypothesis that oxidative injury contributes to the pathogenesis of AMD and suggest that oxidative protein modifications may have a critical role in the formation of undegradable storage bodies, i.e. drusen, lipofuscin, melanolipofuscin.

Lipofuscin Accumulation

Impairment of normal RPE functions is known to result in retinal degeneration and loss of visual function as in AMD. It is therefore hypothesized that age-related deterioration in RPE functions may lead to visual impairment. As a result, factors that may be detrimental to RPE function have been studied to assess any possible contribution to the deterioration of RPE function and vision loss. Like some other postmitotic cells, the RPE accumulates autofluorescent lysosomal storage bodies (lipofuscin) during senescence. Lipofuscin is reported to begin accumulating in the human RPE around age 20 and continues to accumulate throughout an individual's life. This progressive accumulation of lipofuscin can eventually occupy a substantial fraction of the RPE cytoplasmic volume, as much as 20% by age 80.[Feeney-Burns, 1984] The composition and origin of lipofuscin has not previously been completely established, but has been thought to result from the accumulation of undigested material from the phagocytosis of photoreceptor outer segments. Studies have indicated that the formation of lipofuscin may be due to the oxidative alteration of macromolecules by free radicals, rendering them undegradable by the cell.[Winkler, 1999]

It has been proposed that this accumulation of lipofuscin may be detrimental to the RPE and possibly lead to loss of function and eventual vision loss because of its ability to generate reactive oxygen species (ROS). Boulton et al. demonstrated that white light irradiation of RPE lipofuscin granules results in the production of a variety of reactive oxygen species (including superoxide anions, singlet oxygen, hydrogen peroxide and lipid hydroperoxides), their rate of production increasing with increasing light intensity.[Boulton, 1993; Rozanowska, 1995 & 1998] The effect was also shown to be

wavelength dependent, with the greatest generation of reactive oxygen species in granules exposed to blue light (400-520 nm). It has also been demonstrated that lipofuscin causes blue light dependent cell death in cultured RPE cells.[Davies, 2001] The ROS generated when blue light is absorbed by lipofuscin could damage cellular DNA, lipoproteins, and other structures within RPE, and may lead to self-induced cell death (apoptosis).

One constituent of retinal lipofuscin that may contribute to its phototoxicity is the fluorophore A2E. A2E is a combination of two molecules of vitamin A aldehyde and one molecule of ethanolamine which forms in photoreceptor outer segments and eventually ends up in lipofuscin as the result of phagocytosis of discs in these segments.[Sparrow, 2000] A2E has been shown to generate ROS upon photosensitization with blue light and cause blue light dependent cell death in cultured RPE cells.[Sparrow, 2000 & 2001] Although A2E is the most studied photosensitizer of lipofuscin, it is not necessarily the predominant photosensitizer.

Melanosomes in the RPE

RPE cells are highly pigmented due to a high concentration of melanin. Although it has been generally accepted that dermal melanin protects the skin from UV light damage [Kollias, 1991], the biological function of RPE melanin is not completely understood. Melanin is known to absorb excess light passing through the eye, thereby reducing scatter and improving image resolution. It has also been suggested to play a photoprotective role in RPE cells [Sarna, 1992; Schraermeyer, 1999] by scavenging reactive oxygen species [Dunford, 1995; Rozanowska, 1999; Sarna, 1985]. Evidence

also exists for a phototoxic role for melanin in RPE cells, especially in aged cells, including measurable ROS photoproduction [Boulton, 2001; Sarna, 1999; Rozanowski, 1999; Korytowski, 1986; Sarna, 2003]. Melanosomes have been observed to undergo morphological and photophysical changes with age, possibly due to oxidation, which may result in diminished antioxidant potential. Studies have reported that aged human melanosomes are highly photoreactive and can result in RPE dysfunction, while young melanosomes appear to confer photoprotection [Dayhaw-Barker, 2001; Gaillard, 2003; Rozanowska, 2002]. With increasing age, a decrease in melanosomes in the RPE is observed along with an increase in what seem to be melanosome-lipofuscin complexes, termed melanolipofuscin (MLF). [Boulton, 1991; Feeney-Burns, 1978; Schraermeyer, 1994 & 1999].

Although little is known about the origin and composition of MLF, Feeney-Burns et al. have reported that the accumulation of MLF more closely reflects the onset of AMD than the accumulation of LF. Two models for the origin of MLF have been suggested. The first model involves the autophagy of preexisting melansomes and their incorporation into accreting LF granules. This model is supported by the observation that phagosomes containing undegradable material fuse with melanosomes [Schraermeyer, 1999]. The second model is that melanin is synthesized *de novo* in lysosomes, which subsequently fuse with accreting LF granules. This model is supported by evidence that synthesis of melanin in depigmented RPE cells is seen in lysosomal compartments [Dorey, 1990; Schraermeyer, 1994]. Knowledge of the composition of MLF could provide significant insight into the origin of these granules, and determining the

phototoxicity of these granules could be useful for ascertaining MLF's role in the etiology of AMD and other retinal diseases.

AMD Genetics

It seems likely that AMD has a multifactorial etiology, including environmental stimuli, the impact of ageing and genetic predisposition. Genetic defects may render an individual more susceptible to environmental insult or be sufficient to interrupt proper visual functioning. Several studies have provided evidence for a genetic factor to AMD, including Seddon et al. who evaluated first-degree relatives of AMD cases and control individuals without AMD.[Seddon, 1997] The majority of the relatives evaluated were siblings, although living parents and children over the age of 40 were also included. The prevalence of AMD was significantly higher among first-degree relatives of AMD case probands (23.7%) compared to that observed for first degree relatives of control probands (11.6%).

Researchers have also studied the genome of patients suffering from retinal degeneration to assess possible mutations that may contribute to vision loss. Patients suffering from retinal degeneration were found to have heterozygous mutations in both the *ROM1* and *RDS* genes, whereas mutations in either of these genes alone had no effect on phenotype. [Dryja, 1997] The products of both genes are membrane proteins that localize to rod and cone photoreceptor discs, are structurally homologous, and associate *in vivo* as a heterotetrameric complex both at the disc rims and at the site of disc formation.

AMD has several phenotypic similarities with Stargardt's disease, including the accumulation of drusen under the RPE and the progressive atrophy of RPE cells in the macula. Stargardt's disease is the most common form of hereditary, recessive macular dystrophy, is characterized by juvenile-to-young-adult onset and is known to result from a mutation in the *ABCR* gene. To determine if defects in *ABCR* contribute to AMD, researchers screened for *ABCR* sequence alterations in two independent collections of unrelated (n=96) and AMD (n=71) patients. Thirteen different AMD-associated alterations, both deletions and amino acid substitutions, were found in one allele of *ABCR* in 26 patients (16%).[Allikmets, 1997] The identification of a number of rare variants in the *ABCR* gene in individuals with AMD suggests a possible contribution to vision loss associated with AMD.

Another gene, responsible for an autosomal dominant form of Stargardt's, was recently identified as ELOVL4. Transgenic mice expressing a mutant form of ELOVL4 were shown to accumulate lipofuscin in their RPE which was followed by RPE atrophy. RPE atrophy was proceeded by photoreceptor degeneration in the macula in a pattern that resembles Stargardt's and AMD.[Karan, 2005]

Researchers have also utilized gene knockout mice to assess genes implicated in human retinal diseases. Most genes implicated in AMD have been shown to cause accelerated accumulation of lipofuscin in RPE cells. However, again, the accelerated RPE lipofuscin accumulation has not been shown to be the cause of the accompanying macular degeneration. The lack of a definitive link between RPE lipofuscin accumulation and AMD illustrates one of the biggest challenges remaining in lipofuscin research: determining whether lipofuscin accumulation has an impact on cell function.

Dissertation Overview

Although there have been significant advances in our understanding of AMD, knowledge of the mechanisms responsible for its progression remain unclear. My dissertation details experiments that were designed to better understand the factors that may play a causal role in AMD as well as the development of methods to assist in AMD research. Specifically, the protein composition of retinal LF was assessed to elucidate its origin. These findings are reported in chapter 2. The accumulation, composition and phototoxicity of MLF were analyzed to assess MLF's origin and possible contribution to AMD. These results are reported in chapter 3. Because protein oxidation is possibly a common posttranslational modification to proteins which accumulate in lipofuscin and melanolipofuscin granules, a method for the detection and analysis of oxidized proteins was developed and is reported in chapter 4. Chapter 5 details the proteomic differences between ARPE-19 cells - the only human RPE cell line available for research - in their differentiated and undifferentiated states and compares these to the proteome of human RPE cells. These results are also compared to the phenotypic difference of these cells as observed by transmission electron microscopy.

CHAPTER 2

LIPOFUSCIN ORIGIN & COMPOSITION

Summary

Several retinal diseases, including AMD, have been associated with the accumulation of autofluorescent lipofuscin (LF) granules in the retinal pigment epithelium (RPE). LF may relate to the onset of these ocular diseases because it has been shown to generate reactive oxygen species via photosensitization with blue light, which may cause damage and death of the RPE and surrounding cells. The origin of LF has not been completely established, but the granules are thought to result from the accumulation of undigested material from the phagocytosis of photoreceptor discs in RPE lysosomes. To elucidate the origins of biologically active retinal lipofuscin (LF), proteins in this granule were identified by limited-scale proteomic analysis using both two-dimensional (2D) gel electrophoresis and SDS-PAGE coupled with MALDI-QqToF MSMS and automated LCMSMS, respectively. Proteomic analyses identified 41 constituent proteins. Hydrophobic proteins and several proteins specific to photoreceptors, including rhodopsin, that have not previously been reported, were identified. Extensive protein modification, especially oxidative damage, was observed. The proteins identified support the model that LF accumulates in RPE cells as a result of the buildup of undigested material from the phagocytosis of photoreceptor outer segments. Perhaps oxidative damage renders some of these proteins indigestible and thus leads to the accumulation of LF granules.

Introduction

Several retinal diseases including age-related macular degeneration (AMD), Stargardt's disease, and Best's macular dystrophy result from the degeneration of cells in the retina. These diseases have also been associated with the accumulation of autofluorescent lipofuscin (LF) granules in the retinal pigment epithelium (RPE) [Delori, 2001; Mata, 2000]. Many tissues accumulate LF granules, also called age pigments, but the retinal LF that accumulates in RPE cells is probably unique. RPE cells are reported to begin accumulating LF granules around age 20; and by age 80 these granules may constitute up to 20% of the cell volume [Feeney-Burns, 1984]. LF may relate to the onset of these ocular diseases because it has been shown to generate reactive oxygen species via photosensitization with blue light [Beatty, 2000; Winkler, 1999; Rozanowska, 1995; Wassell, 1999], which may cause damage and death of the RPE and surrounding cells. LF is known to be a heterogeneous material composed of a mixture of proteins and lipids, including several different fluorescent compounds. More than ten different fluorophores from LF have been observed by thin layer chromatography [Feeney-Burns, 1983; Eldred, 1988] but the most fully characterized fluorophore is the bis-retinoid, A2E [Eldred, 1993]. One would expect to find an abundance of hydrophobic and highly modified, microheterogenous proteins in LF granules because of their lipophilic nature and the inability of RPE cells to degrade them. Recently another publication reported the identification of proteins in LF granules using two-dimensional (2D) gel electrophoresis [Schutt, 2002]. Due to the limitations of 2D electrophoresis including the lack of solubility of hydrophobic proteins in buffer systems compatible with 2D gel

electrophoresis, and the inability to focus microheterogeneous proteins into observable spots, this method may limit the proteins amenable to identification.

The origin of LF has not been completely established, but the granules are thought to result from the accumulation of undigested material from the phagocytosis of photoreceptor discs in RPE lysosomes. The material is thought to be undegradable by the cell, perhaps because of modifications that inhibit degradation. Knowledge of the composition and origin of lipofuscin granules could be useful for designing therapies to prevent lipofuscin accumulation and the onset of AMD. Elucidating the protein constituents of LF could provide significant insight into the origin of these granules.

In this study we employed both one-dimensional (1D) and 2D gel electrophoresis to provide a view of the proteins in LF, and demonstrated the presence of modifications on these proteins. Our results are compared to a recent publication [Schutt, 2002] reporting the identification of proteins in LF granules in which only 2D electrophoresis was employed. Our findings provide strong evidence for the model that retinal lipofuscin results from an accumulation of undigested material from the phagocytosis of photoreceptor discs in RPE lysosomes, and also suggest a possible mechanism for the inhibition of phagosomal/lysosomal digestion.

Materials and Methods

Lipofuscin isolation and fluorescence - Lipofuscin granules were isolated from human RPE from donor eyes, provided by Dr. Paul Bernstein of the Moran Eye Institute, (University of Utah, Salt Lake City, UT). We used RPE from human donor eyes provided by the Utah Lions Eye Bank, after they had been released for research use. Any unused

tissue was returned to the Eye Bank for proper disposal. No identifying information beyond age, gender, brief ocular history, and cause of death was supplied to our laboratory. All specimens were accepted without regard to gender, race, or ethnic origin. No formal human subjects approval was required by the University for research studies on donated human tissue (E4 exemption). The time between donor death and enucleation was 1-4 h after which the donor eyes were stored at 4 °C until dissection. Dissections were carried out 6-24 h after donor death in a dim light environment by Dr. Bernstein's lab at the Moran Eye Institute. RPE's were shipped to BYU on dry ice and stored at -75 °C until use. RPE's from twenty randomly selected individuals between 20 and 80 years of age were used for each preparation of isolated lipofuscin. The lipofuscin granules were isolated using a sucrose gradient as described by Boulton et al. [Boulton, 1990]. Fluorescence spectra of isolated lipofuscin granules were acquired as described by Boulton et al. [Boulton, 1990] using a Jobin Yvon Fluoromax-3 Spectrofluorometer (Edison, NJ).

Bioactivity assay - ARPE-19 (human retinal pigment epithelial cells-ATCC-CRL-2302) were grown in 96 well tissue culture plates and were maintained in RPMI 1640 media supplemented with 10% fetal bovine serum (FBS). Cells were differentiated by transferring them to Matrigel Basement Membrane Matrix (BD Biosciences, Bedford, MA) and reducing the FBS in the media to 1% for two weeks. Upon differentiation, cells were either maintained in RPMI 1640 media supplemented with 1% FBS or incubated in the same media which also contained about 90 lipofuscin granules/cell for 24 h to allow for ingestion of the granules. After the 24 h incubation, the lipofuscin-fed RPE cells were

transferred back to RPMI 1640 media supplemented with 1% FBS and maintained for 7 days before use in bioactivity assay. To verify the bioactivity of the LF, differentiated ARPE-19 cells that were fed LF or maintained as control cells were either subjected to blue light (390-550 nm) for 24-48 h at an intensity of about 2.8 mW/cm or maintained in the dark. Blue light was introduced into a humidified cell incubator using a Mille Luce M1000 Fiber Optic Illuminator with a 150 W quartz halogen bulb, a 25 mm dichroic blue light filter, and a 48 inch fiber optic cable which obviates heat damage (Edmund Optics, Barrington, NJ). Photocytotoxicity of the lipofuscin granules was assessed using the MTT Colorimetric Assay (Chemicon International, Temecula, CA). MTT (3-(4,5-dimehtylthiazol-2-yl)-2,5-diphenyl tetrasodium bromide) in PBS (pH 7.4) was added to each well and then incubated at 37 °C for 4 h. After incubation, developing solution containing 0.04 N HCl in isopropanol was added to each well and the absorbance was read at 570 nm on a CERES UV900 HDi plate reading spectrophotometer (Bio-Tek Instruments).

Microscopy - LF granules were prepared for scanning electron microscopy (SEM) analysis by drying the granules on a silicon wafer and sputter coating them with gold. The granules were analyzed on a Phillips XL30 ESEM FEG using a 5 kV accelerating potential. For transmission electron microscopy (TEM) analysis LF granules were fixed in glutaraldehyde, postfixed in osmic acid, dehydrated, and embedded in epoxy resin. Slices of the sample (100 nm) were imaged and photographed on a JEOL JEM 2000 FX. LF samples for atomic force microscopy (AFM) were prepared by drying the granules onto a mica slide. Images were taken with a Multimode IIIa AFM instrument with

microfabricated Si cantilever tips (Nanoscience Instruments, Phoenix, AZ). Vibrational noise was dampened using an active isolation system (MOD1-M, Halcyonics, Goettingen, Germany). Typical imaging parameters were: tip resonance frequency, 55-65 kHz; amplitude setpoint, 2.0-2.5 V; scan rate, 2.0 Hz. Images were processed offline to remove the background slope using software bundled with the AFM instrument.

Total lipid determination in lipofuscin - Lipofuscin granules were collected by centrifugation and dried in an evaporative centrifugal concentrator. The granules were weighed using a Mettler UMT2 microbalance (Columbus, OH) to determine the total mass of the granules. After weighing the dried granules, lipids in lipofuscin samples were extracted in chloroform:methanol (2:1, v/v). The lipid extract was dried in an evaporative centrifugal concentrator and weighed using the microbalance to determine the total mass of lipids.

Total protein determination in lipofuscin - After weighing samples of lipofuscin granules as above, the protein in these lipofuscin samples was quantified by solubilizing 150 μg of lipofuscin protein (about 380 μg lipofucin) in 30 μl of 1% (w/v) SDS followed by the BCA Protein Assay (Pierce, Rockford, IL).

2D Gels - LF granules containing 300 μg of protein were collected by centrifugation at 6000x g and solubilized in reswelling buffer (7 M urea, 2 M thiourea, 15 mM dithiothreitol (DTT), and 1% pharmalites) with either 4% Triton X-100 or 0.5% Triton X-100 and 2% ASB-14 (Calbiochem, San Diego, CA). Both cuploading and reswelling

procedures were used to analyze the proteins. Isoelectric focusing was performed using a 7 cm immobilized pH gradient (IPG) pH 4-7 on a Multiphor II Electrophoresis System (Amersham Pharmacia Biotech, Piscataway, NJ). A programmed voltage gradient was used consisting of 200 V for 1 min, linearly increasing to 3500 V over 1.5 h, and held at 3500 V for 1.5 h to reach a total of approximately 8 kVh. Following isoelectric focusing, IPG strips were washed in equilibration buffer (0.05 M Tris, 6 M urea, 30% glycerol, and 1% SDS) containing 32 mM dithiothreitol for 15 min followed by a 15 min wash in equilibration buffer containing 216 mM iodoacetamide. The proteins were then separated according to their molecular weight on a 10% gel (8.3x6.4x0.1 cm) using standard SDS-PAGE conditions. Gels were stained with colloidal coomassie (Pierce), and were analyzed using Melanie 4 software (GeneBio, Geneva, Switzerland [Verhaert, 2001]). Internal pI and molecular weight standards were used to assist in alignment of gels. Excised spots were trypsinized in-gel [Shevchenko, 1996] and desalted using a $ZipTip_{U\text{-}C18}$ (Millipore, Bedford, MA). Sample spots of 1 µl were allowed to co-crystallize on the MALDI plate with 1 µl of α-cyano 4-hydroxycinnamic acid as the matrix. Peptides were analyzed by oMALDI Qq-ToF (orthogonal matrix-assisted laser desorption ionization quadrupole time-of-flight) mass spectrometry on an Applied Biosystems QSTAR Pulsar i instrument (Foster City, CA).

1D Gel and mass spectrometry - Lipofuscin granules containing 100 µg of protein were collected by centrifugation, solubilized in 20 µl 4X Laemmli buffer (3% SDS, 0.17 M Tris pH 6.8, 35% glycerol, 3.5% 2-mercaptoethanol) and separated on a 10% SDS-polyacrylamide gel (8.3x6.4x0.1 cm). The proteins were in-gel digested as described by

Shevchenko et al. [Shevchenok, 1996], injected onto a Jupiter C18 reversed-phase resin capillary column (150 μm IDx20 cm, made in-house) and eluted using a gradient of 5 to 95% acetonitrile in 0.1% formic acid at a flow rate of 5 μl/min. On-line mass spectrometric analysis was performed on an Applied Biosystems QSTAR Pulsar i using an atmospheric pressure ionization (API) source. Automated tandem mass spectrometry using information-dependent acquisition was run, collecting collision induced dissociation (CID) spectra for the three most intense ions from each survey scan excluding peaks chosen in the preceding 2 min. Fragmentation spectra were chosen by hand for submission to the Mascot (Matrix Science) website for peptide identification. The ProID extension of BioAnalyst (Applied Biosystems, Foster City, CA) was also used to identify modifications on RLF proteins.

Immunoelectron microscopy - Granules were collected by centrifugation and fixed with either 2% glutaraldehyde or 2% paraformaldehyde. The granule pellets were dehydrated in ethanol and embedded in LR White resin, one of the most infiltratable resins specifically designed for immunocytochemical techniques. Slices of the samples (100 nm) were collected on formvar-coated gold grids. Grids were incubated first in 4% bovine serum albumin (BSA) for 15 min at room temperature to block nonspecific binding sites, then in either a 1:1000 dilution of anti-rhodopsin IgG (R4, polyclonal antibody Takemoto et al. [Takemoto, 1985]) or anti-phosducin IgG [Thulin, 1999] (negative control) overnight at 4 °C, and finally a 1:100 dilution of anti-rabbit IgG gold-conjugate (10 nm, Sigma, St. Louis, MO) for 2 h at 37 °C. Between each incubation period the grids were washed four times for 2 min each in either Tris Buffer A pH 8.2

(200 mM NaCl, 20 mM Tris, 1% NP40, 0.05% Tween 20) or Tris Buffer B pH 8.2 (200 mM NaCl, 20 mM Tris). The grids were stained with uranyl acetate and lead citrate prior to examining them on a FEI Tecnai 12 (Hillsborough, OR) transmission electron microscope. Micrographs from two samples were used in the analysis, one sample was fixed with paraformaldehyde and washed with Tris Buffer A and the other sample was fixed with glutaraldehyde and washed with Tris Buffer B. Because fixation of the sample requires alteration of protein constituents, this process can block or impede antigen labeling. Therefore, different fixation procedures were explored to ensure appropriate labeling of the sample. The gold particles, associated with the RLF granules and the resin (nonspecific binding), in the micrographs were counted in a total area of about 120 μm^2 containing about 100 granules. Adobe Photoshop was used to determine the area occupied by granules and resin in the micrographs. The area occupied by granules and resin was normalized to half of the total area. That normalization was applied to the gold particle count to accurately determine the fraction of gold particles bound to RLF granules.

Flow cytometric analysis - To determine the size distribution and concentration (granules/unit volume), suspensions of LF granules were diluted 1:100, and 1:1000 with PBS, and 200,000 Flow Check High Intensity Green Alignment Beads (Polysciences, Inc., Warrington, PA), 5.726±0.375 μm in diameter, were added to each sample to serve as an internal standard. The samples were excited with an argon laser at 488 nm on a Beckman Coulter (Beckman, Fullerton, CA) EPICS-XL Flow Cytometer with EXPO 32 ADC software for flow cytometric analysis. The samples were analyzed for light scatter

and autofluorescence by collection of data for 300 s, which allowed visualization of at least 5,000 beads and at least 49,000 LF granules.

Immunoblots -Human retinas were obtained from Dr. Paul Bernstein from the Moran Eye Institute to provide a positive control for rhodopsin. A retina was gently triturated in 0.75 M sucrose, 0.68 mM $CaCl_2$, 20 mM Tris and 1 mM DTT, pH 7.4 to rupture the cells. The suspension was poured over 4 thicknesses of cheesecloth to remove cellular debris. The sample was centrifuged at 1475x g for 20 min and the pellet was resuspended in 1% SDS. Total protein was determined using the BCA assay.

Anti-rhodopsin antibody (R4) was used at 1:1000 dilution in Tris buffered saline with 0.05% (w/v) Tween (TBS-T). Anti-CRALBP antibody (Dr. John C. Saari, University of Washington, Seattle, WA) was used at a 1:1000 dilution in TBS-T. LF protein (30 μg) was separated on a 1D gel and analyzed for malondialdehyde (MDA)-modified proteins using a rabbit antibody to MDA (Calbiochem, San Diego, CA) diluted 1:1000 in TBS-T. Oxidized BSA standards were made by incubating BSA in hypochlorous acid at 37 °C for 30 min. LF and BSA samples were derivatized by incubating them in 5% sodium dodecyl sulfate and 10 mM 2,4-dinitrophenylhydrazine (DNP) in 10% (v/v) trifluoroacetic acid for 30 min at room temperature [Shacter, 1994]. Laemmli buffer and 2 M Tris base was added to the samples until they turned from yellow to blue, indicating that the pH was neutral, before loading the samples onto a gel. Anti-DNP antibody from rabbit was used at a 1:1000 dilution (Sigma, St. Louis, MO).

Results

LF granules, isolated as previously described [Boulton, 1990], were found to be biologically active in retinal pigment epithelial (RPE) cells in culture (Figure 2-1). Several physical measurements of LF granules were made, including electron microscopy, atomic force microscopy, and size distribution using flow cytometric analysis (Figure 2-2). Fluorescence spectra from our LF preparations (Figure 2-3, top panel) showed extensive similarity to those published by Boulton et al. [Boulton, 1990] (Figure 2-3, middle panel), with a broad excitation maximum between 350 and 450 nm and a broad emission maximum near 600 nm. Figure 2-3 also shows a comparison to excitation and emission spectra recently reported from Schutt et al. [Schutt, 2002], which show a narrow excitation peak at 350 nm and a narrow emission peak at 450 nm. Because the LF fluorescence spectra generated by Boulton et al. looks more similar to the fluorescence spectra of A2E than LF granules we would speculate that somewhere in their procedure they separated the lipids and the proteins.

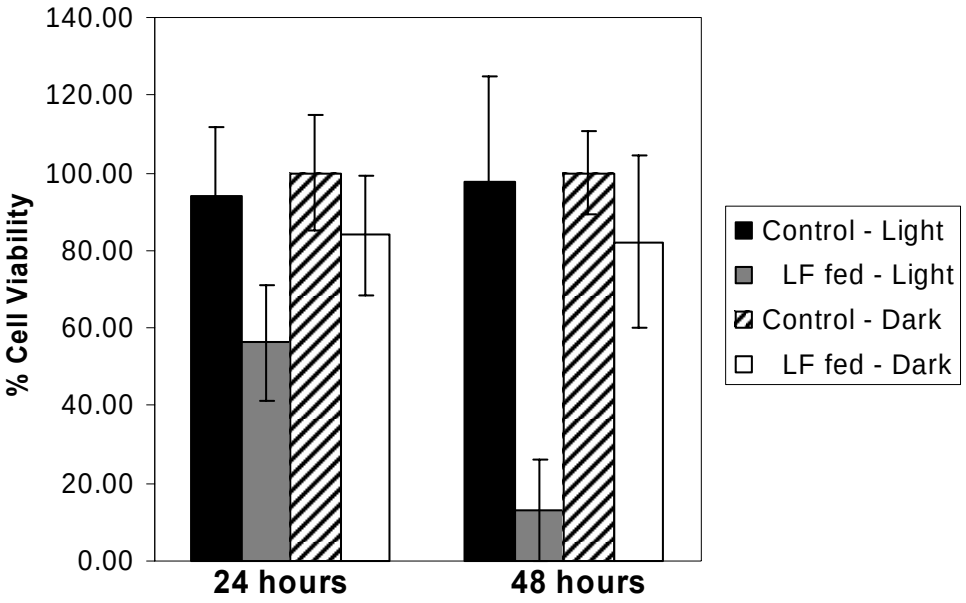

Figure 2-1. Bioactivity of lipofuscin (LF) granules. Isolated LF granules were fed to differentiated ARPE-19 cells which were then allowed to recover for 7 days. Cells that were not fed LF were used as controls. Cells were then subjected to blue light irradiation (solid black or grey bars), or left in the dark (cross-hatched or open bars), for 24 to 48 hours as described in the text. Cell viability was determined using the MTT assay. Values represent means of eight to twelve independent measurements, error bars representing standard deviation.

Transmission and scanning electron microscopy (TEM and SEM) as well as atomic force microscopy (AFM) were employed to examine the structure of LF. TEM (Figure 2-2B) shows granules of approximately 0.7 μm in diameter of fairly uniform density, as has been previously reported [Eldred, 1988; Sohal, 1986; Boulton, 1986]. Despite this apparent uniform density and rather simple circular cross-section, SEM (Figure 2-2C) shows that these granules are mostly spherical but appear to have some globular surface features that suggest aggregation. The aggregate nature of LF is best illustrated by AFM. Figure 2-2C shows AFM phase images of two granules. In one (top panel), surface globules of about 200 nm diameter, noted in SEM, are seen and would seem to suggest growth by accretion. In both this picture and the other AFM view (Figure 2-2C lower

panel), LF appears to be made of smaller (about 50 nm) structures that are aggregated together.

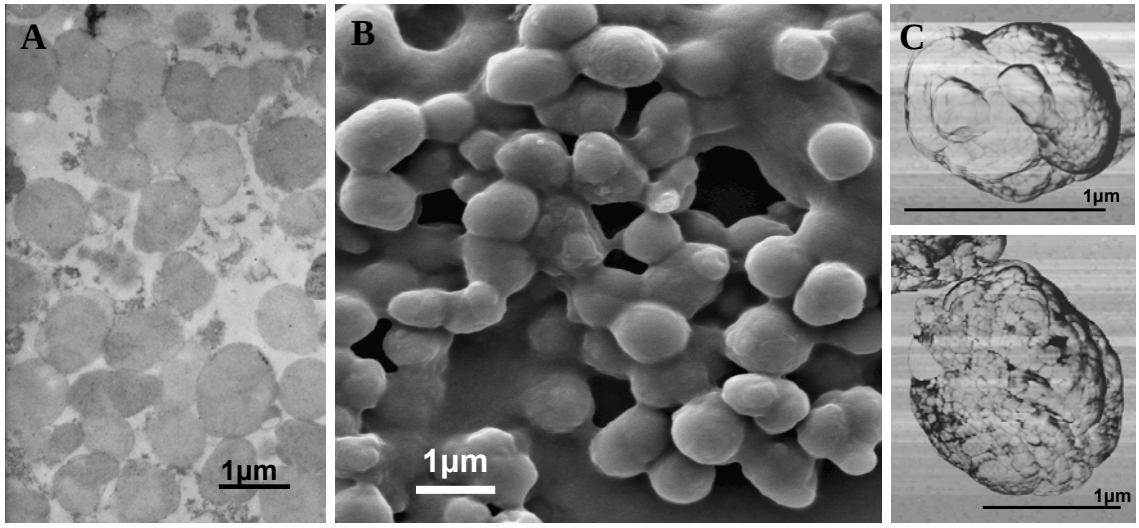

Figure 2-2. Microscopy of lipofuscin granules. **A**: Transmission electron micrograph of LF, showing granules of homogeneous density. **B**: Scanning electron micrograph of LF, showing nearly spherical granules with some surface features. **C**: Atomic force micrographs (phase images) showing LF granules to be aggregates of about 200 nm (upper panel) and about 50 nm (both panels) substructures.

Taken together, the microscopic analyses show LF granules to be composed of smaller structures of fairly uniform density that have accreted together to form the granules themselves. Granule size was more quantitatively determined using flow cytometric analysis (FC). Forward light scatter in FC instruments is directly proportional to the size of the objects passing through the beam. The LF granules were found to be distributed into two populations by size, one (representing 99% of the granules) having a mean diameter of 0.69 µm with a Gaussian distribution and a broad standard deviation of 0.63 µm, and the other population (representing only 1% of the granules) having a mean diameter of 4.8 µm with standard deviation of 0.3 µm. Flow cytometry also enabled a quantitative determination of the concentration of granules in our suspensions. Having a

quantitative count of the LF granules we were able to determine their average weight, which proved to be 1.3±0.2 pg/granule.

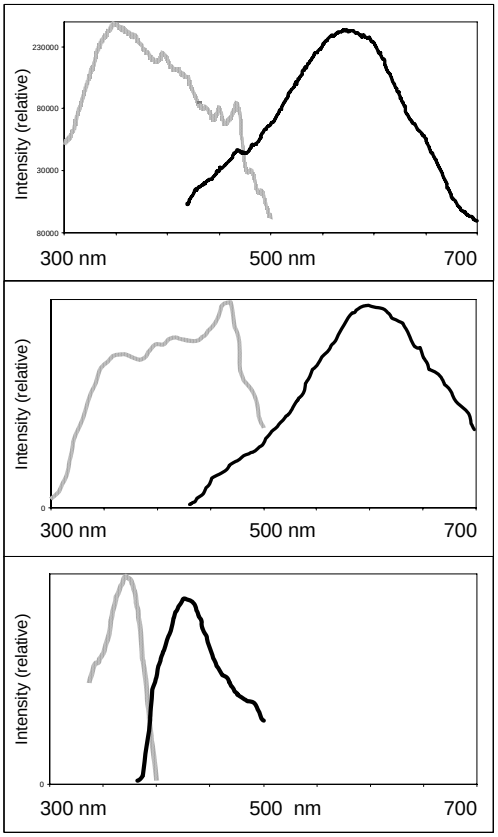

Figure 2-3. Fluorescence of lipofuscin granules (LF). Fluorescence spectroscopy of LF from our preparations (top panel) compared with LF from Boulton et al. [Boulton, 1990] (middle panel) and Schutt et al. [Schutt, 2002] (lower panel). The spectra from their published papers were simply traced. Excitation (gray) monitored with emission at 570 nm, and emission (black) monitored with excitation at 364 nm. These spectra provide evidence that supports the congruence of our preparations with those studied by Boulton et al. [Boulton, 1990].

To determine the composition of the granules, first the lipids from a weighed quantity of granules were extracted in methanol:chloroform, transferred, evaporated to dryness and weighed. This revealed that LF was 49.5%±1.1% extractable lipid by weight. These percentages represent the mean of three independent measurements and indicate the standard deviation. Next, the protein in a known quantity of LF was solubilized in 1% SDS and quantified by BCA assay. LF consisted of 43.5%±2.6% total protein. Thus, these granules were composed nearly entirely of lipid and protein. These percentages represent the mean of three independent measurements and indicate the standard deviation.

In order to analyze the protein component of LF, the granules were subjected to 2D gel electrophoresis. Initial attempts yielded very few protein spots. Only after loading significantly more protein (300 μg) than would typically be needed to examine an entire cell extract (about 100 μg total protein) were significant numbers of spots visible (Figure 2-4A).

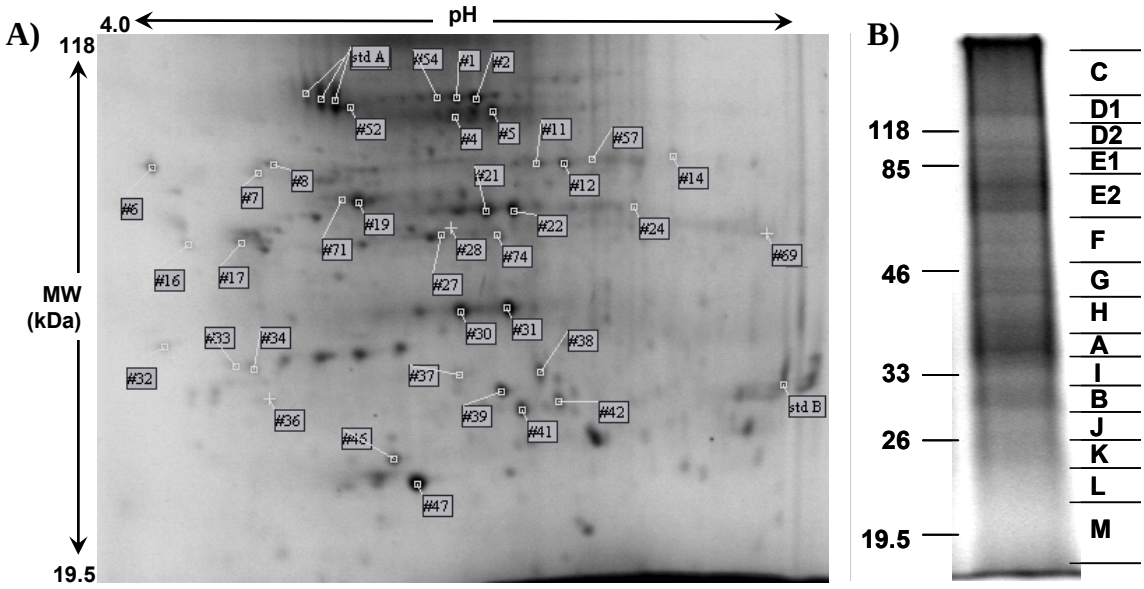

Figure 2-4. Electrophoresis of lipofuscin (LF) proteins. **A**: 2D electrophoresis gel from 300 μg of LF protein. This gel is representative of gels from four separate LF preparations. Spots found in at least three of the four gels are indicated by their identifying spot number (Table 1). Spots lacking a label were unique to this particular preparation. Spots from standard proteins used to align gels are indicated as "std A" and "std B". **B**: Representative lane of SDS-PAGE of 50 μg of LF protein. Mobilities of molecular weight markers are indicated to the left. On the right, gel slices taken for subsequent in-gel digestion are shown. The 1D gel shows relatively few well-resolved bands with much diffuse protein staining; thus 6 fold more total protein is needed in the 2D gel in order to observe a surprisingly small number of well-focused protein spots. Taken together, these observations suggest that the proteins of LF are notably heterogeneous.

2D gel electrophoresis of LF proteins using a common isoelectric focusing buffer that contained 4% Triton X-100 resulted in 37% fewer spots than when the same sample was run in buffer with 0.5% Triton X-100 and 2% ASB-14 (data not shown). ASB-14 is a zwitterionic detergent known to facilitate the entry of transmembrane and other hydrophobic proteins into 2D gels [Santoni, 2003]. The results reported were obtained using ASB-14 in the reswelling buffer.

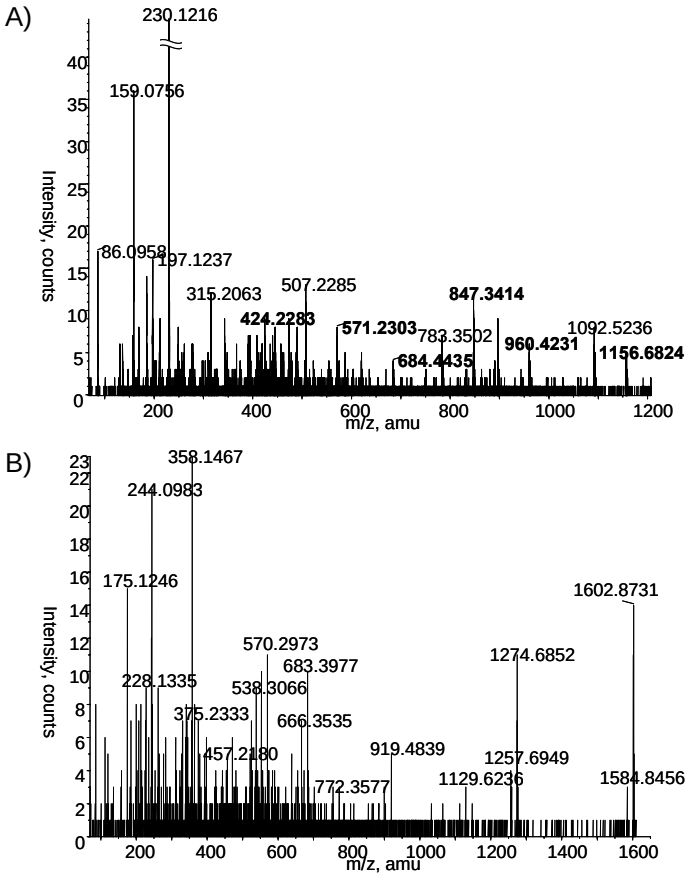

Figure 2-5. Mass spectrometry of peptides from lipofuscin proteins. **A**: CID spectrum from LCMSMS of the peptide identified as SAAIYNPVIYIM$_{O2}$M$_{O}$NK (where M$_{O}$ represents Met sulfoxide and M$_{O2}$ represents Met sulfone) from rhodopsin. Indicated in bold are six y ions that make identification of these modified sites unequivocal. Another spectrum showed the same peptide with Met sulfoxide at the first Met position, and a third spectrum showed Met sulfone at the first Met without Met sulfoxide at the second Met position (data not shown). **B**: Representative CID spectrum from oMALDI MSMS. This peptide was identified as LVDQNIFSFYLSR from cathepsin D. The spectrum in **A** allows the conclusive identification of the modified methionines at positions 308 and 309 of rhodopsin. These spectra show that the fragmentation data obtained by both LCMSMS and oMALDI MSMS are of sufficiently high quality to allow unambiguous identification of the corresponding peptides.

2D gels were run analyzing proteins from four independent preparations of LF granules. These gels showed some variation in number of spots, ranging from 53 to 121 (with an average of 78.5 spots per gel). The image processing program Melanie 4 was used to compare and match spots from the different gels. A "synthetic gel" was constructed in silico using this software, where each spot in the synthetic gel represented a spot present in at least three of the four 2D gels. Forty-four spots were found in the synthetic gel, including the five internal pI standards that had been added before electrophoresis. Nineteen proteins were identified from the 2D gels, corresponding to 37 of the 39 spots (some proteins run as more than one spot due to posttranslational modifications).

Because of the limitations of 2D electrophoresis, we also analyzed LF proteins that had been solubilized in 1% SDS using 1D SDS-PAGE (Figure 2-4B). The overall

pattern of bands seen in Figure 2-4B was qualitatively reproducible from one preparation of LF granules to another. Regions of the 1D gel were cut out and trypsinized for subsequent analysis and protein identification using HPLC with on-line ESI-QqToF tandem mass spectrometry (LCMSMS) techniques (Figure 2-5A). These protein identifications were compared with those for proteins from spots in the 2D gels, which were excised, trypsinized, and identified using MALDI-QqToF mass spectrometry (Figure 2-5B).

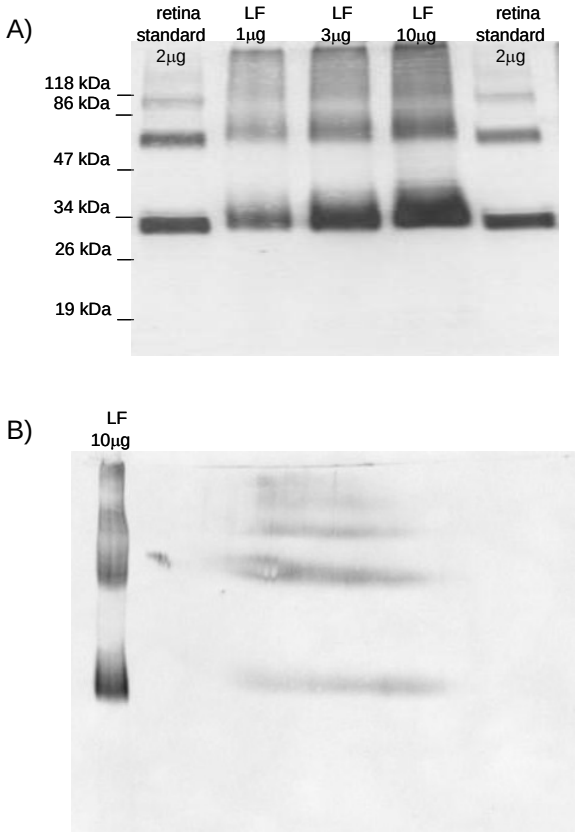

Figure 2-6. Rhodopsin immunoblots of lipofuscin (LF). **A**: Immunoblot following SDS-PAGE of 1, 3, and 10 μg of total LF protein. Shown for comparison is 2 μg of protein from photoreceptor cell membranes enriched from human retina. Rhodopsin runs on SDS-PAGE as a mixture of the monomer (about 30 kDa), dimer (about 60 kDa), and trimer (about 90 kDa). **B**: Immunoblot following 2D electrophoresis of 10 μg of total LF protein. For comparison, 10 μg of LF protein was loaded in the standards lane of the second dimension gel. The diffusion (band broadening, due to modifications) of the rhodopsin in LF as compared with that in photoreceptor cells indicates that the rhodopsin in LF is remarkably heterogeneous.

Twenty-seven proteins were identified in 1D gel regions (Table 2-1), including five that were also found in the 2D spots. Thus, 22 proteins were identified in 1D gel regions that were not identified in the 2D gels. Notably, though 27 proteins were identified, many good quality CID spectra (defined as spectra that have at least four

fragment peaks of signal:noise >5 between 500 and 1300 m/z) did not yield credible protein identification.

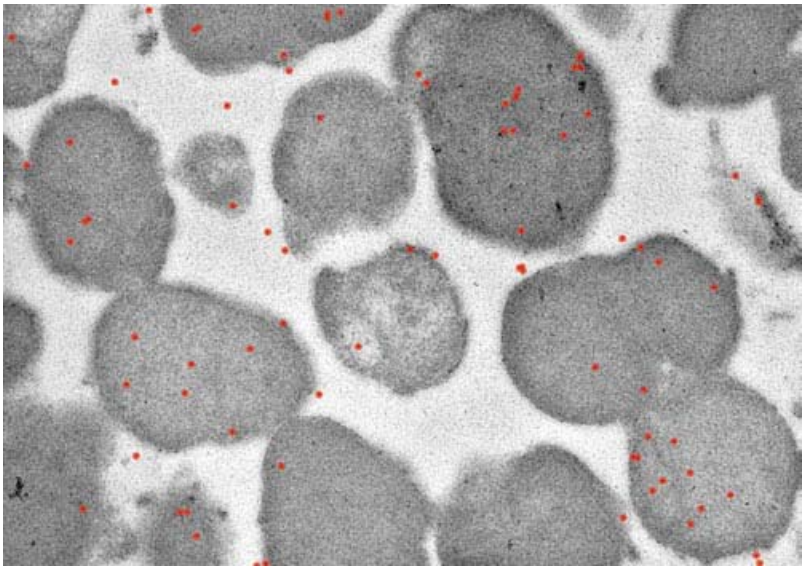

Figure 2-7. Immunocytochemistry of lipofuscin (LF). LF granules were fixed and embedded in resin. Thin sections were collected on gold grids, incubated with an anti-rhodopsin antibody, washed, incubated with gold-conjugated protein A, washed, and examined using transmission electron microscopy (TEM). TEM showed gold-conjugated protein A bound to anti-rhodopsin antibodies on the LF granules as dark black dots, which have been pseudocolored red. Rhodopsin is an integral part of the LF granules.

Among the proteins identified in 1D gel regions but not in the 2D gels was rhodopsin. Because of its importance and abundance in the photoreceptor cells which are phagocytosed by the RPE, we examined the rhodopsin in LF further. Figure 2-6 shows immunoblot analyses of both 1D and 2D separations of LF proteins, probed with an antibody raised against rhodopsin. In both of these blots, the microheterogeneity of the rhodopsin population in LF was evident. The 2D immunoblot explains why no rhodopsin was identified from the 2D gel, since no well-focused spots were observed. This is despite the apparent abundance of LF rhodopsin, based on the 1D immunoblot. Some of the modification responsible for the observed heterogeneity of LF rhodopsin was determined to be oxidative damage. The tryptic peptide containing Met308 and Met309 was found by mass spectrometry bearing one, two, and three extra oxygen atoms which MSMS localized to the tripeptide IMM, residues 307-309 of rhodopsin, indicating

oxidation of one or both of these Met residues to the Met sulfoxide or even the Met sulfone (Figure 2-5A). Rhodopsin was further confirmed to be a component of LF granules by immunocytochemistry. Electron micrographs of LF showed gold-conjugated protein A bound to anti-rhodopsin antibodies on the LF granules (Figure 2-7). Over two-thirds of the gold particles in these micrographs were found on LF granules when corrections were made for the total area within and between granules.

Another protein of significant interest was the cellular retinoid binding protein CRALBP, which can be used as a molecular marker for RPE cells [Schlunck, 2002]. CRALBP was not identified in 1D gel slices of LF proteins, but was identified by mass spectrometry from a lower abundance spot seen in one of the four 2D gels. 1D immunoblots showed that while CRALBP was present in LF protein extracts, it was not very abundant (Figure 2-8).

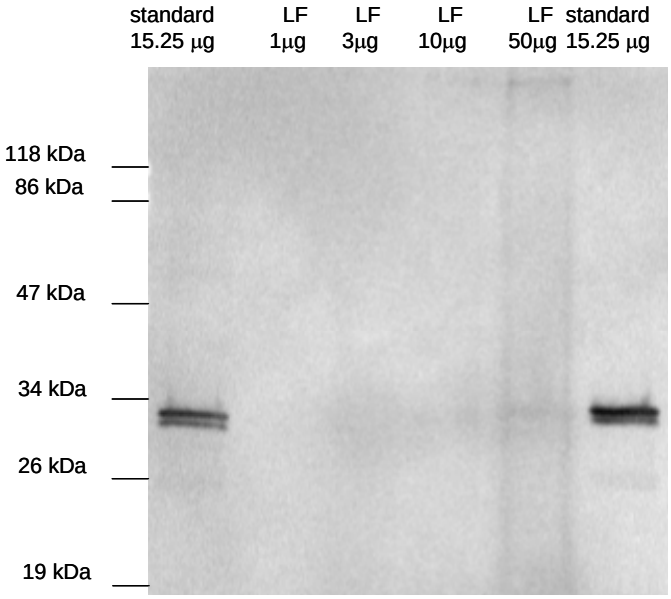

Figure 2-8. CRALBP immunoblot of lipofuscin (LF). Doses of 1, 3, 10, and 50 μg total LF protein were run on SDS-PAGE and blotted with an anti-CRALBP antibody. Shown for comparison are 15.25 μg of total protein extracted from human RPE. CRALBP is nearly absent from LF.

In light of the oxidation seen on rhodopsin, and in view of the hypothesis that oxidative damage may be involved in the generation of LF, we examined the LF proteins for oxidative modifications using DNP, which derivatizes protein carbonyls [Shacter, 2000].

Figure 2-9A shows an immunoblot of DNP-derivatized LF proteins using an anti-DNP antibody which binds to the hydrazones formed by derivatization of the oxidatively formed carbonyls. Additional immunoblots revealed LF proteins containing lipid peroxidation- or glucoxidation-induced damage, specifically malondialdehyde (MDA, Figure 2-9B), and advanced glycation end products (AGE), respectively.

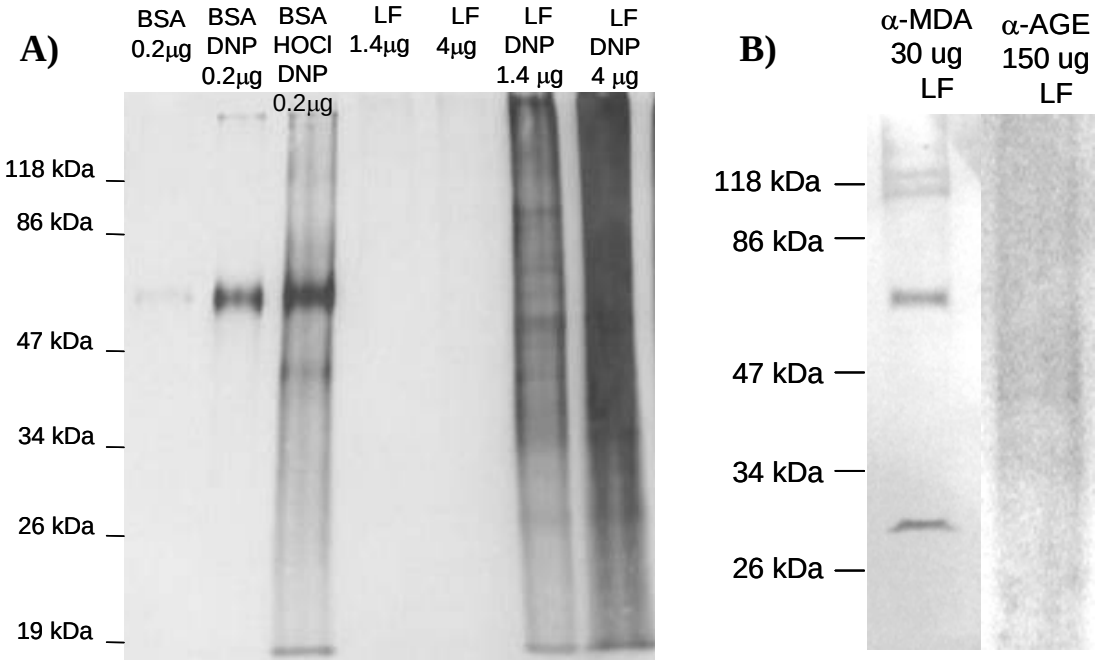

Figure 2-9. Immunoblots of oxidatively damaged lipofuscin (LF) proteins. **A**: LF proteins, 1.4 and 4 μg, that had been derivatized with dinitrophenyl hydrazine (right two lanes) or that were untreated (middle two lanes) were run on SDS-PAGE and blotted with an anti-DNP antibody to show the derivatized protein carbonyls, a common product of protein oxidative damage. Shown for comparison and to demonstrate specificity are lanes of BSA, BSA treated with DNPH, and BSA oxidized with hypochlorite then treated with DNPH. **B**: 30 and 150 μg of LF proteins were separated using SDS-PAGE and blotted with an anti-MDA antibody to show LF proteins containing lipid peroxidation-induced damage. There is extensive oxidative damage to LF proteins.

Protein oxidation was seen to be extensive (proteins across the molecular weight range of the 1D gel were seen to be modified) in the anti-DNP immunoblot. Notably, no well-focused spots of DNP-labeled proteins were detected in 2D immunoblots (data not shown). This suggests that many proteins that were oxidatively damaged were too

heterogeneous to be observed in 2D gels, and therefore cannot be identified using this kind of separation.

Table 2-1. Proteins identified in lipofuscin granules. These proteins were identified from in-gel digestion followed by mass spectrometry from the respective SDS-PAGE gel regions or 2D gel spots. These proteins demonstrate that LF contains components of photoreceptor discs and of lysosomes. Furthermore, 1D- and 2D-based protein identification is complementary, with 1D-based methods identifying significantly more of the heterogeneous and hydrophobic proteins that are found in LF. We could not differentiate between creatine kinase and arginine kinase because of identical peptide sequences. KIAA0617 was only identified from one peptide with relatively low confidence. Items marked with an asterisk (*) were previously reported by Schutt et al. [Schutt, 2002].

Protein	GenBank Number	Gel Area/ Spot #	Tissue Specificity	Subcellular Location	Alternate Names	Gene Ontology
1D Gel						
4F2 antigen heavy chain	177207	D2		type II membrane protein	CD98 antigen	calcium ion / amino acid transport
11-cis retinol dehydrogenase	2492753	I	retinal pigment epithelium	membrane-associated	retinol dehydrogen-ase	visual perception
acyl-CoA dehydrogenase	3273228	F		mitochondrial inner membrane		fatty acid beta-oxidation
alpha 1-antitrypsin[I]	24438	H	plasma	extracellular	alpha-1-antiprotein-ase	Endopeptid-ase inhibitor activity
alpha-tubulin 4[II]	32015	A, D2				protein binding
alpha-tubulin 1[III]	37492	F				protein binding
anion transport protein[I]	28714	D1	erythrocytes	integral membrane protein	AE 1, CD233 antigen	cell ion homeostasis
annexin A2[II, III]	18645167	A		membrane associated	lipocortin II	calcium ion binding
beta-globin[I,III]	29446	B	erythrocytes		hemoglobin beta chain	oxygen transport activity
calnexin[II]	2134858	E1		type I membrane protein		calcium ion binding
cathepsin D[II, III]	494296	B		lysosomal		lysosome
Ceroid-lipofuscinosis	5729770	H		lysosomal	tripeptidyl-peptidase I	
cytochrome c oxidase II subunit	14016	L		integral membrane protein, mitochondiral inner membrane	cytochrome c oxidase	cytochrome-c oxidase activity
Interphoto-	33961	D1	Interphoto-		interstitial	lipid

receptor retinoid-binding protein			receptor matrix		retinol-binding protein	metabolism, visual peception
keratin[III]	30154839	B, F, M				cytoskeleton organization
lysosomal integral membrane protein [IIII]	1362856	E1		type II membrane protein, lysosomal	LIMP II, CD36 antigen like 2	integral to plasma membrane
myelin protein zero	127721	A, B, D1/2, E1/2, F, I, J, L	peripheral nervous system schwann cells	type I membrane protein		structural molecule activity, synaptic transmission
NADH-ubiquinone oxidoreductase	128826	E1		Mitrochon-drial inner membrane	NADH dehydrogen-ase	electron carrier activity
Na+/K+-exchanging ATPase	88214	D1		integral membrane protein	sodium pump 3	ATP hydrolysis, proton transport
peripherin	4506465	A	Photo-receptor rod rim region	integral membrane protein	retinal degeneration slow protein	visual perception
phospholipase C-alpha	303618	F		endoplasmic reticulum	protein disulfide isomerase A3	signal transduction
rhodopsin	4506527	D1/2, E1/2, F, G, H, I	Photo-receptor rod	integral membrane protein	Opsin 2	Phototrans-duction, G-protein coupled receptor activity
rod outer segment membrane protein [I]	4506575	A, D2, H, I	Photo-receptor rod rim region	integral membrane protein	ROSP1	visual perception
retinal pigment epithelium-specific protein	4506591	D2, E1/2	retinal pigment epithelium		RPE65	visual perception
retinal S-antigen[III]	4506781	F, G	retina and pineal gland		rod photo-receptor arrestin	signal transduction
Serum albumin[I,III]	28592	A	plasma	secreted		body fluid osmoregulat-ion
Transducin	31865	A	Photo-receptor rod	membrane associated		visual perception
trypsin[I]	136429	A, D1/2, E1/2, F, G, H, I, M		extracellular		protease

2D Gel						
ATP synthase, beta subunit[II, III]	32189394	19,47, 71		mitochondria, membrane protein		tranpsorter activity
calnexin[II]	2134858	3		type I membrane protein, ER		calcium ion binding
calreticulin[II, III]	4757900	6		endoplasmic reticulum lumen		protein folding
calumenin	2809324	16	ubiquitously expressed	endoplasmic reticulum lumen and secreted	crocalbin	calcium ion binding
Creatine kinase/arginine kinase[III, IV]	180570	74		cytoplasmic		creatine kinase activity
cathepsin D[II, III]	494296	37,38		lysosomal		lysosome
Ceroid-lipofuscinosis, neuronal 2	5729770	21,24		lysosomal		
dnaK-type molecular chaperone HSPA5	87528	4,5,52		endoplasmic reticulum lumen		
heat shock protein gp96[III]	15010550	7		endoplasmic reticulum lumen	GRP94, tumor rejection antigen	response to unfolded protein
KIAA0908	4240305	57	ubiquitous	lysosomal	Prenyl-cysteine oxidase	lysosome, lyase activity
KIAA0617[V]	40788303	30	widely expressed	nuclear and golgi		cell cycle arrest
motor protein[III]	516764	74		mitochondrial inner membrane	mito. inner memb. protein, mitofilin	Mitochond-rial inner membrane
mutant beta-actin	28336	27		cytoplasmic		Acetyl-transferase complex
NADH-ubiquinone oxidoreductase	128826	1,2,32, 33,41, 54		Mitrochond-rial inner membrane	NADH dehydrogen-ase	electron carrier activity
phospholipase c-alpha	303618	11		endoplasmic reticulum		signal transduction
pre-mRNA splicing factor SF2p32	338043	32		mitochondrial matrix	hyaluronan-binding protein 1	immune response
prohibitin[II, III]	4505773	39	widely expressed	cytoplasmic		regulation of cell cycle
protein disulfide isomerase	5031973	7,12,1 9		endoplasmic reticulum lumen		
vimentin[II, III]	4507895	17	highly			structural

			expressed in fibroblasts			constituent

[I] These proteins were preparation contaminants.
[II] These proteins were identified as components of the macrophage phagosome proteome. [Garin, 2001]
[III] These proteins were reported in Schutt et al. [Schutt, 2002] as LF components.
[IV] We were unable to differentiate between these two proteins because of their possessing identical peptide sequences.
[V] This protein was only identified from one peptide with relatively low confidence.

Discussion

Detecting membrane and microheterogeneous proteins

We report the identification of proteins in retinal lipofuscin (LF) granules. Because of the lipophilic nature of LF granules and the apparent inability of RPE cells to degrade them, one would expect to find an abundance of hydrophobic and highly modified, microheterogeneous proteins in LF granules. Due to the limitations of 2D electrophoresis, including the lack of solubility of hydrophobic proteins in buffer systems compatible with 2D electrophoresis and the inability to focus microheterogeneous proteins into observable spots, 1D electrophoresis was also used to identify proteins in LF. The previous report [Schutt, 2002] employed only 2D electrophoresis, which limited the proteins amenable to identification. We have identified 41 total proteins, only five of which were found in both 1D and 2D gels. Of the 41 proteins that we identified and the 65 nonredundant proteins identified by Schutt et al. [Schutt, 2002], only 12 (11%) were common to both studies.

An aspect influencing the discrepancy between protein identifications from the two types of gels is the ability to detect highly hydrophobic proteins, which we expected to be abundant in LF granules. We found 17 integral membrane and membrane-associated proteins (about 50% of all LF-specific proteins we identified). The previous report of LF proteins [Schutt, 2002], which used 2D electrophoresis, found fewer membrane proteins.

Of the 17 membrane associated proteins that we identified, 13 were found exclusively in our 1D gel slices, again testifying to the limitations of 2D electrophoresis in analyzing lipophilic proteins.

Another cause of the inconsistency in proteins identified from 1D and 2D gels may be from contaminants of LF preparations. Contaminants of LF preparations are likely to be greatly exacerbated in 2D electrophoresis because they might run as well focused spots, whereas many of the authentic LF proteins are microheterogeneous and therefore do not focus on 2D gels (rhodopsin being a notable example, Figure 2-6). Whenever preparations of subcellular structures are made using centrifugation for separation based on density, some contamination is inevitable. Indeed, as several others have noted, such preparations are not truly purifications but are enrichments [Brunet, 2003]. While these are nonetheless valuable preparations, caution should be exercised in drawing conclusions when analyzing them. We found that we had to load significantly more material onto the 2D gels than we would have expected for an enriched subcellular granule. This may have resulted in an overloading of the focusable protein contaminants, such that they became visible as spots that were subsequently identified (CRALBP as an example, Figure 2-8). For this reason, we also employed complementary protein identification from 1D gels. We are aware that the methods we have used do not identify every protein in the preparations we have studied. Attempting to exhaustively identify all of the proteins in an enriched preparation such as lipofuscin granules would be misleading because many contaminating proteins would be identified. Nonetheless, the proteins we have identified give us a useful, even if somewhat incomplete, view of the protein constituents of LF.

We have shown that these granules exhibit the fluorescence characteristics and microscopic structure previously reported [Boulton, 1990]. We also show that the granules that we have isolated and characterized physically are biologically active, causing blue-light-dependent cell death to RPE cells in culture (Figure 2-1), as others have previously reported [Winkler, 1999]. The only physical characterization of the granules offered by Schutt et al. [Schutt, 2002] of their LF preparation was fluorescence spectroscopy. As shown in Figure 2-3, the excitation and particularly the emission spectra reported by these authors were significantly dissimilar from our fluorescence spectra and from spectra previously reported in the literature.

Identifying phagosomal, lysosomal, and photoreceptor proteins

Our protein identifications are supportive of the hypothesis that LF has a lysosomal/phagosomal origin. Four proteins that are lysosomal in subcellular localization were found in our LF preparations. The proteome of macrophage phagosomes has recently been published [Garin, 2001], and 10 of the 41 proteins in our LF preparations, which presumably have a phagosomal origin, are shared with the phagosomal proteome as reported [Garin, 2001].

The prevailing model of LF origin is that there is a breakdown in the lysosomal machinery responsible for the degradation of the photoreceptor outer segments that are phagocytosed diurnally by the RPE, leading to an accumulation of indigestible material that becomes LF. Our protein identifications strongly support such a model. Six of the LF proteins that we identified are specific to photoreceptors and their outer segments. Only one of these was previously reported as a constituent of LF [Schutt, 2002].

Identifying rhodopsin

One of the most significant proteins that we observed in LF, not observed previously, is rhodopsin, one of the most abundant proteins of photoreceptor outer segments. We did not observe rhodopsin among our 2D gel spots. Immunoblotting of our 2D gels showed that this was due to the lack of focusing of the microheterogeneous rhodopsin population in LF (Figure 2-6). It is significant that the rhodopsin observed is rather extensively modified, at least in part due to oxidative damage. Though we were not able to quantify LF rhodopsin precisely, our immunoblot evidence suggests that this protein is fairly abundant in LF. Although Feeney-Burns et al. [Feeney-Burns, 1988] were unable to observe rhodopsin in LF granules, we believe that this was due to the antibody they used. As shown in Figure 2-7 our anti-rhodopsin antibody (R4) specifically bound to LF granules confirming that the rhodopsin observed is a component of the granules and not merely a contaminant. The opsin we identified was exclusively rhodopsin, and no evidence was found that cone opsins were present in LF. It has been previously noted that the cone-rich fovea is not as high in LF as the rest of the macula [Sparrow, 2003].

Other specific proteins of interest

Two LF proteins of interest, found in both 1D and 2D gels, are the ceroid lipofuscinosis protein and cathepsin D. Ceroid lipofuscinosis proteins are found to be mutated in Batten's disease, a condition in which there is significant accumulation of lipofuscin in neuronal tissue [Yin, 1996]. The ceroid lipofuscinosis proteins accumulate

in the lipofuscin granules, along with ATP synthase, other proteins, and lipids [Yin, 1996; Ryan, 1996]. Finding cathepsin D in LF was not surprising. This lysosomal protease is highly expressed in RPE lysosomes, and is employed by these cells in degrading rhodopsin [Zimmerman, 1983].

Another protein of interest in these studies is the cellular retinoid binding protein CRALBP, a protein sometimes used as a molecular marker for RPE cells (but also found in the Müller cells of the neural retina [Johnson, 1997]). Schutt et al. [Schutt, 2002] found CRALBP to be one of the most abundant proteins in their preparations (approximately the fifth most intense spot on the 2D gel, though two proteins were identified from this spot). In contrast, we find CRALBP to be the 69th most abundant of 121 spots in one gel, and absent from the other three 2D gels (data not shown). We did not identify CRALBP from our 1D gels, presumably because it was lost among more abundant proteins. As seen in Figure 2-8, immunoblotting shows that while CRALBP is present in gels of RLF, it is not very abundant. It is probable that CRALBP is a contaminant of these preparations.

Detecting protein modifications

A notable observation from this work is the nature and extent of modifications seen in LF proteins. Derivatization using DNPH followed by immunoblot analyses with the anti-DNP antibody shows the presence of abundant protein carbonyl groups in LF, indicating extensive oxidative damage to proteins. While protein carbonyls are diagnostic of oxidative damage to proteins [Shacter, 2000, Berlett, 1997], they are certainly not the only covalent modification that occurs to proteins as a result of such damage. Neither

Met-sulfoxide nor Met-sulfone are derivatized with DNPH. A notable modification to proteins under oxidative stress is their fragmentation into smaller polypeptides by the breakage of backbone bonds [Berlett, 1997]. Such damage would result in peptides upon trypsinization that have amino or carboxy termini that would not be predicted from the sequence databases, and may be further modified in terms of covalent structure. Additionally, covalent modifications of proteins due to oxidative damage are not yet completely understood, and many unknown modifications could be present, further complicating the proteomic analyses of the in-gel digest mass spectrometry data. Indeed, we observed a remarkably high fraction (about 75%) of our "good" CID spectra (criteria given in Results) that did not yield peptide identification, possibly because many of the peptides in question are modified in unknown ways. The only modification that we were able to identify precisely was oxidation of two methionine residues on rhodopsin, including the formation of the sulfone and the sulfoxide (Figure 2-5A). Ryan et al. [Ryan, 1996] showed oxidation of methionine in ceroid lipofuscinosis protein in lipofuscin of neural tissue. We mention their findings, because we find the parallel between LF and neural lipofuscin suggestive. We find that both the ceroid lipofuscinosis protein itself and methionine oxidation are found in LF. Though we believe that there are significant differences between retinal LF and LF in other tissues such as neurons; we also believe that they are not wholly dissimilar. The facts that methionine oxidation is seen in both types of lipofuscin, and ceroid lipofuscinosis protein (a lysosomal component) occurs in both types suggests to us that oxidative protein damage inhibiting lysosomal function may be a shared characteristic (or even causal factor) in the two types of lipofuscin.

A previous report on LF proteins [Schutt, 2002] was followed up with an article showing immunological analyses of LF proteins modified by hydroxynonenol (HNE), malonyldialdehyde (MDA), and advanced glycation end-products (AGE) [Schutt, 2003]. Many of these modifications would be derivatized by DNPH, and thus would be part of the modified proteins that we observed in Figure 2-7A. For example, HNE has been shown to react with proteins resulting in a loss of sulfhydryls and a concomitant increase in DNPH reactivity [Esterbauer, 1991]. In addition, 22% of the MDA incorporated into polylysine became amino-propenal, which has a DNPH-reactive aldehyde moiety [Esterbauer, 1991]. Furthermore, one of the two aldehydes in MDA can react with a protein yielding the imine and possibly leave the other aldehyde to react with the hydrazine. Glycation, through a Maillard reaction, creates Amadori products that have free carbonyl groups [Yin, 1996]. The previous report [Schutt, 2003] identified 32 2D gel spots that react with an anti-MDA antibody, 15 spots that react with an anti-HNE antibody, and four spots that react with an anti-AGE antibody. Notably, all of these are well-focused spots, as opposed to the heterogeneously modified proteins we observed with DNP derivatization (Figure 2-9A). We observed that an anti-MDA antibody reacted with only a handful of LF proteins (Figure 2-9B), and that an anti-AGE antibody reacted weakly with a heterogeneous smear of proteins from LF (data not shown). Thus, it is eminently possible that the general oxidative damage that we describe might well include specific modifications such as those resulting from MDA, HNE, and AGE. Our specific efforts to duplicate the findings of Schutt et al. [Schutt, 2003] using our LF preparations yielded different findings, suggesting the need for further study of the roles of these specific modifications in the biochemistry of LF.

Much has yet to be learned about the modifications of proteins in LF granules. Perhaps it is the oxidative modification of proteins (and possibly of lipids as well) that inhibits the degradative machinery of the RPE lysosomes, and leads to the accumulation of LF within these cells. Protease inhibition causes lipofuscin formation in myocytes [Brunk, 2002]. Oxidative stress causes accelerated lipofuscinogenesis in various cells, and there is a dramatic synergy between oxidative stress and inhibition of lysosomal proteases (allowing more time for oxidation) in lipofuscin formation in cultured cells [Brunk, 2002]. Nilsson et al. [Nilsson, 2003] found greatly enhanced accumulation of LF in RPE cells cultured in 40% ambient oxygen when compared with cells cultured in 8% ambient oxygen. We are pursuing experiments aimed at understanding the possible role of oxidative damage of proteins in lipofuscinogenesis and other aspects of LF origins and activities.

CHAPTER 3

MELANOLIPOFUSCIN ORIGIN & COMPOSITION

Summary

Melanolipofuscin (MLF) is a complex granule, exhibiting properties of both melanosomes and lipofuscin (LF) granules. MLF accumulates in retinal pigment epithelial (RPE) cells and may contribute to the etiology of age-related macular degeneration (AMD). MLF accumulation has been reported by Feeney-Burns to more closely reflect the onset of AMD than the accumulation of lipofuscin. In an effort to assess the possible contribution MLF may have to the onset of AMD, we analyzed the phototoxicity and protein composition of MLF and compared those results to that of LF. Specifically, we observed the accumulation of MLF in human RPE from different decades of life, and assessed the phototoxicity of these granules. We also employed fluorescence spectroscopy, atomic force microscopy, transmission and scanning electron microscopy and proteomic analysis to examine the composition of MLF granules in an effort to ascertain their origin. Our results show that MLF granules are phototoxic and their accumulation more closely reflects the onset of AMD than does LF accumulation. Our compositional analysis of MLF has shown that while these granules contain some similarities to LF granules, MLF is substantially different. Of significant interest is the finding that MLF, in contrast to LF, does not contain photoreceptor-specific proteins, suggesting that MLF may not originate from the phagocytosis of photoreceptor outer segments. Instead the presence of RPE- and melanosome-specific proteins would suggest that MLF accumulates as a result of the melanosomal autophagocytosis of RPE cells.

Our results provide significant insight into understanding the formation and toxicity of MLF and support its role in the etiology of retinal disease.

Introduction

Several retinal diseases, including age-related macular degeneration (AMD), have been associated with the accumulation of autofluorescent granules in retinal pigment epithelial (RPE) cells. One such autofluorescent granule, lipofuscin (LF), may relate to the onset of these ocular diseases because it has been shown to generate reactive oxygen species via photosensitization with blue light [Beatty, 2000; Winkler, 1999; Wassell, 1999; Rozanowska, 1995]; which may cause damage and death of the RPE with subsequent death of the surrounding cells. However, as Feeney-Burns has reported [Feeney-Burns, 1984], the accumulation of LF in human RPEs is not consistent with the onset of AMD. The most dramatic increase of LF in human RPEs, a 95% increase, occurs between young and middle-aged groups (defined as ages 1-20 and 21-60 respectively) while there is only a 21% increase between middle-aged and old-aged groups (ages 61-100) [Feeney-Burns, 1984]. The presence of significant quantities of LF in young eyes may cast doubt on its contribution to the etiology of AMD.

Another autofluorescent granule that accumulates in RPE cells and may contribute to the etiology of AMD is a complex granule exhibiting properties of both melanosomes and lipofuscin granules called melanolipofuscin (MLF). In contrast with the accumulation of LF in the RPE, MLF accumulation has been reported by Feeney-Burns to more closely reflect the onset of AMD. MLF exhibits a 15% increase between

young and middle aged groups and a 50% increase between middle-aged and old-aged groups {Feeney-Burns, 1984].

MLF may contribute to the etiology of AMD, but little is known about the composition and origin of these complex granules. Two models for the origin of MLF have been suggested. The first model involves the autophagy of preexisting melansomes and their incorporation into accreting LF granules. This model is supported by the observation that phagosomes containing undegradable material fuse with melanosomes [Schraermeyer, 1999]. The second model is that melanin is synthesized *de novo* in lysosomes, which subsequently fuse with accreting LF granules. This model is supported by evidence that synthesis of melanin in depigmented RPE cells is seen in lysosomal compartments [Dorey, 1990; Schraermeyer, 1994]. Knowledge of the composition of MLF could provide significant insight into the origin of these granules, and determining the phototoxicity of these granules could be useful for ascertaining MLF's role in the etiology of AMD and other retinal diseases.

In the present study we observed the accumulation of MLF in human RPE from different decades of life and assessed the phototoxicity of these granules. We also employed fluorescence spectroscopy, atomic force microscopy, transmission and scanning electron microscopy and proteomic analysis – using 1D gel electrophoresis coupled with ESI mass spectrometry – to examine the composition of MLF granules in an effort to ascertain their origin. Collectively these data provide significant insight into understanding the formation and toxicity of MLF and support its role in the etiology of retinal diseases. Specifically, these data do not provide direct support for either previously suggested hypothesis for the origin of MLF, but instead suggest that MLF

accumulates as a result of the melanosomal autophagocytosis of RPE cells. To our knowledge this is the first report of the phototoxicity and biochemical analysis of retinal melanolipofuscin.

Materials and Methods

Lipofuscin and Melanolipofuscin Isolation and Fluorescence - Lipofuscin granules were isolated as previously described [Warburton, 2005] and MLF granules were isolated from these preparations. Briefly, granules were isolated from human RPE from donor eyes, provided by Dr. Paul Bernstein of the Moran Eye Institute, University of Utah, Salt Lake City, UT. The time between donor death and enucleation was 1-4 hours, after which the donor eyes were stored at 4ºC until dissection. Dissections were carried out 6-24 hrs after donor death in a dim light environment. RPE's were stored at -75°C until use. Lipofuscin granules were isolated from the band at the 0.3M/1.0M interface and melanolipofuscin granules were isolated from the bands at the 1.0M/1.2M and 1.2M/1.4M interface. Sucrose gradients were only briefly exposed to light while photographs of the gradients were taken. Fluorescence spectra of isolated lipofuscin and melanolipofuscin granules were acquired as described by Boulton et al. [Boulton, 1990] using a Jobin Yvon Fluoromax-3 Spectrofluorometer (Edison, NJ).

LF and MLF Accumulation - To study the accumulation of LF and MLF over time, sucrose gradient centrifugation was employed using four groups of RPE, each consisting of 6 RPE and representing a different decade of life. The first group had an average age

of 33 ± 1.6 yrs; the second group had an average age of 43 ± 0.9 yrs; the third group had an average age of 54.3 ± 1.9 yrs; and the fourth group had an average age of 64 ± 0.0 yrs. To compare the LF and MLF content in young and old eyes, sucrose gradients were run with 11 RPE from young eyes (average age of 21.2 ± 5.9 yrs) and 14 RPE from old eyes (average age of 66.5 ± 5.9 yrs). Pictures of the gradients were taken using an Olympus Camedia digital camera. Image J (National Institutes of Health) was used to measure the optical density of LF and MLF bands in the sucrose gradients.

All other experiments were performed using LF and MLF isolated from RPE's taken from a random donor population between 40 and 80 years old.

Cell Culture - ARPE-19 (human retinal pigment epithelial cells – ATCC-CRL-2302) were grown in 24-well tissue culture plates in RPMI 1640 media supplemented with 10% fetal bovine serum (FBS). Upon reaching confluency the FBS in the media was reduced to 1%. Cells were either maintained in RPMI 1640 media supplemented with 1% FBS or incubated in the same media which also contained ~300 melanolipofuscin or lipofuscin granules/cell for 24 hours to allow for ingestion of the granules. After the 24 hour incubation, the melanolipofuscin- or lipofuscin-fed RPE cells were transferred back to RPMI 1640 media supplemented with 1% FBS and maintained for 3 days before bioactivity assay.

Bioactivity Assay - To investigate the bioactivity of MLF, ARPE-19 cells that were fed LF, MLF or neither (control cells) were either subjected to blue light (390-550 nm) for 48 hr at an intensity of ~2.8 mW/cm or maintained in the dark. Blue light was introduced

into a 5% CO_2 humidified cell incubator using a Mille Luce M1000 Fiber Optic Illuminator with a 150 W quartz halogen bulb, a 25-mm dichroic blue light filter, and a 48 inch fiber optic cable which obviates heat (Edmund Optics, Barrington, NJ). Photocytotoxicity of the lipofuscin and melanolipofuscin granules was assessed using Sulforhodamine B (JNCI 82, p1107 (1990)) to measure cell viability. Briefly, cultures were fixed with trichloroacetic acid and stained with 0.4% sulforhodamine B in 1% acetic acid. The cultures were washed 4 times with 1% acetic acid to remove any unbound dye; protein-bound dye was extracted with 10 mM unbuffered Tris base and transferred to a 96 well culture plate. Absorbance was measured at 570 nm on a CERES UV900 HDi plate reading spectrophotometer (Bio-Tek Instruments).

Microscopy - MLF granules were prepared for scanning electron microscopy (SEM) analysis by drying the granules on a silicon wafer and sputter coating them with gold. The granules were analyzed on a Phillips XL30 ESEM FEG using a 5kV accelerating potential. For transmission electron microscopy (TEM) analysis MLF granules were fixed in glutaraldehyde, postfixed in osmic acid, dehydrated and embedded in epoxy resin. 100 nm slices of the sample were imaged and photographed on a JOEL JEM 2000 FX.

MLF samples for atomic force microscopy (AFM) were prepared by drying the granules onto a mica slide. Images were taken with a Multimode IIIa AFM instrument with microfabricated Si cantilever tips (Nanoscience Instruments, Phoenix, AZ). Vibrational noise was dampened using an active isolation system (MOD1-M, Halcyonics, Goettingen, Germany). Typical imaging parameters were (a) tip resonance frequency,

55-65 kHz; (b) amplitude setpoint, 2.0-2.5 V; (c) scan rate, 2.0 Hz. Images were processed offline to remove the background slope using software bundled with the AFM instrument.

Flow Cytometric Analysis - To determine the size distribution and concentration (granules/unit volume), suspensions of MLF granules were diluted 1:100 and 1:1000 with PBS and 200,000 Flow Check High Intensity Green Alignment Beads (Polysciences, Inc., Warrington, PA), 5.726 ± 0.375 μm in diameter, were added to each sample to serve as an internal standard. The samples were excited with an argon laser at 488 nm on a Beckman Coulter (Beckman, Fullerton, CA) EPICS-XL Flow Cytometer with EXPO 32 ADC software for flow cytometric analysis. The samples were analyzed for forward light scatter and autofluorescence by collection of data for 300 sec, which allowed visualization of at least 10,000 beads and at least 95,000 MLF granules.

Total Protein Determination in Melanolipofuscin - Melanolipofuscin granules were pelleted using centrifugation and lyophilized in an evaporative centrifugal concentrator. The granules were weighed using a Mettler UMT2 microbalance (Columbus, OH) to determine their total mass. After weighing the dried granules, the protein in these melanolipofuscin samples was quantified by solubilizing the granules in 1% SDS followed by the BCA Protein Assay (Pierce, Rockford, IL). Three independent measurements were used to calculate the percent protein and standard deviation.

1D Gel Electrophoresis and Mass Spectrometry - Melanlolipofuscin and lipofuscin granules containing 100 μg of protein were pelleted by centrifugation, solubilized in 4X Laemmli buffer (3% SDS, 0.17 M Tris pH 6.8, 35% glycerol, 3.5% 2-mercaptoethanol) and separated on a 10% SDS-PAGE gel (8.3 x 6.4 x 0.1 cm). The gel lanes were sliced into sections and the proteins were digested in-gel as described by Shevchenko et al.[Shevchenko, 1996], injected onto a Jupiter C18 reversed-phase resin capillary column (150 μm ID, made in-house), and eluted using a gradient of 5 to 95% acetonitrile in 0.1% formic acid at a flow rate of 5 μl/min. On-line mass spectrometric analysis was performed on an Applied Biosystems QSTAR Pulsar i (Foster City, CA) using an API (atmospheric pressure ionization) source. Automated tandem mass spectrometry using information-dependent acquisition was run, collecting CID spectra for the three most intense ions from each survey scan excluding peaks chosen in the preceding 2 min. Fragmentation spectra were submitted to the Mascot (Matrix Science) website (www.matrixscience.com) for peptide identification. Proteins in MLF granules from three independent preparations were examined. Each 1D gel lane containing MLF or LF proteins was cut into 24 gel slices for mass spectrometric analysis. Four gel slices (numbers 15, 16, 17, and 19) from two preps of LF granules were selected for analysis to provide a direct comparison of the differences in LF and MLF proteins. Relative quantitation of proteins was estimated using the method of spectral counting [Old, 2005].

Immunoblots - Human retinas were obtained from Dr. Paul Bernstein from the Moran Eye Institute to make a positive control for rhodopsin. A retina was gently triturated in 0.75 M sucrose, 0.68 mM calcium chloride, 20 mM tris and 1 mM DTT pH 7.4 to rupture

the cells. The suspension was poured over 4 thicknesses of cheesecloth to remove debris. The sample was spun at 1475 x g for 20 min and the pellet was resuspended in 1% SDS. Total protein was determined using the BCA assay. An α-rhodopsin antibody (R4, polyclonal antibody, see Takemoto et al.[Takemoto, 1985]) was used at 1:1000 dilution in TBS-T.

Oxidized BSA samples were made by incubating BSA in hypochlorous acid at 37°C for 30 minutes. LF, MLF and BSA samples were derivatized by incubating them in 5% sodium dodecyl sulfate and 10 mM 2,4-dinitrophenylhydrazine(DNPH) in 10% (v/v) trifluoroacetic acid for 30 minutes at room temperature. The solutions were neutralized by adding 2M Tris and Laemmli buffer (3% SDS, 0.17 M Tris pH 6.8, 35% glycerol, 3.5% 2-mercaptoethanol) and loaded directly onto a gel. Anti-DNP antibody from rabbit was purchased from Sigma.

Results

Side by side comparison of the LF and MLF content in RPE from young (21.2 ± 5.9 yr) and old (66.5 ± 5.9 yr) individuals as seen in sucrose gradients is shown in Figure 3-1A. This figure confirms the presence of significant quantities of LF in RPEs from young individuals where very little if any MLF is present. In contrast RPEs from older individuals show significant quantities of MLF. This accumulation pattern is further evident when the optical density of the MLF and LF bands in sucrose density gradients is plotted versus the age of the RPE donor. (Figure 3-1B)

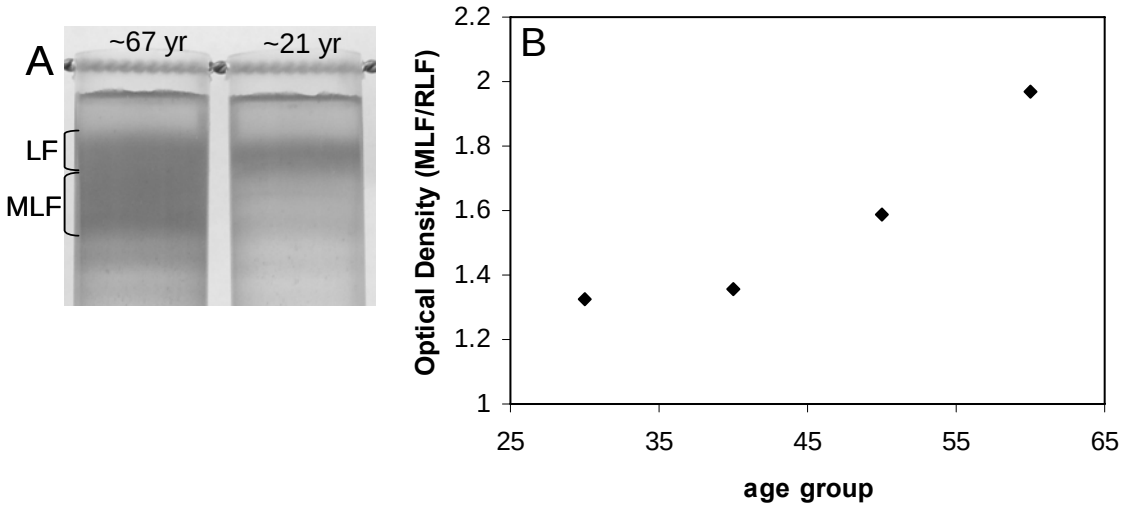

Figure 3-1. Melanolipofuscin (MLF) Accumulation. A) Comparison of MLF granules from RPE of young (21.2 ± 5.9 yrs) and old (66.5 ± 5.9 yrs) human donors. B) Age of RPE donor versus optical density of MLF/LF plotted to show the accumulation of MLF throughout life. LF granules are observed in human RPE from young individuals, whereas significant quantities of MLF do not appear to accumulate for decades afterward.

Analysis of the phototoxicity of MLF revealed that these granules cause a 58% decrease in cell viability in ARPE-19 cells fed with MLF and exposed to blue light for 48 hours. This is compared to an 80% decrease in cell viability in ARPE-19 cells fed with the same number of granules of LF (Figure 3-2). Although this colorimetric assay provides an informative approximation of the phototoxicity of these granules, we are aware that the nature of ARPE-19 cells makes it difficult to precisely determine the phototoxicity of these granules. ARPE-19 cells migrate up the sides of tissue culture plates as they proliferate and phagocytose far fewer granules in this sideways position. These cells depress phototoxicity results because their inability to phagocytose granules inhibits them from undergoing light dependent cell death. Thus, these phototoxicity measurements are overly conservative. However, the relative comparison of LF & MLF phototoxicity is not affected.

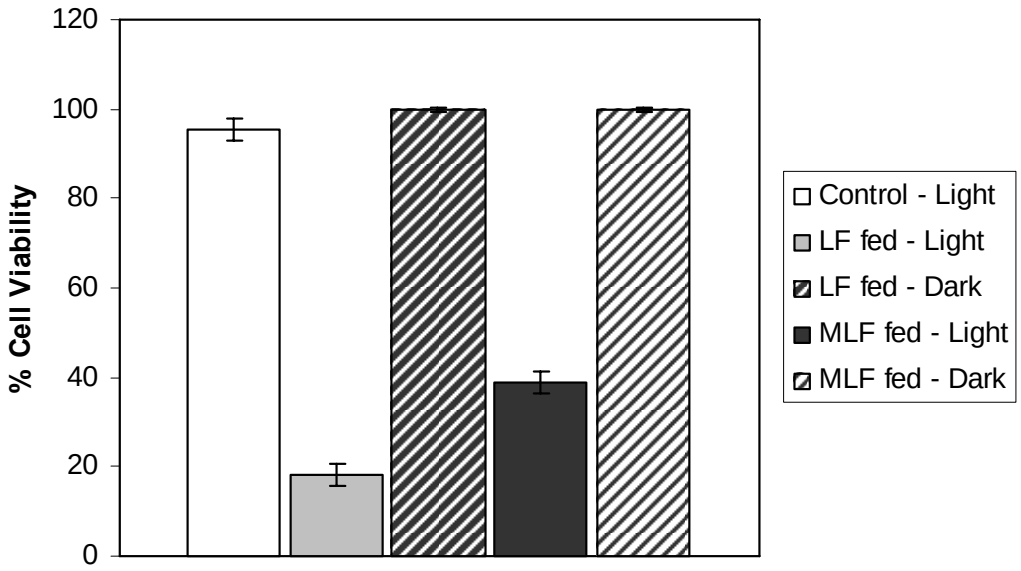

Figure 3-2. Bioactivity of LF & MLF Granules. Isolated LF & MLF granules were fed to ARPE-19 cells. Cells that were not fed LF or MLF were used as controls. Cells were then subjected to blue light irradiation (solid bars), or left in the dark (cross-hatched), for 48 hours. Cell viability was determined using the Sulforhodamine B assay. Values represent mean of at least four independent measurements, error bars represent standard deviation. The phototoxicity of MLF granules in ARPE-19 cells is at least 72% as potent as that of LF granules, showing that MLF granules have the potential for deleterious affects on RPE cells in the retina.

Several physical measurements of MLF granules were made using fluorescence spectroscopy, electron microscopy, atomic force microscopy, and flow cytometry.

Fluorescence of MLF and LF granules is shown in Figure 3-3. Both granules produce similar excitation spectra (data not shown), however, MLF granules have an emission maximum at 554 nm, whereas LF granules have an emission maximum at 578 nm. The similarity between the fluorescence spectra of these two granules is expected because of the A2E fluorophore present in both granules which dominates the spectra [Vollmer-Snarr, 2004]. Apparently, melanin in MLF produces significantly less emission and appears to be negligible in comparison to the fluorescence of A2E (data not shown). The shoulder at ~470nm in the fluorescence spectrum of MLF increased over time when exposed to light eventually becoming the maximum in the spectrum (data not shown).

This change may result from the accumulation of damage on the proteins within MLF granules as a result of light exposure or from photo-isomerization of A2E or other lipids. This trend was also observed with LF (data not shown).

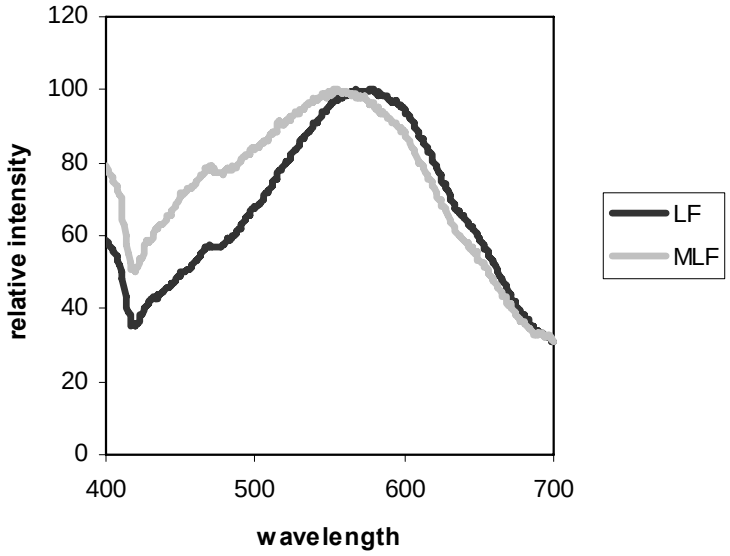

Figure 3-3. Fluorescence Emission Spectra of LF & MLF. Fluorescence emission of LF & MLF monitored with excitation at 364 nm. Both granules produce similar excitation spectra (data not shown), however, MLF granules have an emission maximum at 554 nm, whereas LF granules have an emission maximum at 578 nm.

SEM and AFM analyses of MLF granules (Figure 3-4A-C) show nearly spherical granules with some surface features which suggest these granules are aggregates of smaller substructures. Transmission electron micrographs of MLF (Figure 3-4D) show these granules to contain inclusions of higher density, demonstrating that these granules are complex and not a mixed population of different granules.

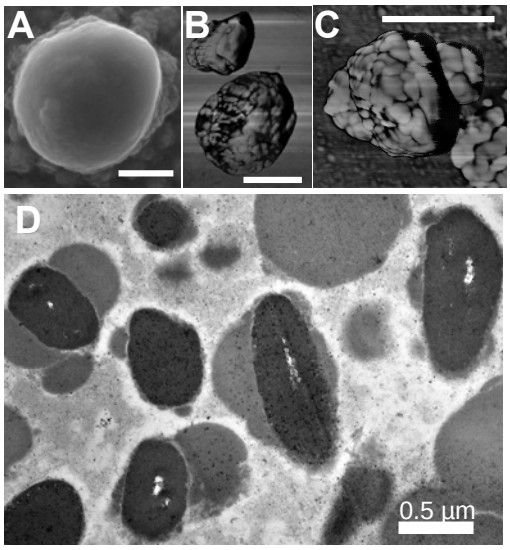

Figure 3-4. Microscopic Structure of MLF. A) Scanning electron micrograph of MLF, showing nearly spherical granules with some surface features. B,C) Atomic force micrographs (phase images) showing MLF granules to be aggregates of ~200 nm and ~50 nm substructures. D) Transmission electron micrograph of MLF, shows these granules to contain inclusions of higher density, demonstrating that these granules are complexes of lipofuscin and melanin. Each bar represents 0.5 um.

Flow cytometric (FC) analysis allowed a quantitative determination of granule size. Forward light scatter in FC instruments is directly proportional to the size of the objects passing through the beam. The MLF granules were found to have a mean diameter of 0.93 µm and a broad standard deviation of 0.60 µm. Flow cytometry also enabled a quantitative determination of the concentration of granules in our suspensions. Having a count of the MLF granules, we were able to determine their average weight, which proved to be 2.2 ± 0.1 pg /granule. When compared to LF, MLF is ~35% larger but weighs ~69% more, again indicating the presence of a more dense substance.

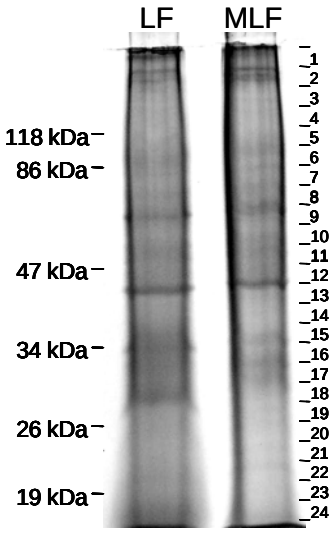

Figure 3-5. Electrophoresis of LF & MLF Proteins. Representative SDS-PAGE lanes of 50 µg of LF and MLF proteins. Mobility of molecular weight markers are indicated to the left. On the right, gel slices taken for subsequent in-gel digestion are shown. The lack of well-focused bands in the gel lane indicates microheterogeneous populations of the proteins, probably resulting from extensive modifications.

To determine the percent protein composing MLF granules, the protein in a known quantity of MLF was solubilized in 1% SDS and quantified by BCA assay. MLF proved to consist of 60.7 ± 6.4% total protein. Compared to LF, MLF contains more protein and therefore less extractable lipids [Warburton, 2005].

Table 3-2. MLF proteome comparison with other organelles. The proteome of MLF was compared to the proteome of several relevant organelles. Organelles are listed in order of decreasing number of proteins in common with MLF.

organelle	total proteins	no. of common	percent	reference
melanolipofuscin	110	–	–	this study
RPE melanosomes	102	23	22.5	Azarian et al.
phagosomes	140	18	12.9	Garin et al.
lipofuscin	36	14	38.9	Warburton et al.
melanocyte melanosomes	68	7	10.3	Basrur et al.

Because of the possibility that the proteins in MLF granules are highly modified exhibiting highly heterogeneous populations and therefore unfocusable on 2D gels, we employed 1D SDS-PAGE coupled with automated LCMSMS to identify the protein constituents of MLF. Figure 3-5 shows representative 1D lanes of LF and MLF proteins and indicates the gel slices removed from the lanes. Proteomic analyses of the proteins in the 1D gel slices identified 110 proteins in MLF granules which are listed in Table 3-1 (found at the end of the results section in this chapter). The proteome of MLF granules was compared to the proteome of other relevant organelles including RPE melanosomes, macrophage phagosomes, retinal LF, and melanocyte melanosomes. As indicated in Table 3-2, 23 proteins were previously identified in mature RPE melanosomes [Azarian, 2006], 18 proteins were previously identified as part of the macrophage phagosome proteome [Garin, 2001], 14 proteins were previously identified in LF granules [Warburton, 2005], and 7 proteins were identified in melanocyte melanosomes [Basrur, 2003].

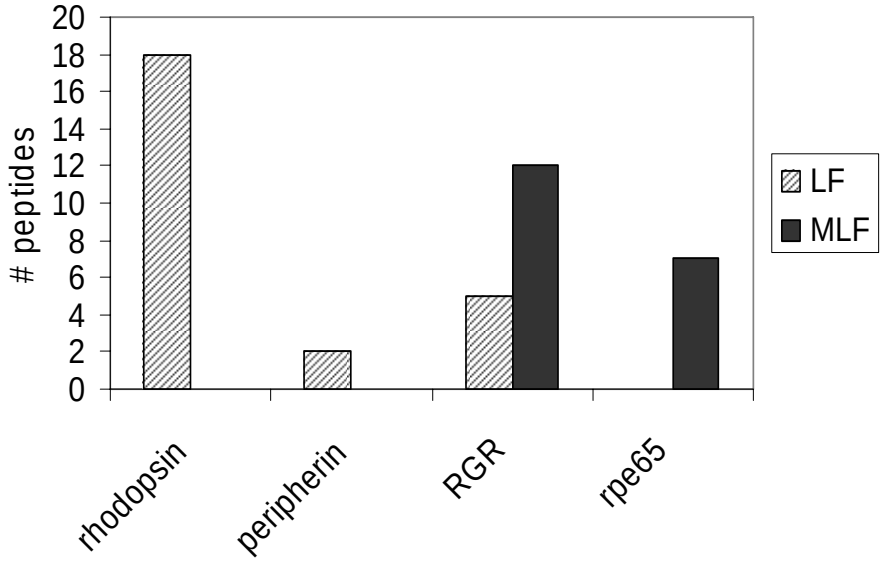

Figure 3-6. Semi-quantitative analysis of photoreceptor- and RPE-specific proteins in LF and MLF granules. Spectral counting was performed on two photoreceptor-specific proteins, rhodopsin and peripherin, and two RPE-specific proteins, RGR and rpe65, in 4 gel slices from LF & MLF 1D gels. Photoreceptor-specific proteins were only identified in LF granules, while RPE-specific proteins were mainly identified in MLF granules. Although RGR was identified in LF granules it appeared to be ~58% less abundant than in MLF granules. This supports the hypothesis that LF granules originate from photoreceptors while MLF granules appear to originate from autophagy of RPE cells.

Four gel slices from MLF and LF 1D gels were analyzed for a direct semi-quantitative comparison of RPE- and photoreceptor-specific proteins in these granules. Spectral counting of two photoreceptor-specific proteins, rhodopsin and peripherin, and two RPE-specific proteins, RGR and rpe65, from these four gel slices is show in Figure 3-6. The two photoreceptor-specific proteins were identified in LF granules but absent from MLF granules while RPE-specific proteins were more abundant in MLF granules. Although RGR was identified in LF granules, it appears to be ~58% less abundant than in MLF granules. A more comprehensive study of the proteins in LF granules was previously published by Warburton et al.[Warburton, 2005].

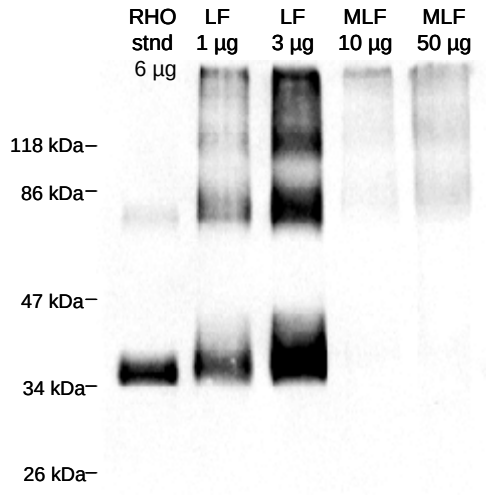

Figure 3-7. Rhodopsin Immunoblot. Immunoblot following SDS-PAGE of 1 and 3 µg of total LF protein and 10 and 50 µg of total MLF protein. Shown for comparison is 6 µg of protein from photoreceptor cell membranes enriched from human retina. Rhodopsin runs on SDS-PAGE as a mixture of the monomer (~30 kDa), dimer (~60 kDa), and trimer (~90 kDa). Although rhodopsin is seen to be present in abundance in LF granules, no significant quantity of rhodopsin is detected in MLF granules.

Rhodopsin was previously shown to be abundant in LF granules [Warburton, 2005], however; this protein was only identified in a single gel slice from 1 of the 3 MLF preparations analyzed. In order to more quantitatively examine this apparent lack of rhodopsin in MLF granules, we performed an immunoblot of MLF proteins in which we used an α-RHO antibody to detect rhodopsin. Figure 3-7 shows that indeed no significant amount of rhodopsin was detected in MLF granules.

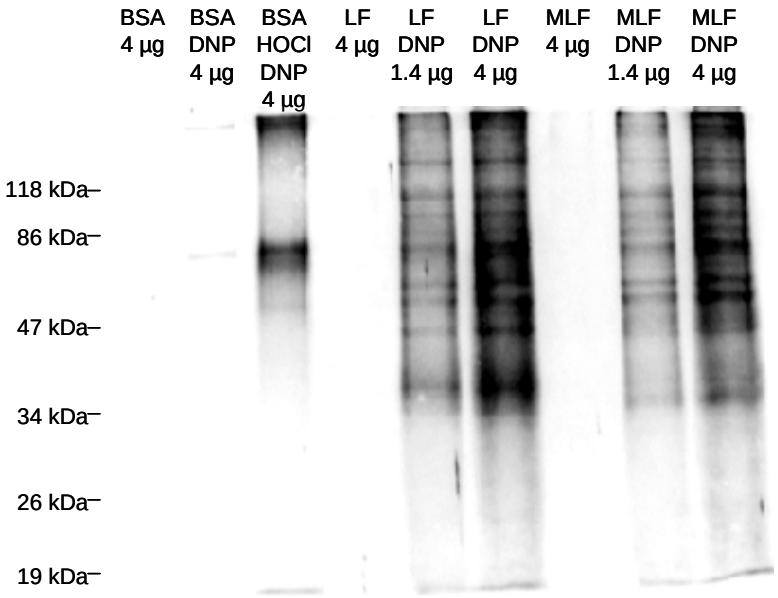

Figure 3-8. DNP Immunoblot. LF and MLF proteins, 1.4 and 4 µg, that had been derivatized with dinitrophenylhydrazine (DNPH) or not (control) were run on SDS-PAGE, transferred to nitrocellulose, and probed with an α-DNP antibody to show the derivatized protein carbonyls, a common product of protein oxidative damage. Shown for comparison and to demonstrate specificity are lanes of BSA, BSA treated with DNPH, and BSA oxidized with hypochlorite then treated with DNPH. Oxidative damage on proteins in LF and MLF granules is both extensive and comparable, though not identical.

Because of the extensive modifications on proteins in LF granules that have been previously reported [Warburton, 200], we used immunoblot techniques to detect oxidative modifications on proteins in MLF granules. Dinitrophenylhydrazine (DNPH) was used to derivatize protein carbonyls, a common product of protein oxidation, and was detected using an α-DNP antibody. Figure 3-8 shows that the degree of oxidative modifications on proteins in MLF and LF granules is both extensive and comparable, though not identical.

Table 3-1. Proteins identified in melanolipofuscin granules. MLF proteins were fractionated on a 1D gel. The gel lanes were sliced into sections and the proteins were digested and analyzed using automated LC-MSMS and then identified using Mascot. Gel number refers to three separate preparations that were analyzed.

Gel	Protein	Gel Slice	Genbank Ascession #	Synonyms	Subcellular location	Tissue Specificity
1,2	acid ceramidase[III]	13	3860240	putative heart protein	Lysosomal.	Widely expressed
1,2,3	actin, beta[III]	11,12,13,14,15,16	14250401			
2	alpha actinin 4[II]	6	12025678	F-actin cross linking protein	Nuclear and cytoplasmic	Widely expressed
1	alpha tubulin, ubiquitous	1,2,4,5,6,7,9,10,13,15,17,18,19,21	5174477			
3	alpha tubulin 2	9,10,11,24	37492			
3	alpha tubulin 4[I]	10	13376539			
1,2,3	alpha tubulin 6[III]	1,5,10,11,12,13,14,18,20,21,23,24	13436317			
3	Ankyrin 1[IV]	3,4	105337		Cytoplasmic surface of erythrocytic plasma membrane.	Erythrocyte
1,2,3	Annexin A2[I]	12,13,14,15	18645167			
2	Annexin A5[III]	15,16	12655149			
2,3	aspartate aminotransferase	14	4504069	transaminase A, Glutamate oxaloacetate transaminase-2	Mitochond-rial matrix.	
3	ATP Synthase subunit g	24	3659901			
2,3	ATP Synthase, H+ transporting, mitochondrial F0 complex, subunit 6	22	29690552			
1,2,3	ATP Synthase, H+ transporting, mitochondrial F0 complex, subunit b	18	13543618		Mitochond-rial.	
2,3	ATP Synthase, H+ transporting, mitochondrial F0 complex, subunit d	22	5453559			
1,2,3	ATP Synthase, H+ transporting, mitochondrial F0 complex, subunit f	23	13277542			
1,2,3	ATP Synthase,	2,9,10	30583257			

	H+ transporting, mitochondrial F1 complex, alpha subunit					
1,2,3	ATP Synthase, H+ transporting, mitochondrial F1 complex, beta subunit[II,III]	10	32189394			Widely expressed
2,3	ATP Synthase, H+ transporting, mitochondrial F1 complex, gamma subunit	16	16877071		Mitochond-rial.	
1,2,3	ATP Synthase, H+ transporting, mitochondrial F1 complex, subunit o	20	54696534		Mitochond-rial matrix.	
1,2,3	beta tubulin[II,III]	10,11,14,15,23	20809886			Ubiquitously expressed
3	beta tubulin polypeptide	10,11,12,13,21	12804971			
1,2,3	calnexin[I,II,III]	6	2134858	MHC I antigen binding protein p88	Type I membrane protein. Endoplas-mic reticulum.	
2,3	Cathepsin D[I,II,III]	15,16,17	30582659		Lysosomal.	
1,2	cell death-regulatory protein GRIM19	23	21361822	NADH-ubiquinone oxidoreductase B16.6 subunit, Gene associated with retinoic-interferon-induced mortality 19 protein	Mitochond-rial inner membrane	Widely expressed
2,3	Cerebroside sulfate activator protein	23	337760			
2,3	Ceroid-lipofuscinosis[I,II]	12,13	15928808	tripeptidyl-peptidase I precursor, lysosomal pepstatin insensitive protease	Lysosomal.	All tissue
1,2,3	chromosome 10 open reading frame 58	19,21	37183236	SFLQ611		
3	chromosome 10 open reading	24	37590612			

	frame 70					
3	chromosome 20 open reading frame 3	12	37183270		Type II membrane protein	
3	chromosome 8 open reading frame 2	13	37181322		Membrane-associated	Ubiquitous
2,3	crystallin, alpha B[II]	22	30582379	heat shock protein B5		Lens as well as other tissues.
2,3	cytochrome c oxidase subunit II[I]	22	14016		Integral membrane protein. Mitochond-rial inner membrane.	
2	cytochrome c oxidase subunit IV	23	54696512		Mitochondri al inner membrane.	Ubiquitous
1	cytokeratin 9[IV]	1	435476			Terminal differentiated epidermis of palms and soles
1	Epidermal cytokeratin 2[IV]	1	181402			Epidermal tissue, squamous metaplasias and carcinomas
2	erythryocyte membrane protein band 4.2[IV]	7,8	4557559		Membrane-associated and cytoplasmic	Erythrocyte
2	Gamma-glutamyltransfer-ase-like activity 1	10,11	4758432		Type II membrane protein	
2	glucose regulated protein[III]	7	6900104	dnaK-type molecular chaperone, BiP protein, hsp A5	Endoplas-mic reticulum lumen.	
1	gp25L2	19	996057		Type I membrane protein. Endoplas-mic reticulum	
2,3	Guanine nucleotide binding protein	16	386750	G(o) alpha subunit I		
1	Guanine-nucleotide binding protein, alpha transducin	13	22027522	G protein		
1,2	heat shock 70 kD protein 9B[III]	8,9	21040386	mortalin-2		

1	heat shock protein 27	18,19	662841	estrogen-regulated protein, stress responsive protein	Mitotic spindles in mitotic cells; nucleus during heat shock.	
2	heat shock protein 60[III]	10	306890	chaperonin 60, mitochondrial matrix protein	Mitochond-rial matrix.	
2,3	heat shock protein gp96	6	15010550	tumor rejection antigen, 94kD glucose regulated protein	Endoplas-mic reticulum lumen.	
1,2,3	hemoglobin beta chain[IV]	23	4378804			Red blood cells
3	hemoglobin, alpha 2[IV]	24	22671717			Red blood cells
3	hemoglobin, beta, mutant[IV]	24	4837723			
2	hydroxyacyl dehydrogenase, subunit A	8	20127408	Long chain 3-hydroxyacyl-CoA dehydrogenase	Mitochond-rial.	
2,3	hydroxyacyl dehydrogenase, subunit B	12	4504327			
1,2,3	hypothetical protein MGC5508	20,21	13129092			
1,2,3	keratin 1[IV]	11	17318569			
2,3	keratin 10[IV]	16	71528			
2	keratin 2a[IV]	6	47132620			
1	keratin 6B[IV]	1	21961227			Epithelial in oral mucosa, esophagus, papillae of tongue & hair follicle
2,3	Microsomal epoxide hydrolase 1[II]	12	537526		Membrane-bound on microsomes.	Liver
2	microsomal glutathione S-transferase 3	23	34732734		Integral membrane protein. Microsomal	Widely expressed
2	motor protein	6,7	516764	inner memberane protein, mitochondrial; mitofilin,	Mitochond-rial inner membrane.	
2	myelin protein zero[I]	15,19	469517			
2,3	myosin heavy chain 11[II]	2	13124879	KIAA0866		
2,3	Myosin heavy chain nonmuscle	2,4	41406064			

	10[II]					
2,3	Myosin heavy chain nonmuscle form A[III]	2	625305	MYH9		
3	myosin light chain 3	24	188590			
1,2,3	Na+/K+ ATPase alpha chain[I,II]	4,5,6	88214		Integral membrane protein.	Skin and kidney
2	NAD(P) transhydrogenase	5	1000704		Outside the mitochond-rial inner membrane on the matrix side	
3	NADH cytochrome b5 reductase	14,15	3413789	Diaphorase 1	Membrane bound on ER and mitochond-rial outer membrane.	
2	NADH dehydrogenase (ubiquinone) 1 alpha subcomplex 10	14	4758768			
2	NADH dehydrogenase (ubiquinone) 1 alpha subcomplex 9	15,16	6681764			
1,2,3	NADH dehydrogenase (ubiquinone) flavoprotein 2	19	10835025			
1,2	NADH dehydrogenase (ubiquinone), Fe-S protein 1[I]	6,7,8	21411235	NADH ubiquinone oxidoreductase	Matrix and cytoplasmic side of mitochond-rial inner membrane.	
2,3	NADH dehydrogenase (ubiquinone), Fe-S protein 2	12,13	55665941			
1,2,3	NADH dehydrogenase (ubiquinone), Fe-S protein 3	17,18	4758788	NADH ubiquinone reductase		
1,2	NADH dehydrogenase (ubiquinone), Fe-S protein 8	19,20,21	4505371	NADH-coenzyme Q reductase		
2	NADH dehydrogenase	7,8	38079		Matrix and cytoplasmic	

	precursor				side of mitochond-rial inner membrane.	
3	NADH ubiquinone oxidoreductase	4	14198176	NDUFV1 protein	Matrix side of the mitochond-rial inner membrane.	
2,3	Peptidylprolyl isomerase B	22	68399	cyclophilin B		
3	peroxiredoxin 1	20	55959887		Cytoplasmic .	
1	peroxiredoxin 2[III]	21	438069	thioredoxin peroxidase, thio-specific antioxidant protein	Cytoplasmic .	
2	peroxiredoxin 3[II]	19	54696876		Mitochond-rial.	
2,3	Predicted: similar to RIKEN cDNA 4732495G21 gene	12,15,16	29736622			
3	prenylcysteine oxidase 1[I]	10	33620751	KIAA0908, PCL1	Lysosomal.	Ubiquitous
3	progesterone membrane binding protein	18	5453916			
1,2,3	progesterone receptor membrane component 1	19	5729875		Microsomal; membrane-bound	Widely expressed
1,2	prohibitinI,[III]	17	46360168			
2,3	protein disulfide isomerase[III]	10	1085373	glucose regulated protein 58 kD, ER 60 precursor	Endoplas-mic reticulum lumen	
2,3	RAB11B[II,III]	21	4758986	RAS oncogene family		
2,3	RAP1B[III]	22	50418419	RAS oncogene family		
2,3	retinal G protein coupled receptor	13,15,17	21361329	peropsin, RGR		Retinal pigment epithelium
1,2,3	retinal pigment epithelium specific protein[I,II]	2,6,7,8,9,10,11 ,12,13,15,17,2 4	4506591	RPE65		Retinal pigment epithelium
2,3	retinol binding protein 3	4	55666366			
2	retinol dehydrogenase 11	15	12652725	androgen-regulated short-chain dehydrogenase/ reductase 1	Type II membrane protein. Endoplas-mic	

					reticulum.	
1,2,3	retinol dehydrogenase 5 (11-cis and 9-cis)[I,II]	15,16	20271410	11-cis retinol dehydrogenase	Membrane-associated.	Retinal pigment epithelium
3	ribophorin II	11	12803531	KIAA0115, dolichyl-diphosphooligosaccharide-protein glycosyltransferase 48kDa subunit	Type I membrane protein. Endoplasmic reticulum.	
3	ribophorin II precursor	9	88567	Dolichyl-diphosphooligosaccharide-protein glycosyltransferase 63 kDa subunit	Type I membrane protein. Endoplasmic reticulum.	Expressed in all tissues tested
2	serum albumin[IV]	9	28592		Secreted.	Plasma
2,3	solute carrier family 2, member 1[II]	11	5730051	Glucose transporter type 1	Integral membrane protein; primarily at the cell surface	
2	solute carrier family 25, member 1	17	21389315			
2	solute carrier family 25, member 12	9	21361103		Integral membrane protein. Mitochondrial inner membrane.	Widely expressed
2	solute carrier family 25, member 13	9	7657581		Integral membrane protein. Mitochondrial inner membrane.	Widely expressed
2	solute carrier family 25, member 24	12,13	33598954			
2	solute carrier family 25, member 3	16	6031192			
2	solute carrier family 25, member 3 isoform b	17	47132595			
1	solute carrier family 25, member 4	15,16,17	55749577	ADP/ADT	Integral membrane protein. Mitochondrial inner	

					membrane.	
2,3	solute carrier family 25, member 4	15,17,18	55749577			
2	solute carrier family 25, member 5[II]	10,14,18	4502099	ADP/ATP carrier protein		
3	solute carrier family 25, member 6	17	339723	ADP.ATP translocase		
2,3	solute carrier family 25, member A6	10,16	27764863			
1,2,3	solute carrier family 4, anion exchanger, member 1	2,4,18	4507021			
1,2,3	spectrin, alpha[II]	1,2,4	4507191			
1,2,3	spectrin, beta[II]	1,2	4507195			
1	succinate dehydrogenase comlex, subunit B, iron sulfur	17	9257242	succinate-ubiquinone oxidoreductase iron sulfur subunit	Mitochond-rial inner membrane.	
3	succinate dehydrogenase complex, subunit A[II]	9	4759080		Mitochond-rial inner membrane.	
1,2,3	ubiquinol-cyctochrome c reductase, rieske iron-sulfur protein	19,20	5042402		Mitochond-rial inner membrane.	
2	ubiquinol-cytochrome-c reductase	18	87242			
2	ubiquinol-cytochrome-c reductase core protein [III]	12,13	46593007		Mitochond-rial inner membrane.	
3	ubiquinol-cytochrome-c reductase core protein [II]	12	12653427	UQCRC2	Mitochond-rial inner membrane; matrix side.	
1,2,3	vimentin[I,II,III]	13	340219	beta tubulin, polypeptide		Highly expressed in fibroblasts, some expression in T & B lymphocytes
1,2,3	voltage dependent anion channel 1[III]	15,16,18	4507879	porin	Outer membrane of mitochond-	Heart, liver and skeletal muscle

					ria and plasma membrane.	
1,2,3	voltage dependent anion channel 2[II]	15	55664663	porin		
1,2,3	voltage dependent anion channel 3	16	25188179		Outer mitochond-rial membrane.	Widely expressed

[I] These proteins were previously identified as components of lipofuscin granules.
[II] These proteins were previously identified as part of the melanosome proteome.
[III] These proteins were previously identified as part of the macrophage phagosome proteome.
[IV] These proteins are preparation contaminants.

Discussion

MLF accumulation

Sucrose density gradients of human RPE from different decades of life illustrated that MLF is virtually non-existent in the RPE of younger individuals even though LF granules appear to be abundant in these RPE and has been detected in RPE as young as 18 years of age (data not shown). Consistent with Feeney-Burns' results [Feeney-Burns, 1984], MLF does not begin to accumulate significantly until midlife. This accumulation of MLF later in life is consistent with the onset of AMD which affects 2% of individuals over 50 and 30% of individuals over 75 [Group, 1993]. This correlation would suggest that MLF may play a more significant role in the etiology of AMD.

Bioactivity

Of significant interest is the fact the MLF is biologically active, showing a light-dependent decrease in cell viability in ARPE-19 cells fed MLF and placed in blue light for 48 hours. To our knowledge this is the first report of the phototoxicity of MLF. The phototoxicity of MLF granules in ARPE-19 cells is at least 72% as potent as that of LF

granules. These data show that MLF granules have the potential for deleterious affects on RPE cells in the retina.

Protein composition and modifications

The physical characteristics of MLF granules support the description of MLF as a complex granule with characteristics of both melanosomes and LF. The most compelling characteristic of MLF is the protein complement identified in the granules. Of the 110 proteins identified as components of MLF, 23 were previously identified in mature RPE melanosomes [Azarian, 2006], 18 were previously identified as part of the macrophage phagosome proteome [Garin, 2001], 14 were previously identified in LF granules [Warburton, 2005], and 7 were identified in melanocyte melanosomes [Basrur, 2003]. As expected, MLF granules appear to be considerably more similar to RPE melanosomes than to melanocyte melanosomes. While LF and MLF granules contain a significant number of similar proteins, these proteins appear to be related to the lysosomal processes which these granules both participate in. However, the lack of similar cell specific proteins would suggest different origins of the material being degraded.

Of interest is the presence of RPE65, which we previously identified in LF granules where it appeared to be far less abundant than we observe in MLF granules. RPE65 was previously identified in 3 of 15 gel slices from a 1D lane of LF proteins and in 12 of 24 gel slices from a 1D lane of MLF proteins. RPE65 plays a key role in the isomerization of retinol as part of the visual cycle in the RPE and is therefore crucial to proper visual acuity. In contrast to RPE65, rhodopsin – which is abundant in LF – is practically absent from MLF.

Of significant interest is the finding that MLF, in contrast to LF, does not contain photoreceptor-specific proteins, suggesting that MLF does not originate from the phagocytosis of photoreceptor outer segments. Instead, the presence of RPE- and melanosome-specific proteins would suggest that MLF accumulates as a result of the melanosomal autophagocytosis of RPE cells. Our results appear to support neither of the two previously proposed hypotheses for the origin of MLF (see introduction) and instead suggest a new hypothesis for its origin. This new hypothesis for the formation of MLF granules is also supported by recent evidence that melanosomes function as specialized lysosomes. Evidence for this specialized function includes the related biogenesis of melanosomes and lysosomes [Orlow, 1995; Raposo, 2002], the observed fusion between phagosomes and melanosomes [Schraermeyer, 1999], and the presence of lysosomal enzymes in melanosomes [Azarian, 2006].

The proteins in MLF granules were shown to be extensively modified by oxidative damage. The degree of oxidative damage is comparable to that found on LF proteins. The prevalence of oxidative damage on these proteins may render them undegradable by the cell and therefore lead to their accumulation in MLF granules.

Collectively these data provide significant insight into understanding the formation and toxicity of retinal MLF and suggest a new theory for its formation as well as support its role in the etiology of retinal diseases. Our findings suggest that MLF might result from the accumulation of undegradable material—perhaps undegradable due to oxidative damage—in the autophagocytic melanosomes of RPE cells. Furthermore, MLF granules might pose serious risk of photosensitization of these cells allowing blue

light to produce cell death by liberation of reactive oxygen species, perhaps contributing to AMD.

CHAPTER 4

A NOVEL METHOD FOR THE DETECTION AND ENRICHMENT OF OXIDIZED PROTEINS

Summary

Protein oxidation has been implicated in the development of various pathologies including ischemia/reperfusion, aging, cataract formation, etc. Although protein oxidation has been associated with numerous human diseases, a definitive casual role of protein oxidation in many diseases is still lacking. Because of its wide applicability to disease states, protein oxidation has become the subject of extensive research. However, because of the high heterogeneity and low stoichiometry of these post translational modifications, studying protein oxidation has been a formidable challenge to researchers. One major problem that impedes research of oxidized proteins involves the difficulty of isolating and identifying the oxidized proteins and their modified peptides. It therefore becomes requisite to develop more efficient techniques for the analysis of oxidatively damaged proteins. The development of new methods for the analysis of protein oxidation may help establish definitive ties between certain pathologies and oxidative modifications. To this end we have developed a novel method for the isolation and identification of oxidized proteins using an Oxidized Protein Affinity Tag (OPAT). OPAT employs a hydrazine moiety to derivatize oxidized proteins, thereby acting as an identifier of oxidative damage. In addition, OPAT has been conjugated to biotin, facilitating isolation of oxidized proteins through a biotin/avidin interaction. We herein report a comparison of 2,4-dinitrophenylhydrazine (DNPH) and OPAT in the detection of

protein oxidation as well as demonstrate OPAT's ability to affinity purify oxidized proteins from a mixture as complex as a cell lysate.

Introduction

Oxidative damage to proteins can lead to aggregation, denaturation and degradation of the protein. Such damage can result in loss of protein function, disruption of cell signaling, and eventual cell death. For these and additional reasons, protein oxidation has been implicated in the development of various pathologies including ischemia/reperfusion, aging, cataract formation, etc. Although protein oxidation has been associated with numerous human diseases, a definitive casual role of protein oxidation in many diseases is still lacking. This disparity between protein oxidation and pathology might only be resolved when new methods become available for the analysis of modified proteins. Protein oxidation research is a formidable challenge to researchers because of the low stoichiometry of this modification and the high heterogeneity of the resulting protein population. One specific impediment in analysis of oxidation research is the inability to isolate and identify the oxidized proteins and their modified peptides. It therefore becomes requisite to develop more efficient techniques for the analysis of oxidatively damaged proteins.

Currently the primary method used to study protein oxidation involves the use of 2,4-dinitrophenylhydrazine (DNPH).[Shacter, 2000] DNPH derivatizes non-backbone carbonyl groups on protein residues, a common form of oxidative damage. DNP-derivatized peptides can then be detected spectrophotometrically or with anti-DNP

antibodies. Although DNPH has been useful in the analysis of protein oxidation, it is only an identifier of protein oxidation.

To further oxidation research we have developed a novel method for the isolation and identification of oxidized proteins using an Oxidized Protein Affinity Tag (OPAT). Similarly to DNPH, OPAT employs a hydrazine moiety to derivatize oxidized proteins, thereby acting as an identifier of oxidative damage. However, unlike DNPH, OPAT has been conjugated to biotin, facilitating isolation of oxidized proteins through a biotin/avidin interaction.

We herein report a comparison of DNPH and OPAT in the detection of protein oxidation as well as demonstrate OPAT's ability to affinity purify oxidized proteins from a mixture as complex as a cell lysate.

Materials and Methods

OPAT Synthesis - The reagent that we use as our oxidized protein affinity tag (OPAT) is 4-(biotinamido) phenylacetylhydrazide (BPH), the synthesis of which was previously described by Shinohara et al.[Shinohara, 1996] The synthesis of BPH was performed by David Harris and is outlined in Figure 4-1. Briefly, p-aminophenyl-acetic acid (compound 1) was esterified to yield 4-aminophenylacetic acid methyl ester hydrochloride (compound 2). Biotin was coupled with compound 2 to yield 4-(biotinamido)phenyl-acetic acid methyl ester (compound 3). Hydrazinolysis of compound 3 yielded 4-(biotinamido)phenylacetylhydrazide (BPH). BPH was solubilized by sonicating in 70% 2N HCl and 30% dimethylsulfoxide for use in derivatization procedures. BPH was stored in the dark at 4°C because of its light sensitivity.

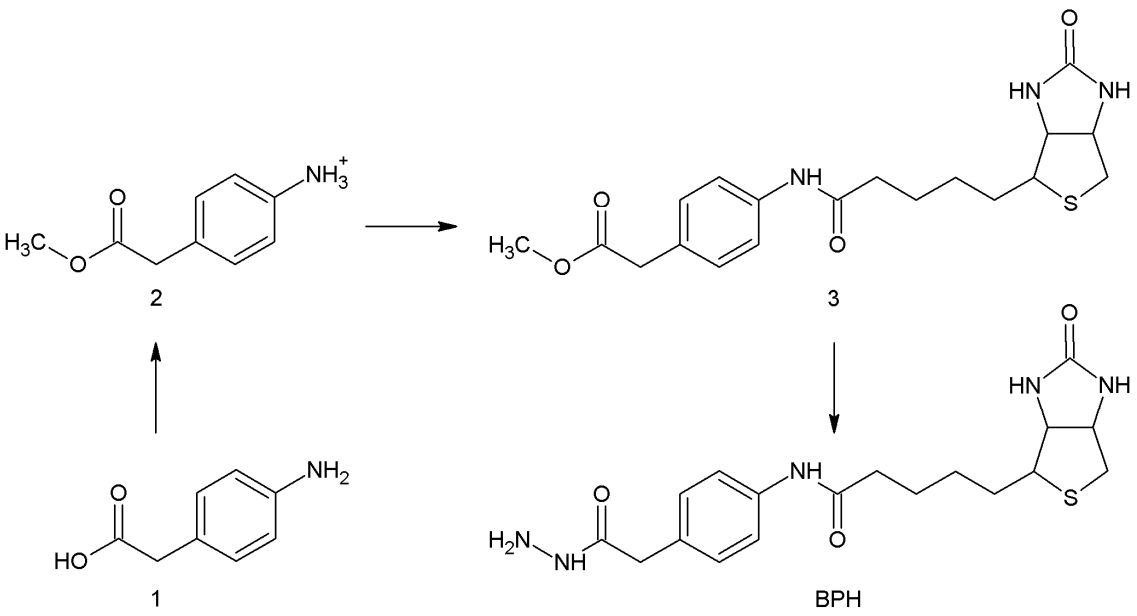

Figure 4-1. Synthesis of 4-(biotinamido)phenylacetylhydrazide (BPH). P-aminophenyl-acetic acid (compound 1) was esterified to yield 4-aminophenylacetic acid methyl ester hydrochloride (compound 2). Biotin was coupled with compound 2 to yield 4-(biotinamido)phenyl-acetic acid methyl ester (compound 3). Hydrazinolysis of compound 3 yielded 4-(biotinamido)phenylacetylhydrazide (BPH). This figure was recreated from Shinohara 1996.

Oxidative Damage to Proteins and Derivatization with OPAT and DNPH - Oxidative damage to ovalbumin and bovine serum albumin (BSA) was accomplished by incubating the protein for 30 minutes at 37°C in the following concentrations of sodium hypochlorite; 1, 3, 10, 30, 100, 300, 1000 mM. The proteins were then derivatized by incubating in either 3 mM 2,4-dinitrophenylhydrazine(DNPH) or 3 mM OPAT for 1 hour at room temperature. The proteins were precipitated by adding 20% (v/v) trifluoroacetic acid, and the pellets were resuspended in Laemmli buffer (3% SDS, 0.17 M Tris pH 6.8, 35% glycerol, 3.5% 2-mercaptoethanol) and 2M Tris (to neutralize the pH) and loaded onto a 10% SDS-PAGE gel (8.3 x 6.4 x 0.1 cm).

Immunoblots - Proteins were transferred to nitrocellulose blots and stained for total protein by incubating in 0.1% fast green in 10% acetic acid and 30% ethanol and destained in 10% acetic acid and 30% ethanol. The blots were then washed with TBS-T blocked with 5 mg/mL BSA and incubated in either 1:1,000 dilution of α-DNP (Sigma, St. Louis) for 3 hours and then a 1:10,000 dilution of goat anti-rabbit antibody, or a 1:1000 dilution of streptavidin-horse radish peroxidase (HRP) conjugate (Calbiochem, Darmstadt) in TBS-T for 1 hour.

Densitometry of the lanes was determined using ImageMaster 2D Platinum software (GE Healthcare, Piscataway, NJ), the background signal (from the zero HOCl added reaction) was subtracted, and the signal was normalized to the maximum signal observed. The data were plotted and fit to the equation $y=ax/(b+x)$, where a=maximum signal and b is defined as the [HOCl] yielding half-maximal binding, using Kaleidograph software (Synergy Software, Reading, PA). The data plotted represent the mean and mean standard error of three independent measurements.

Dynabead Protocol - Ovalbumin was oxidized by incubating in 30 mM sodium hypochlorite, acetone precipitated and resuspended in 3% SDS. HEK 293 cell lysate (100μg) was added to the ovalbumin and the sample was derivatized by incubating in 3 mM OPAT for 1 hour at room temperature. Two control samples, used to detect non-specific binding, contained 1) 100 μg of HEK 293 cell lysate and 3 mM OPAT without oxidized ovalbumin, and 2) oxidized ovalbumin and 100 μg HEK 293 cell lysate without OPAT. After derivitization the samples were acetone precipitated and resuspended in 8M urea. Once the proteins were solubilized the 8M urea was diluted to 2M urea. M-

280 streptavidin beads (Dynal Biotechn, Oslo, Norway) were washed 3 times with 0.01% tween-20 in PBS and then added to the samples which were placed on a rocker and incubated with the dynabeads for 30 minutes at room temperature. The samples were then washed 3 times with 0.01% tween-20 in PBS with 10 minute incubations on a rocker between each wash. After the final wash, the enriched oxidized proteins bound to the dynabeads were resuspended in 100 mM ammonium bicarbonate and then incubated first in 4mM dithiothreitol at 60°C for 15 min and next in 10mM iodoacetamide at room temperature for 15 min. The beads were then washed with 100 mM ammonium bicarbonate and incubated in 2M urea, 25mM ammonium bicarbonate and 10% w/w trypsin overnight at 37°C.

Mass Spectrometry - Peptides were injected onto a Jupiter C18 reversed-phase resin capillary column (150 μm ID, made in-house), and eluted using a gradient of 5 to 95% acetonitrile in 0.1% formic acid at a flow rate of 5 μl/min using a LC Packing Ultimate pump system. On-line mass spectrometric analysis was performed on an Applied Biosystems QSTAR Pulsar i (Foster City, CA) using an API (atmospheric pressure ionization) source. Automated tandem mass spectrometry using information-dependent acquisition was run, collecting CID spectra for the three most intense ions from each survey scan excluding peaks chosen in the preceding 2 min. Fragmentation spectra were submitted to the Mascot (Matrix Science) website (www.matrixscience.com) for peptide identification.

The number of peptides identified from each protein was used for spectral counting data. Spectral counting has been shown to be an effective method to relatively

quantify protein abundance in a sample. [Old, 2005] The method is based on the assumption that the more abundant a protein is in a complex mixture, the more frequently its proteolytic peptides will be identified. It is therefore an indirect way to infer protein abundance.

Results

We have developed a novel method for the isolation and identification of oxidized proteins using BHP (shown in Figure 4-2) as an Oxidized Protein Affinity Tag (OPAT). OPAT employs a hydrazine moiety to derivatize oxidized proteins, thereby acting as an identifier of oxidative damage. OPAT has also been conjugated to biotin, facilitating isolation of oxidized proteins through a biotin/avidin interaction.

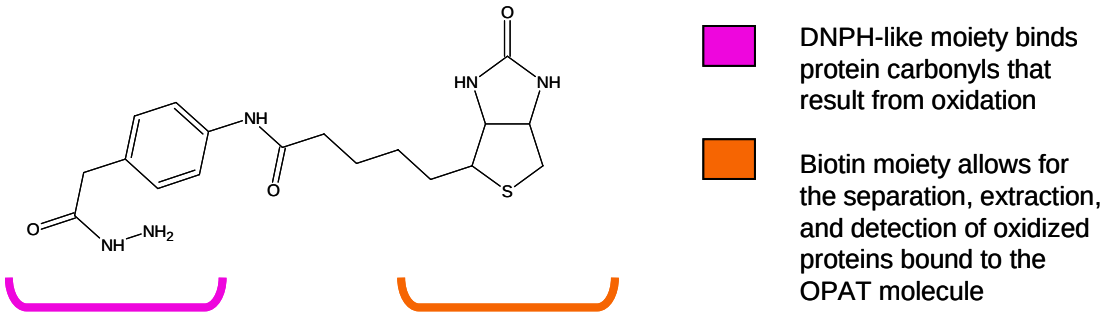

Figure 4-2. 4-(biotinamido) phenylacetylhydrazide (BHP) as an Oxidized Protein Affinity Tag (OPAT). Our OPAT molecule has two functional ends; 1) a hydrazine moiety which derivatizes oxidized proteins, thereby acting as an identifier of oxidative damage, and 2) a biotin moiety which facilitates isolation of oxidized proteins through a biotin/avidin interaction.

Qualitative comparison of ovalbumin derivatized with DNPH and OPAT (Figure 4-3) indicates that these two reagents are comparable in detecting oxidized proteins. In each blot the left lane is protein alone, the middle lane is protein with derivatizing reagent, and the right lane is protein oxidized with sodium hypochlorite with derivatizing

reagent added. There is some signal in the unoxidized protein lanes, derivatized with OPAT or DNPH, indicating an endogenous level of oxidative damage to these proteins. The lack of signal in the protein only lanes shows the high specificity of the detection.

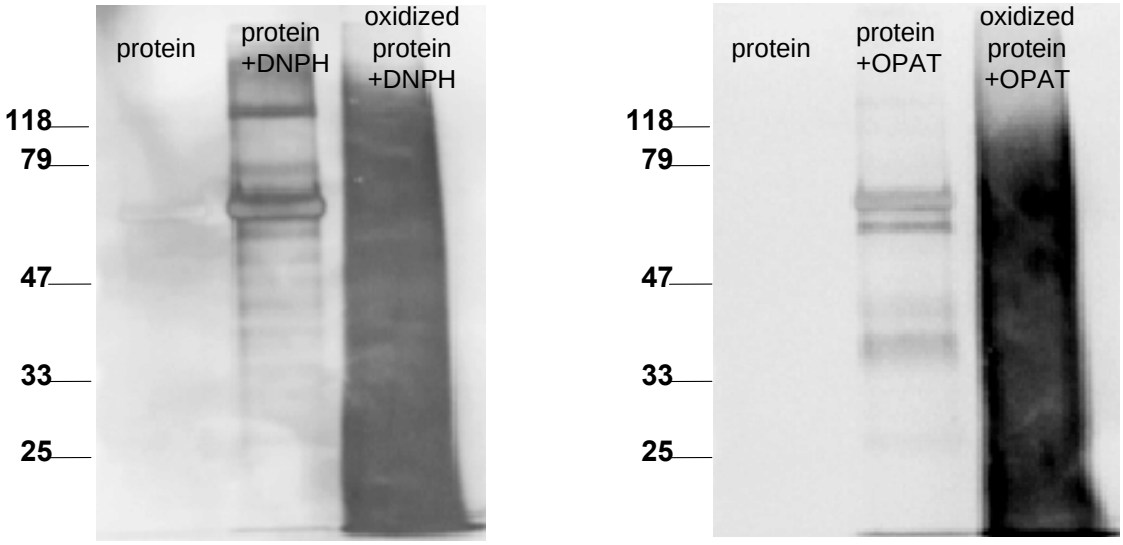

Figure 4-3. Qualitative comparison of derivatization with DNPH and OPAT. In each blot the left lane is bovine serum albumin (BSA) alone, the middle lane is BSA with derivatizing reagent, and the right lane is BSA oxidized with 1mM HOCl with derivatizing reagent added. There is some signal in the unoxidized protein lanes, derivatized with OPAT or DNPH, indicating an endogenous level of oxidative damage to these proteins. The lack of signal in the protein only lanes shows the high specificity of the detection.

The amount of oxidation detected by OPAT and DNPH, when various concentrations of HOCl were used to oxidize ovalbumin, was quantified by densitometry of the immunoblot lanes. These values were plotted and fit to an equation for a saturating process, shown in Figure 4-4. This revealed that the concentration of sodium hypochlorite at which half the maximal oxidation was detected was 93 ± 31 mM for DNPH and 33 ± 9.9 mM for OPAT. This indicates that OPAT is at least as efficient as DNPH at derivatizing oxidized protein.

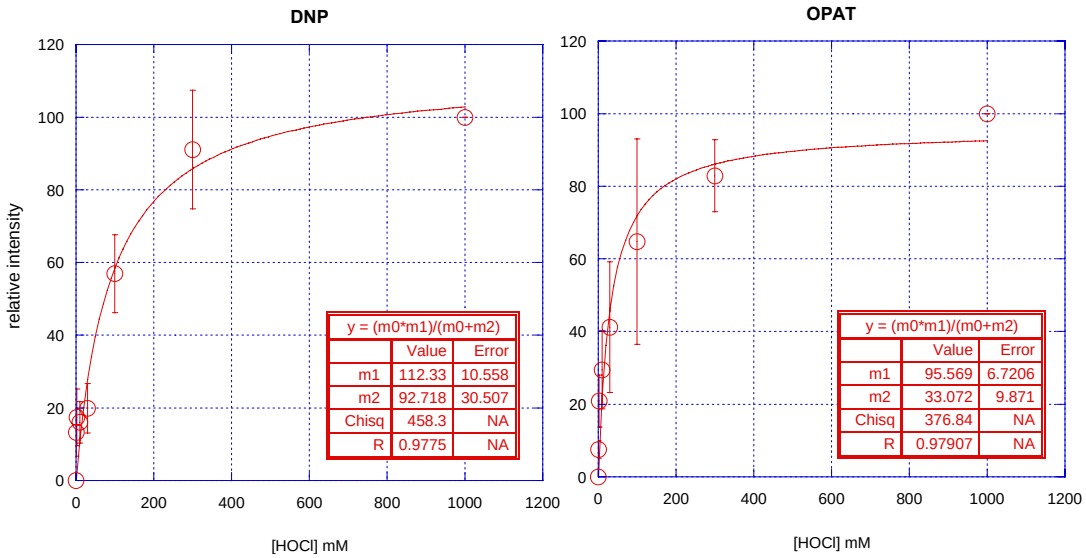

Figure 4-4. Quantitative comparison of derivatization with DNPH and OPAT. Ovalbumin was oxidatively damaged using various concentrations of HOCl and subsequently derivatized and detected using either DNPH or OPAT. Densitometry of blots using ImageMaster software was done on each lane, the background signal (from the zero HOCl added reaction) was subtracted, and the signal was normalized to the maximum signal observed. In addition to the data points, graphs display curves fit to the equation y=ax/(b+x), where a=maximum signal and b is defined as the [HOCl] yielding half-maximal binding (b=92.718 ± 30.507 for DNPH and 33.072 ± 9.871 for OPAT, indicating that OPAT is at least as efficient as DNPH at derivatizing oxidized protein).

Next we set out to use the OPAT reagent to enrich an oxidized protein from a complex mixture. Ovalbumin was oxidized, added to HEK 293 cell lysate and the entire sample was derivatized with OPAT. Control samples, used to detect non-specific binding, contained cell lysate and OPAT without oxidized ovalbumin, or oxidized ovalbumin and cell lysate without OPAT. The oxidized proteins were enriched using magnetic dynabeads conjugated to streptavidin and identified using mass spectrometry. The number of peptides identified from each protein was used for spectral counting data. Figure 4-5 lists the proteins that were identified in the samples with or without OPAT and shows spectral counting of the peptides. Spectral counting of the samples showed that ovalbumin was the only protein which specifically bound to the dynabeads. Bovine serum albumin was identified in all of our samples because it is used to coat the outside

of the dynabeads. A few proteins were found to non-specifically bind to the beads, probably due to endogenous levels of oxidation or non-specific interactions with the beads. No proteins were detected that bound to the dynabeads from the control sample that contained cell lysate and OPAT. Although this is most likely due to the modest quantity of oxidation, because we know there is some endogenous oxidation in these cells.

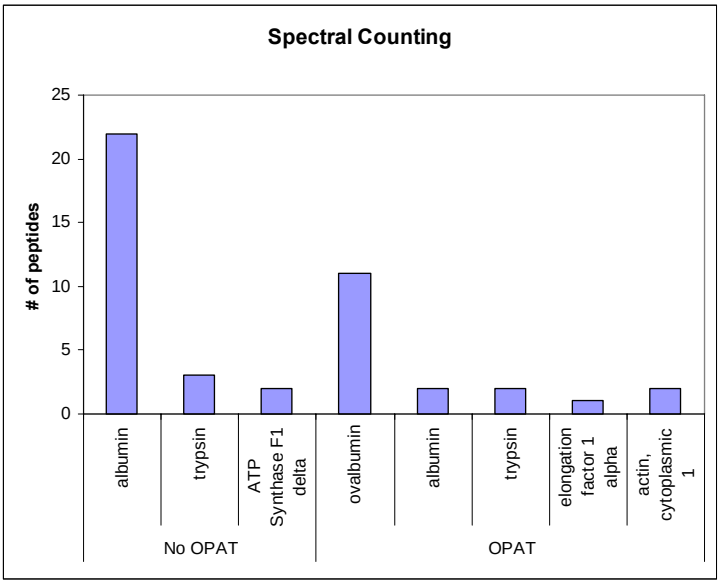

Figure 4-5. Spectral counting of proteins enriched with OPAT. Ovalbumin was oxidatively damaged using HOCl and added to HEK 293 cell lysate. Samples were either incubated with OPAT or not. Magnetic beads coupled to streptavidin were used to remove any OPAT bound proteins. The enriched proteins were digested and analyzed on a mass spectrometer. Spectral counting was used to relatively quantify protein abundance in the samples. The oxidized ovalbumin was enriched using the OPAT reagent. A few proteins were found to non-specifically bind to the beads. Bovine serum albumin is detected because the magnetic beads are coated with it to reduce non-specific binding.

Discussion

We have developed a method for the detection and enrichment of oxidized proteins. This method utilizes the reagent BPH as an oxidized protein affinity tag (OPAT) that not only derivatizes protein carbonyls, but that also tags them with a biotin affinity tag. The OPAT reagent has been shown to derivatize and detect oxidatively damaged proteins as efficiently as the standard reagent used for detection of protein

carbonyls (DNPH). Using the affinity tag, we have been able to enrich OPAT-derivatized proteins from a mixture as complex as a cell lysate and identified them using mass spectrometry.

As oxidized proteins can often represent a minor fraction of the total protein population, they are often masked by other more abundant proteins. Also, because protein oxidation does not typically result in a homogeneous population of modified protein, the amount of protein in a single modification state can be a very small fraction of the total protein present. The affinity tag on the OPAT molecule helps to overcome these impediments by enabling enrichment of the oxidized proteins from a complex sample.

Once the modified proteins have been enriched, enzymatic digestion of the proteins into peptides followed by fragmentation of the peptides using mass spectrometry would allow identification of the residues on which the modifications lie. This method would also provide insight into the nature of the modification as well as suggest a possible oxidizing source.

Recently, 2D-oxyblots have been proposed as a proteomic approach to study oxidatively damaged proteins. This process employs two-dimensional gel electrophoresis (2DE) for the separation and resolution of oxidized proteins which are then detected using immunoblotting techniques. We have previously shown that 2DE is severely limited in its ability to resolve microheterogeneous proteins into detectable spots [Warburton, 2005]. Oxidized proteins appear as smears on 2D gels instead of focused spots. This can lead to inaccurate conclusions when the non-specific binding of an antibody to a well-focused protein gives a false positive or when proteins are not

accurately correlated between a gel and an immunoblot. Our OPAT reagent will provide a superior alternative to 2D-oxyblots for the analysis of these proteins.

The development of this method will prove useful in the advancement of protein oxidation research by assisting in the isolation and identification of protein oxidation associated with various pathologies. This method may also help establish definitive ties between certain pathologies and oxidative modifications.

CHAPTER 5

PROTEOMIC AND PHENOTYPIC ANALYSIS OF RPE CELLS

Summary

The retinal pigment epithelium is a monolayer of cells located directly behind photoreceptor cells in the retina. During embryongenesis these cells differentiate to form a polarized epithelium. Once epithelialized, RPE cells have little or no turn over for the remainder of the organism's life. Although RPE cells in the adult monolayer are quiescent, the cells are capable of proliferating when placed in culture. When RPE cells are removed to culture there is a rapid loss in polarity and epithelial phenotype.[Huotari, 1995; Burke, 1996] However, researchers have been able to induce differentiation of RPE cells in culture through the use of humoral substances, substrate association or tissues interactions.[Campochiaro and Hackett, 19931; Song and Lui, 1990] Although cultured human RPE cells can be induced to differentiate the process is costly and time consuming and as a result most scientists perform research on undifferentiated RPE cells. The following chapter details the proteomic differences in differentiated and undifferentiated ARPE-19 cells (the only human RPE cell line available for research) and compares these results to the proteome of human RPE cells. The phenotypic differences of these cells as revealed by transmission electron microscopy are also reported.

Introduction

During ocular development, signaling events induce RPE morphogenesis to produce a fully differentiated monolayer of tightly packed cells. Signals for these events have not been completely established, but it has been shown that cues from adjacent tissues contribute to the development of an epithelial organization and polarity in these cells.[Rizzolo and Heiges, 1991] The lateral, apical and basal cell surfaces in the RPE monolayer are functionally and structurally specialized. Neighboring RPE cells are linked at their lateral margins by tight junctions, enabling these cells to act as a selective barrier. The plasma membrane on the basal surface is highly infolded and lies adjacent to Bruch's membrane. The apical surface consists of microvilli that interdigitate with photoreceptor outer segments and assist in their phagocytosis. These structural specializations are necessary for proper RPE functioning. Once epithelialized, RPE cells have little or no turnover for the remainder of the organism's life.

Although RPE cells in the adult monolayer are quiescent, the cells are capable of proliferating when placed in culture. When RPE cells are removed to culture there is a rapid loss in polarity and epithelial phenotype.[Huotari, 1995; Burke, 1996] However, researchers have been able to induce differentiation of RPE cells in culture through the use of humoral substances, substrate association or tissues interactions.[Campochiaro and Hackett, 19931; Song and Lui, 1990]

Currently the only human RPE cell line available for research is the ARPE-19 cell line. Although cultured RPE cells can be induced to differentiate, the process is costly and time consuming. As a result most investigators perform research on undifferentiated

RPE cells in culture. To ascertain the proteomic differences in differentiated and undifferentiated ARPE-19 cells, we have examined the proteomes from these cells and compared them to the proteome of human RPE cells. These proteomic results were also compared to the phenotypic characteristics of these cells detected by transmission electron microscopy (TEM).

Materials and Methods

ARPE-19 Differentiation-ARPE-19 (human retinal pigment epithelial cells – ATCC-CRL-2302) cells were grown in T-75 tissue culture flasks in RPMI 1640 media supplemented with 10% fetal bovine serum (FBS). Undifferentiated cells were harvested at 95% confluency. The cells were differentiated by transferring the confluent cells to T75 flasks coated with matrigel and reducing the FBS in the media to 1%. Cells were allowed to differentiate for 3 weeks. Cells were solubilized in either 3% SDS or phosphate buffered saline (PBS) containing 2.3 μM E-64 and 0.6 mM PMSF to examine either the complete proteome or the soluble proteome of the cells, respectively.

2D Gel Electrophoresis and Mass Spectrometry- 100 μg of ARPE-19 cell lysate was acetone precipitated and solubilized in reswelling buffer (7 M urea, 2 M thiourea, 15 mM dithiothreitol (DTT), 1% pharmalites, 0.5% Triton X-100 and 2% ASB-14 (Calbiochem, San Diego, CA)). Immobilized pH gradient (IPG) strips (pH 4-7, 7 cm) were rehydrated in this solution for 12 h under mineral oil. Isoelectric focusing (IEF) was performed at 20°C, on a Multiphor II Electrophoresis System (Amersham Pharmacia Biotech, Piscataway, NJ). A programmed voltage gradient was used consisting of 200 V for 1 min,

linearly increasing to 3500 V over 1.5 h, and held at 3500 V for 1.5 h to reach a total of approximately 8 kVh. Following isoelectric focusing, IPG strips were washed in equilibration buffer (0.05 M Tris, 6 M urea, 30% glycerol, and 1% SDS) containing 32 mM dithiothreitol for 15 min followed by a 15 min wash in equilibration buffer containing 216 mM iodoacetamide. The proteins were then separated according to their molecular weight on a 10% gel (8.3x6.4x0.1 cm) using standard SDS-PAGE conditions. Gels were stained with colloidal coomassie (Pierce), and gel spots were excised for analysis. Excised spots were trypsinized in-gel [Schevchenko, 1996] and desalted using a $ZipTip_{U\text{-}C18}$ (Millipore, Bedford, MA). Sample spots of 1 µl were allowed to co-crystallize on the MALDI plate with 1 µl of α-cyano 4-hydroxycinnamic acid as the matrix. The peptides were analyzed by oMALDI Qq-ToF (orthogonal matrix-assisted laser desorption ionization quadrupole time-of-flight) mass spectrometry on an Applied Biosystems QSTAR Pulsar i instrument (Foster City, CA).

Analysis of 2D Gels - 2D gels were analyzed using Image Master software (GeneBio, Geneva, Switzerland). Image Master calculates the volume of a spot as the volume above the spot border, situated at 75% of the spot height (measured from the peak of the spot). The spot volumes were then used to determine the percent volume of each spot in the gels. The percent volume of a spot was calculated as the volume of the spot divided by the combined volumes of all spots in the gel, multiplied by one hundred. Percent volume was used to semi-quantitatively determine the protein abundance of spots in the gels. Internal pI and molecular weight standards were used to assist in the alignment of gels.

Microscopy of Differentiated and Undifferentiated ARPE-19 Cells - ARPE-19 cells were grown on either membrane alone in media containing 10% FBS until confluent (undifferentiated) or membrane coated with matrigel in media containing 1% FBS for three weeks (differentiated). Cells on the membrane were fixed in glutaraldehyde, postfixed in osmic acid, dehydrated, and embedded in epoxy resin. Slices of the samples (100 nm) were imaged and photographed on a JEOL JEM 2000 FX scanning electron microscope.

Results

The proteins in undifferentiated and differentiated ARPE-19 cells and human RPE cells were harvested and fractionated on 2D gels, shown in Figure 5-1. Initially, the complete proteome of the aforementioned cells (as harvested with 3% SDS) was analyzed.

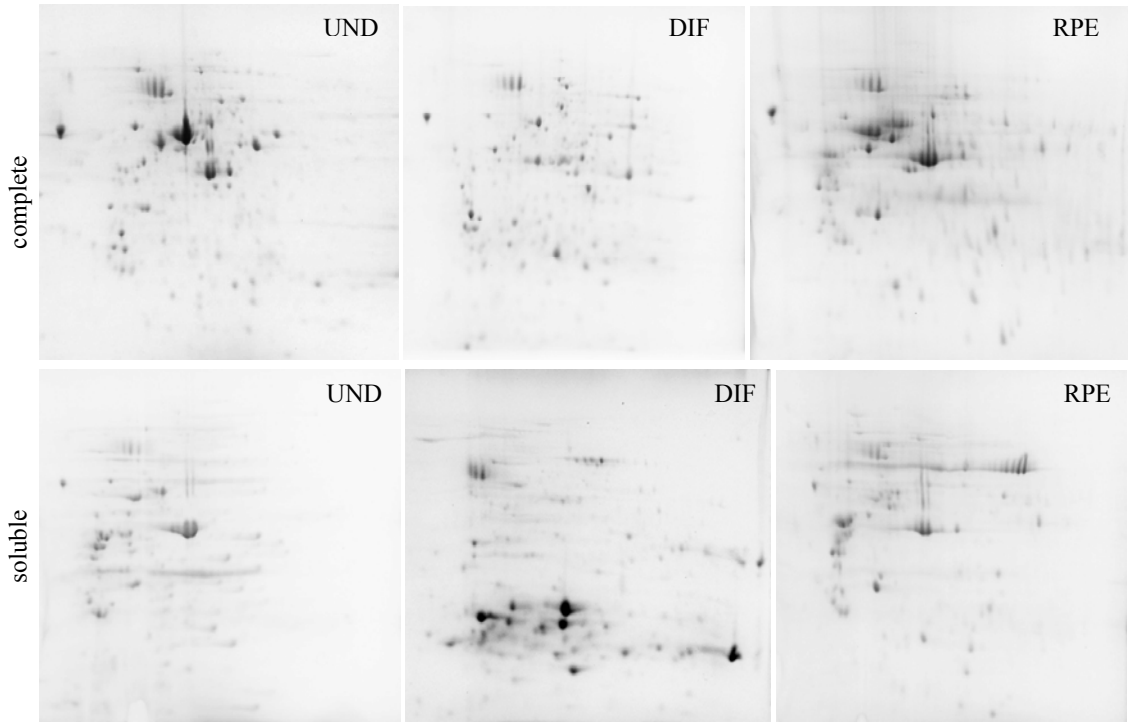

Figure 5-1. 2D gels of undifferentiated (UND) ARPE-19, differentiated (DIF) ARPE-19 and human RPE cells (RPE). The cells were solubilized in either 3% SDS or phosphate buffered saline (PBS) containing 2.3 μM E-64 and 0.6 mM PMSF to examine either the complete proteome or the soluble proteome of the cells, respectively.

However, because of the high number of cytoskeletal proteins identified, we undertook the analysis of the soluble proteome of these cells by harvesting the proteins in phosphate buffered saline (PBS). The spots that were excised and analyzed by mass spectrometry from the 2D gels are indicated on the gels in Figures 5-2A-C. The proteins identified in each of the six gels, along with the proteins subcellular location, tissue specificity, synonyms, ascession number and function are listed in Tables 5-1A-F (located at the end of the results section in this chapter).

undifferentiated

complete

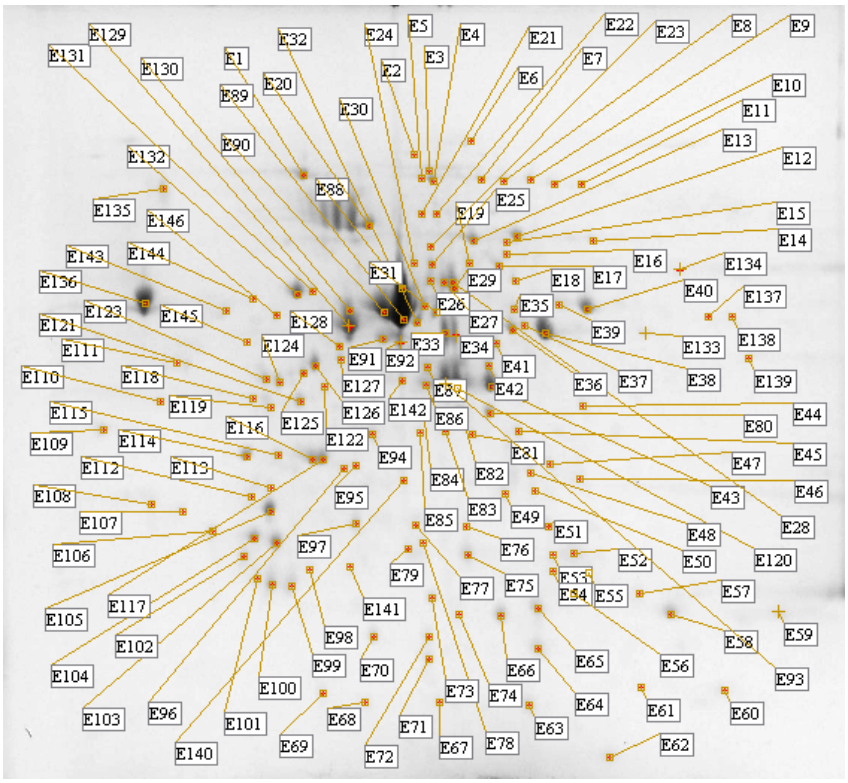

soluble

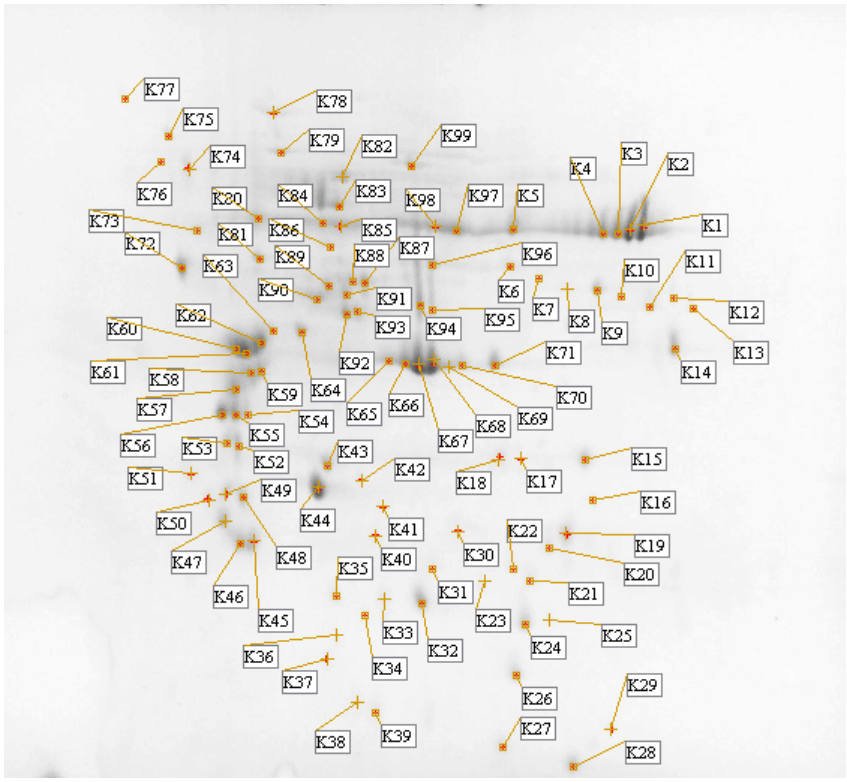

Figure 5-2A. 2D gels of complete and soluble proteome of undifferentiated ARPE-19 cells. The spot location and identification number are indicated on the gel.

differentiated

complete

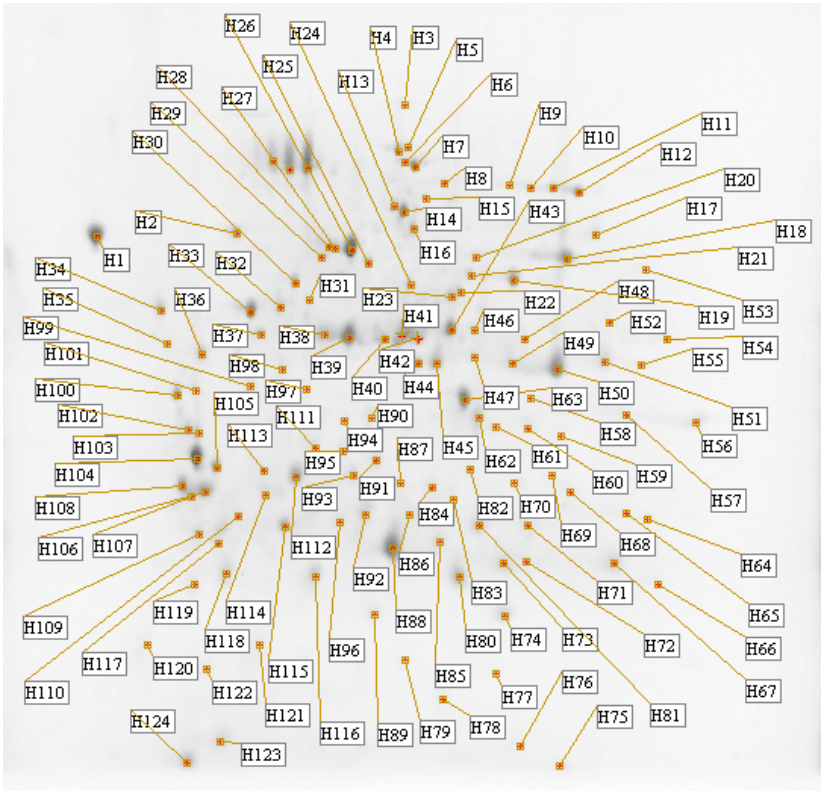

soluble

Figure 5-2B. 2D gels of complete and soluble proteome of differentiated ARPE-19 cells. The spot location and identification number are indicated on the gel.

human RPE

complete

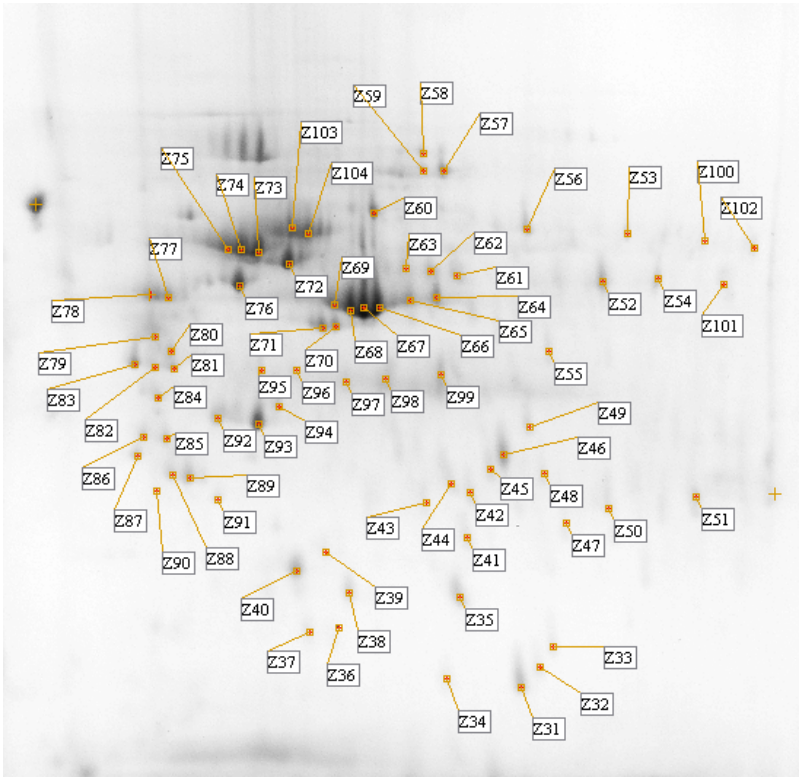

soluble

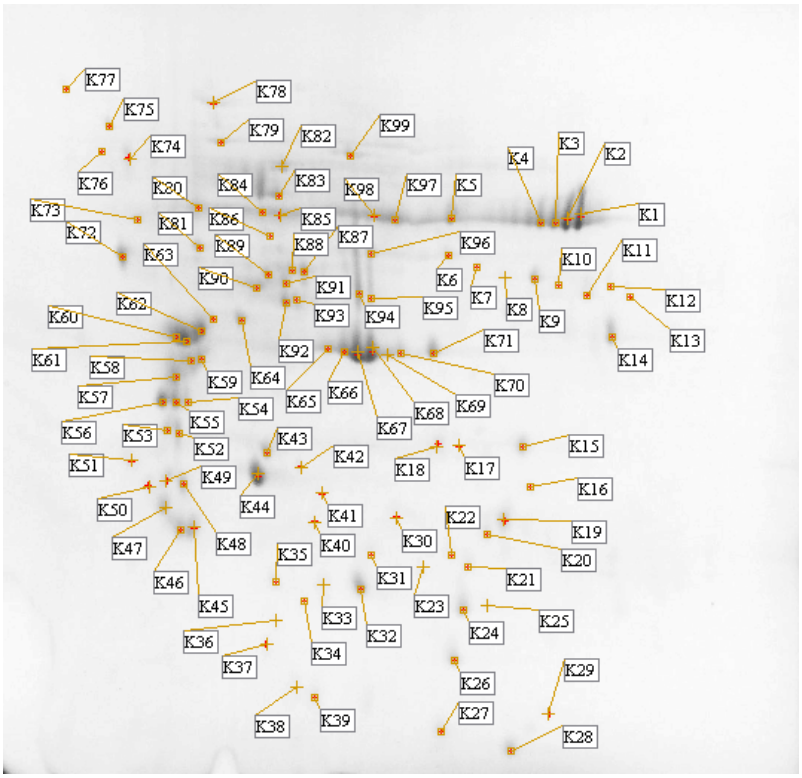

Figure 5-2C. 2D gels of complete and soluble proteome of human RPE cells. The spot location and identification number are indicated on the gel.

To assess the relatedness of the proteomes, Venn diagrams were used to display the number of proteins in common to each other, Figure 5-3.

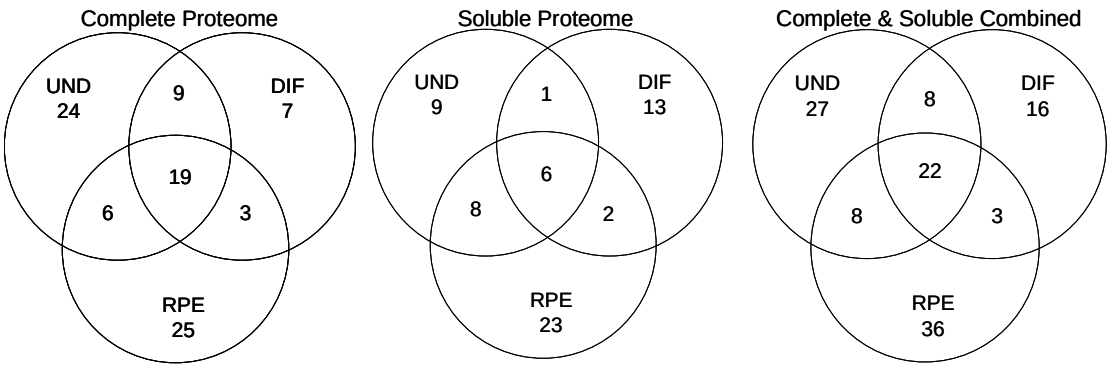

Figure 5-3. Venn diagrams of proteins identified in differentiated ARPE-19 (DIF), undifferentiated ARPE-19 (UND) and human RPE cells (RPE). Proteins in DIF, UND or RPE cells were solubilized in either 3% SDS or PBS with protease inhibitors to examine the complete or soluble proteome, respectively.

The ten most abundant, non-cytoskeletal, proteins from each gel were established by determining the percent volume of each spot using ImageMaster software and are listed in Table 5-2. The cytoskeletal proteins that were excluded from Table 5-2 include actin, tubulin, vimentin and tropomyosin.

Complete Proteome								
undifferentiated			differentiated			RPE		
spot	protein	%Vol	spot	protein	%Vol	spot	protein	%Vol
E136	calreticulin	4.669	H1	calreticulin	3.113	Z72	ATP synthase, H+ transporting, mitochondrial F1 complex, beta subunit	4.040
E40	protein disulfide isomerase	1.480	H112	annexin A5	1.473	Z93	annexin A5	3.681
E132	protein disulfide isomerase	1.413	H73	cathepsin H	1.278	Z76	enolase	3.379
E20	heat shock 70 protein 5	1.156	H56	enolase	1.174	Z64	creatine kinase	2.467
E117	nucleophosmin 1	1.040	H74	glutathione S-transferase	1.052	Z46	3-hydroxyisobutryrate dehydrogenase	2.263
E91	ATP synthase beta subunit	0.992	H7	myosin, heavy polypeptide 9	0.880	Z35	peroxiredoxin 2	2.187
E29	mitochondrial matrix protein P1	0.920	H14	myosin, heavy polypeptide 9	0.834	Z103	ATP synthase, H+ transporting, mitochondrial F1 complex, beta subunit	2.118
E116	nucleophosmin 1	0.757	H2	protein disulfide isomerase precursor	0.775	Z40	recoverin	1.977
E1	heat shock protein 70 gp96	0.736	H107	heat shock 70 protein 5	0.702	Z89	14-3-3	1.832
E58	heat shock protein 27	0.724	H34	heat shock protein gp96	0.662	Z52	tripeptidyl peptidase 1	1.703

Soluble Proteome								
undifferentiated			differentiated			RPE		
spot	protein	%Vol	spot	protein	%Vol	spot	protein	%Vol
J69	glyceraldehyde 3-phosphate dehydrogenase	2.630	A59	annexin A5	4.854	K97	heat shock 70 protein 8	2.035
J52	glutathione-s-transferase	2.060	A60	annexin A5	3.635	K32	glutathione s-transferase	1.562
J92	protein kinase	1.982	A87	glutathione-s-transferase	2.794	K14	tripeptidyl peptidase	1.488
J1	calreticulin	1.721	A56	14-3-3	1.986	K72	calreticulin	1.486
J32	annexin A5	1.298	A49	enolase	1.476	K46	14-3-3	1.350
J31	annexin A5	1.257	A48	enolase	1.302	K24	glutathione s-transferase	1.079
J53	glutathione s-transferase	1.008	A105	phosphoglycerate mutase 1	1.243	K52	glyceraldehyde 3-phosphate dehydrogenase	0.990
J30	glyceraldehyde 3-phosphate dehydrogenase	0.940	A85	phosphoglycerate kinase 1	1.238	K15	lactate dehydrogenase C	0.960
J39	14-3-3	0.917	A47	enolase	1.153	K43	retinaldehyde binding protein	0.899
J105	heat shock 70 protein 8	0.809	A104	cathepsin H	1.030	K26	peroxiredoxin 2	0.792

Table 5-2. Ten most abundant spots in 2D gels. The ten most abundant, non-cytoskeletal, proteins from each gel were established by determining the percent volume of each spot using ImageMaster software Initially the volume of a spot was calculated as the volume above the spot border, situated at 75% of the spot height (measured from the peak of the spot). The spot volumes were then used to determine the percent volume of each spot in the gels. The percent volume of a spot was calculated as the volume of the spot divided by the combined volumes of all spots in the gel, multiplied by one hundred. Percent volume was used to semi-quantitatively determine the protein abundance of spots in the gels. The cytoskeletal proteins that were excluded are actin, tubulin, vimentin and tropomyosin.

The phenotypic characteristics of differentiated and undifferentiated ARPE-19 cells were examined using transmission electron microscopy (TEM), Figure 5-4. This enabled a qualitative comparison of the specialized structures on these cells which are required for proper RPE functioning. Specifically cell size, cell shape and the presence or absence of apical microvilli where among the characteristics examined.

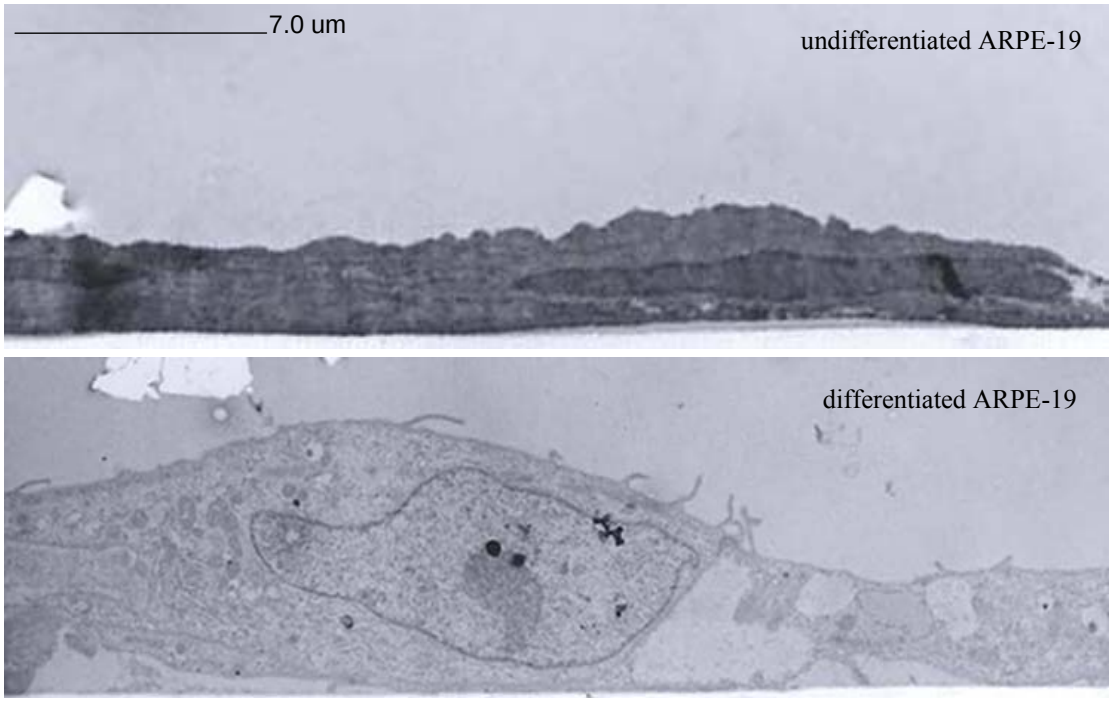

Figure 5-4. Transmission electron micrograph (TEM) of differentiated and undifferentiated ARPE-19 cells. ARPE-19 cells were grown on either membrane alone in media containing 10% FBS until confluent (undifferentiated) or membrane coated with matrigel in media containing 1% FBS for three weeks (differentiated). Cells on the membrane were fixed in glutaraldehyde, postfixed in osmic acid, dehydrated, and embedded in epoxy resin. Slices of the samples (100 nm) were imaged and photographed on a JEOL JEM 2000 FX.

Table 5-1A. Proteins identified from the complete proteome of undifferentiated ARPE-19 cells.

Protein	NCBI asscession	Spot	synonym	subcellular location	tissue specificity	function
14-3-3	AAD48408	E99, E100, E101, E102		cytoplasm	widely expressed	adapter protein implicated in regulation of signaling pathways
3-hydroxyisobuty-rate dehydrogenase	NP_689953	E52		Mitochond-rion		catalytic enzyme
6-phosphoglucono-lactonase	AAH14006	E55				hydrolyzes 6-phosphoglucono-lactone
actin, beta	CAA45026	E29, E33, E34, E44, E84, E86, E87, E93, E110, E120		cytoplasm	ubiquitous	involved in cell motility
annexin A1	1AIN	E46, E139, E140				promotes membrane fusion, involved in exocytosis and

						regulates phospholipase A2
annexin A3	NP_005130	E51				inhibitor of phospholipase A2, possesses anti-coagulation properties
annexin A5	AAH18671	E97				anticoagulant
ATP synthase beta subunit	AAA51808	E91	H(+)-transport-ing ATPase beta subunit	Mitochond-rion		produces ATP from ADP in the presence of a proton gradient across the membrane
calreticulin	AAP36116	E136		cytoplasm, nucleus, mitochondria	widely expressed	probable oxidoreductase and plays a role in apoptosis
calumenin	AAB97725	E111	crocalbin	endoplasmic reticulum	ubiquitous	involved in regulation of carboxylation to amino acid residues
cathepsin D	AAP35556	E52, E75, E76, E79		lysosome		breaks down proteins
cathepsin H	CAA30428	E57		lysosome		degrades proteins in lysosomes
chaperonin containing TCP1, subunit 5	NP_036205	E18	KIAA009 8 protein			molecular chaperone involved in folding of actin and tubulin
dynactin 2	NP_006391	E92	DCTN2 protein, p50 dynamitin	cytoplasm, peripheral membrane protein		modulates cytoplasmic dynein binding to an organelle and plays a role in prometaphase chromosome alignment and spindle organization
enolase	CAA32505	E128		cytoplasm	most adult tissues	
eukaryotic translation initiation factor 3, subunit 2 beta	AAH00413	E48	PRO2242			binds the 40S ribosome and promotes the binding of tRNAi and mRNA
F-actin capping protein alpha-1 subunit	NP_006126	E49				binds end of actin filaments, blocking the exchange of subunits
glutathione S-transferase	CAA30894	E64, E65				conjugates reduced glutathione to hydrophobic electrophiles
heat shock 70	NP_005337	E13, E23	dnaK-type			stabilizes proteins

protein 1B			molecular chaperone			against aggregation and mediates protein folding
heat shock 70 protein 5	NP_005338	E20	glucose regulated protein, BiP, dnaK-type molecular chaperone			involved in folding and assembly of proteins in the ER
heat shock 70 protein 9B	AAH30634	E12	dnaK-type molecular chaperone, mortalin-2			mediates protein folding
heat shock protein 27	AAA62175	E58, E65		cytoplasm, nucleus		involved in stress resistance and actin organization
heat shock protein gp96	AAK74072	E1	glucose-regulated protein 94, GRP94, tumor rejection antigen 1	endoplasmic reticulum		molecular chaperone that functions in the processing and transport of secreted proteins
lactate dehydrogenase B	AAH71860	E46		cytoplasm		catalytic enzyme involved in anaerobic glycolysis
laminin-binding protein	CAA43469	E121		cytoplasm		possibly involved in cell adhesion
mannose 6 phosphate receptor binding protein 1	AAH01590	E87		cytoplasm		required for transport of mannose 6-phosphate receptors from endosomes to the trans-Golgi network
mitochondrial matrix protein P1	NP_002147	E28, E29	Heat shock protein 60, chaperon-in	mitochondrion		involved in mitochondrial protein import, macromolecular assembly and correct folding of imported proteins
nucleophosmin 1	AAH12566	E96, E116, E117		nucleus		associated with nucleolar ribonucleoprotein structures and binds single stranded nucleic acids
peroxiredoxin 2	CAA80269	E63	thiol-specific antioxid-ant protein	cytoplasm		involved in redox regulation; reduces peroxides

peroxiredoxin 4	CAG46469	E56	Thio-redoxin peroxide-ase	cytoplasm		involved in redox regulation; reduces peroxides
peroxiredoxin 6	NP_004896	E59		cytoplasm		involved in redox regulation; reduces peroxides
proliferating cell nuclear antigen	CAG38740	E112		nucleus		involved in regulation of DNA replication
proteasome activator subunit 1 isoform 1	NP_006254	E55				involved in cleavage of proteins
protein disulfide isomerase	BAA03759	E39, E40	Phospho-lipase c alpha, glucose regulated protein	endoplasmic reticulum		catalyzes the rearrangement of disulfide bonds in proteins
protein disulfide isomerase precursor	NP_000909	E131, E132	prolyl 4-hydroxyla se	endoplasmic reticulum		catalyzes the formation, rearrangement and breakage of disulfide bonds
protein disulfide isomerase-related protein 5	AAB50217	E91, E92		endoplasmic reticulum		catalyzes the rearrangement of disulfide bonds in proteins
protein kinase C substrate	AAA98668	E135				regulatory subunit of glucosidase II
pyridoxal kinase	NP_003672	E46	Chromo-some 21 open reading frame 97	cytoplasm	ubiquitous	required for synthesis of pyridoxal-5-phosphate from vitamin B6
pyruvate dehydrogenase, chain D	1NI4D	E49				
rho GDP dissociation inhibitor alpha	AAP35530	E70		cytoplasm		regulates GDP/GTP exchange reaction of Rho proteins
SET translocation	NP_003002	E109	myeloid leukemia-associated	nucleus		possibly involved in nucleosome assembly
tat-associated protein	2110369A	E108				
Tat-binding protein-1	107855	E92	PSMC3 protein			
transformation upregulated nuclear protein	CAA51267	E17, E24, E25,	heterogen eous nuclear ribonucleo protein K, isoform B	cytoplasm, nucleus		pre-mRNA binding protein, plays a role in nuclear metabolism of hnRNAs
transformation	AAH03394	E94	Hetero-	nucleus		binds pre-mRNA

upregulated nuclear protein			geneous nuclear ribonucleo -protein C			and nucleates the assembly of hnRNP particles
transformation upregulated nuclear protein	NP_062543	E133	Hetero- geneous nuclear ribonucleo -protein H	nucleus		a component of the hrRNP complex which processes pre-mRNAs
translation elongation factor eEF-1 delta	1085404	E95				possible signal transducer
tropomyosin 1	A23562	E103				binds to actin filaments
tropomyosin 3	A27674	E114				binds to actin filaments
tropomyosin 4	NP_003281	E104				binds to actin filaments
tubulin, alpha	CAA25855	E74, E88, E89, E90				major constituent of microtubules
tubulin, beta	0805287A	E129, E130				major constituent of microtubules
ubiquitin thiolesterase	A25856	E66				ubiquitin thiolesterase activity
UMP-CMP kinase	AAH14961	E63		nucleus, cytoplasm	ubiquitous	catalyzes phosphoryl transfer from ATP to UMP and CMP
vimentin	NP_003371	E32, E80, E82, E88, E89, E90, E118, E119			widely expressed	class three filaments found in various non-epithelial cells
VLA-3 alpha subunit	BAA00845	E7, E8, E9, E10, E11	Integrin alpha-3 precursor	membrane	widely expressed	receptor for fibronectin, laminin, collagen, epiligrin, thrombospondin and CSPG4
WD-40 repeat protein	BAA75544	E94	serine/ threonine kinase receptor associated protein			interacts with RNA binding protein
WW domain binding protein-2	AAD10951	E45			ubiquitous	binds to the WW domain of YAP1, WWP1, and WWP2

Table 5-1B. Proteins identified from the complete proteome of differentiated ARPE-19 cells.

protein	NCBI asscession	spot	synonym	subcellular location	tissue specificity	function
14-3-3	AAD48408	H109, H117	cytosolic phospho-lipase A2	cytoplasm	widely expressed	adapter protein implicated in signaling pathways
actin, beta	CAA45026	H18, H22, H24, H35, H36, H38, H40, H41, H42, H43, H44, H45, H47, H48, H50, H51, H52, H58, H62, H63, H72, H80, H81, H82, H83, H84, H88, H90, H91, H95, H96, H110, H113, H114, H115, H116		cytoplasm	ubiquitous	involved in cell motility
alpha-actinin	CAA38970	H28		cytoplasm		F-actin cross-linking protein thought to anchor actin to a variety of intracellular structures
annexin A3	NP_005130	H68, H70				inhibitor of phospholipase A2, possesses anti-coagulation properties
annexin A4	NP_001144	H68, H69				promotes membrane fusion and is involved in exocytosis
annexin A5	AAH18671	H112, H113	lipocortin V	cytoplasm		involved in signal transduction and apoptosis
ATP synthase beta subunit	AAA51808	H78, H83		Mitochond-rion		produces ATP from ADP in the presence of a proton gradient across the membrane
calreticulin precursor	NP_004334	H1	calcium binding protein	Endoplasm-mic reticulum		chaperone promotes folding, oligomeric assembly and quality control in the ER

cathepsin B	2007265A	H89		lysosome		degradation of proteins
cathepsin D	AAP35556	H71, H96		lysosome		breaks down proteins
cathepsin H	CAA30428	H73		lysosome		degrades proteins in lysosomes
dimethylarginine dimethylamino-hydrolase	NP_036269	H61	Dimethyl-arginase-1			hydrolyzes inhibitors of NOS
enolase	CAA32505	H32, H33, H56, H57, H60, H61		cytoplasm	most adult tissues	
F-actin capping protein beta subunit		H71	CapZB			binds to the end of actin filaments blocking the exchange of subunits
filamin	AAA92644	H102		cytoplasm	ubiquitous	promotes orthogonal branching of actin filaments and links actin to membrane glycoproteins
glutathione S-transferase	CAA30894	H74				conjugates reduced glutathione to hydrophobic electrophiles
heat shock 70 protein 5	NP_005338	H48, H54, H55, H107, H108	glucose regulated protein, BiP, dnaK-type molecular chaperone			
heat shock protein 27	AAA62175	H66, H72, H73	p24k-1, estrogen receptor related protein	cytoplasm, nucleus		involved in stress resistance and actin organization
heat shock protein 90		H121				
heat shock protein gp96	AAK74072	H34	Tumor rejection antigen/ endoplasm-mic reticular heat shock protein gp96 homolog protein	Endoplas-mic reticulum		molecular chaperone that functions in the processing and transport of secreted proteins
mitochondrial matrix protein P1	NP_002147	H16	HSP 60, chaperon-in	Mitochond-rion		involved in mitochondrial protein import,

						macromolecular assembly and correct folding of imported proteins
myosin, heavy polypeptide 9, non-muscle	NP_002464	H4, H5, H6, H7, H14, H69				possible ATP binding protein, may be involved in motor activity
osteonectin	NP_003109		Extra-cellular matrix protein			may be involved in calcium ion binding
peroxiredoxin 2	CAA80269	H77, H79	thiol-specific anti-oxidant protein	cytoplasm		involved in redox regulation; reduces peroxides
peroxiredoxin 4	CAG46469	H72	Thio-redoxin peroxidase	cytoplasm		involved in redox regulation; reduces peroxides
protein disulfide isomerase	BAA03759	H53, H58	Phosphor-lipase c alpha, glucose regulated protein	Endo-plasmic reticulum		catalyzes the rearrangement of disulfide bonds in proteins
protein disulfide isomerase precursor	NP_000909	H2, H94, H101	prolyl 4-hydroxy-ase	Endo-plasmic reticulum		catalyzes the formation, rearrangement and breakage of disulfide bonds
protein disulfide isomerase-related protein 5	AAB50217	H54		Endo-plasmic reticulum		catalyzes the rearrangement of disulfide bonds in proteins
pyridoxal kinase	NP_003672	H59	Chromo-some 21 open reading frame 97	cytoplasm	ubiquitous	required for synthesis of pyridoxal-5-phosphate from vitamin B6
transglutaminase 2 isoform a	NP_004604	H81				
tripeptidyl-peptidase I	NP_000382	H52	ceroid lipo-fuscinosis	lysosome	widely expressed	lysosomal serine protease
tropomyosin 1	A23562	H105, H108				binds to actin filaments
tropomyosin 3	A27674	H103, H104				binds to actin filaments
tropomyosin 4	NP_003281	H100, H107				binds to actin filaments
tubulin, alpha	CAA25855	H76, H78, H123				major constituent of microtubules
tubulin, beta	0805287A	H30, H95, H111				major constituent of microtubules

UMP-CMP kinase	AAH14961	H77		nucleus, cytoplasm	ubiquitous	catalyzes phosphoryl transfer from ATP to UMP and CMP
Vimentin	NP_003371	H27, H28, H29, H30, H31, H33, H63, H72, H106, H110, H117, H124			widely expressed	class three filaments found in various non-epithelial cells

Table 5-1C. Proteins identified from the complete proteome of human RPE cells.

protein	NCBI asscession	spot	synonym	subcellular location	tissue specificity	function
14-3-3	AAD48408	Z87, Z88, Z89, Z91	protein kinase C inhibitor protein-1 epsilon isoform	cytoplasm	widely expressed	adapter protein implicated in signaling pathways
3-hydroxy-isobutyrate dehydrogenase	NP_689953	Z24, Z46		Mitochond-rion		catalytic enzyme
actin, beta	CAA45026	Z43, Z60, Z65, Z66, Z67, Z68, Z69, Z70, Z71, Z92		cytoplasm	ubiquitous	involved in cell motility
aldehyde dehydrogenase 1	AAC51652	Z102		cytoplasm		binds free retinal and CRALBP-bound retinal; can oxidize retinaldehyde to retinoic acid
annexin A4	NP_001144	Z49				promotes membrane fusion and is involved in exocytosis
annexin A5	AAH18671	Z15, Z91, Z93, Z95		cytoplasm		involved in signal transduction and apoptosis
annexin A6	AAH17046	Z21		stress fibers		associates with CD21 and regulates the release of Ca from intracellular stores
annexin A7	AAP35851	Z11				involved in calcium ion binding
ATP synthase beta subunit	AAA51808	Z29		Mitochond-rion		produces ATP from ADP in the presence of a proton gradient across the membrane

ATP synthase, H+ transporting, mitochondrial F0 complex, subunit d	NP_006347	Z38		Mitochond-rion		catalyzes ATP synthesis
ATP synthase, H+ transporting, mitochondrial F1 complex, beta subunit	NP_001677	Z72, Z103		Mitochond-rion		catalyzes ATP synthesis
ATPase, H+ transporting, lysosomal, V1 subunit A	AAP36699	Z30		lysosome		
calumenin	AAB97725	Z3	crocalbin	endoplasmic reticulum	ubiquitous	involved in regulation of carboxylation to amino acid residues
cathepsin B	2007265A	Z39		lysosome		degradation of proteins
cathepsin D	AAP35556	Z24, Z45, Z46		lysosome		breaks down proteins
clusterin isoform	NP_001822	Z95		secreted protein		associated with apoptosis
creatine kinase	AAC31758	Z19, Z62, Z64, Z65, Z66		cytoplasm		reversibly catalyzes the transfer of phosphate between ATP and various phosphogens
endoplasmic reticulum protein 29 precursor	NP_006808	Z48		endoplasmic reticulum	ubiquitous	processes secretory proteins within the ER
enolase	CAA32505	Z11, Z16, Z54, Z76, Z101		cytoplasm	most adult tissues	
glutathione S-transferase	CAA30894	Z41				conjugates reduced glutathione to hydrophobic electrophiles
glutathione-insulin transhydrogenase	CAA30112	Z27	prolyl 4-hydroxyl-ase, thryoid hormone binding protein	endoplasmic reticulum		catalysis formation, breakage and rearrangement of disulfide bonds
glyceraldehyde-3-phosphate dehydrogenase	CAA25833	Z99		cytoplasm		catalyist for carbohydrate degradation and glycolysis
guanine nucleotide-binding protein, beta 1	NP_002065	Z97, Z98, Z99				modulator of various transmembrane signaling systems, required for GTPase

						activity
heat shock 70 protein 1B	NP_005337	Z30	dnaK-type molecular chaperone			stabilizes proteins against aggregation and mediates protein folding
heat shock 70 protein 9B	AAH30634	Z21, Z57, Z59	dnaK-type molecular chaperone, mortalin-2			mediates protein folding
heat shock protein 27	AAA62175	Z42, Z50	p24k-1, estrogen receptor related protein	cytoplasm, nucleus		involved in stress resistance and actin organization
heat shock protein gp96	AAK74072	Z12	tumor rejection antigen, glucose regulated protein	endoplasmic reticulum		molecular chaperone that functions in the processing and transport of secreted proteins
motor protein	BAA04654	Z4, Z5, Z6	Mito-chondrial inner membrane protein	Mito-chondrion		
NADH dehydrogenase (ubiquinone) Fe-S protein 1	AAH30833	Z13, Z58	NADH-ubiquin-one oxido-reductase	Mito-chondrion		large subunit of complex where NADH is oxidized
NADH dehydrogenase (ubiquinone) Fe-S protein 3	NP_004542	Z42, Z43	NADH-coenzyme Q reductase			may be involved in mitochondrial electron transport
NADH dehydrogenase (ubiquinone) Fe-S protein 8	NP_002487	Z39	NADH-coenzyme Q reductase			may donate electrons to ubiquinone
NADH dehydrogenase (ubiquinone) flavoprotein 2	NP_066552	Z47	NADH-ubiquin-one oxido-reductase			may be involved in mitochondrial electron transport
mitochondrial matrix protein P1	NP_002147	Z26, Z60	Chaperon-in (HSP60)	Mito-chondrion		involved in mitochondrial protein import, macromolecular assembly and correct folding of imported proteins
nucleophosmin 1	AAH12566	Z81		nucleus		may function in the assembly and/or transport of ribosome
nucleoside-diphosphate	NP_000260	Z33	nm23 protein			

kinase 1 isoform b						
peroxiredoxin 2	CAA80269	Z35, Z37	thiol-specific anti-oxidant protein	cytoplasm		involved in redox regulation; reduces peroxides
peroxiredoxin 6	NP_004896	Z50, Z51		cytoplasm		involved in redox regulation; reduces peroxides
prenylcysteine oxidase 1	NP_057381	Z53	KIAA-0908	lysosome	ubiquitous	degradation of prenylated proteins
prohibitin	NP_002625	Z44		Mito-chondrion	widely expressed	inhibits DNA synthesis, regulates proliferation
protein disulfide isomerase	BAA03759	Z9, Z56	Phosphor-lipase c alpha, glucose regulated protein	endoplasmic reticulum		catalyzes the rearrangement of disulfide bonds in proteins
protein disulfide isomerase precursor	1MEK	Z27	prolyl 4-hydroxyl-ase, thryoid hormone binding protein	endoplasmic reticulum		catalyzes the formation, rearrangement and breakage of disulfide bonds
RAP1B	NP_056461	Z33	RAS related protein RAP1B			displays low GTPase activity
recoverin	AAP88840	Z40	guanylate cyclase activator			involved in calcium ion binding
retinaldehyde-binding protein 1	NP_000317	Z94	CRALBP	cytoplasm	retina and pineal gland	carries 11-cis retinol and 11-cis retinaldehyde as endogenous ligands
serum albumin	CAA23754	Z8				
transmembrane anchor protein 1	P84157	Z1		membrane		
tripeptidyl-peptidase I	NP_000382	Z10, Z52	ceroid lipo-fuscinosis	lysosome	widely expressed	lysosomal serine protease
tropomyosin 1	A23562	Z83, Z84				binds to actin filaments
tropomyosin 3	A27674	Z85				binds to actin filaments
tropomyosin 4	NP_003281	Z86				binds to actin filaments
tropomyosin, beta	AAF17621	Z14				major constituent of microtubules
tubulin, alpha	CAA25855	Z97, Z103, Z104				major constituent of microtubules
tubulin, beta	0805287A	Z25, Z61,				major constituent of

		Z62, Z63, Z73, Z74, Z75				microtubules
vimentin	NP_003371	Z28, Z77, Z78, Z79			widely expressed	class three filaments found in various non-epithelial cells

Table 5-1D. Proteins identified from the soluble proteome of undifferentiated ARPE-19 cells.

protein	NCBI asscession	spot	synonym	subcellular location	tissue specificity	function
14-3-3	AAD48408	J39		cytoplasm	widely expressed	adapter protein implicated in regulating signaling pathways
actin, beta	CAA45026	J19, J29, J59, J60, J62, J65, J76, J77, J78, J79, J80, J82, J83, J99, J100, J102, J103		cytoplasm	ubiquitous	involved in cell motility
annexin A1	1AIN	J27, J28, J29				promotes membrane fusion, involved in exocytosis and regulates phospholipase A2
annexin A2	AAH09564	J44, J45		secreted membrane, basement matrix		calcium regulated membrane binding protein
annexin A3	NP_005130	J67				inhibitor of phospholipase A2, possesses anti-coagulation properties
annexin A5	AAH18671	J31, J32		cytoplasm		involved in signal transduction and apoptosis
annexin A6	AAH17046	J106		stress fibers		associates with CD21 and regulates the release of Ca from intracellular stores
calreticulin	AAP36116	J1		cytoplasm, nucleus, mitochondria	widely expressed	probable oxidoreductase and plays a role in apoptosis
chloride intracellular channel 1	CAI17827	J64		membrane		chloride ion binding and transport
enolase, gamma	AAA52388	J10, J11		cytoplasm	most adult tissues	

glutathione S-transferase	CAA30894	J52, J53				conjugates reduced glutathione to hydrophobic electrophiles
glyceraldehyde-3-phosphate dehydrogenase	CAA25833	J30, J68, J69, J70		cytoplasm		catalyist for carbohydrate degradation and glycolysis
heat shock 70 protein 5	NP_005338	J2	glucose regulated protein, BiP, dnaK-type molecular chaperone			involved in folding and assembly of proteins in the ER
heat shock 70 protein 8	NP_694881	J3, J4, J105				involved in protein folding
laminin-binding protein	CAA43469	J17		cytoplasm		possibly involved in cell adhesion
peroxiredoxin 2	CAA80269	J46	thiol-specific anti-oxidant protein	cytoplasm		involved in redox regulation; reduces peroxides
protein kinase	CAI13015	J92				kinase activity
pyruvate kinase	CAA39849	J104, J109				catalytic enzyme in carbohydrate degradation and glycolysis
rho GDP dissociation inhibitor alpha	AAP35530	J55		cytoplasm		regulates GDP/GTP exchange reaction of Rho proteins
ribonuclease/angiogenin inhibitor	AAH00677	J9				
tubulin, alpha	CAA25855	J57, J58, J92, J93				major constituent of microtubules
tubulin, beta	0805287A	J6, J7, J8, J65, J95				major constituent of microtubules
UMP-CMP kinase	AAH14961	J51		nucleus, cytoplasm	ubiquitous	catalyzes phosphoryl transfer from ATP to UMP and CMP
vimentin	NP_003371	J15, J16, J22, J23, J24, J25, J26			widely expressed	class three filaments found in various non-epithelial cells

Table 5-1E. Proteins identified from the soluble proteome of differentiated ARPE-19 cells.

Protein	NCBI asscession	spot	synonym	subcellular location	tissue specificity	function
14-3-3	AAD48408	A52, A56		cytoplasm	ubiquitous	involved in regulation of signaling pathways
actin, beta	CAA45026	A25, A27,		cytoplasm	ubiquitous	involved in cell

		A28, A38, A61, A62, A63, A64, A65, A66, A67, A68, A69, A70, A73, A77, A78, A79, A80, A81, A82, A84, A94				motility
alpha actinin	CAA38970	A9		cytoplasm		actin bundling protein
aminoacylase 1	AAH00545	A40		cytoplasm	kidney, brain, placenta, spleen	involved in hydrolysis of amino acids
annexin A5	AAH18671	A59, A60, A62		cytoplasm		involved in signal transduction and apoptosis
cathepsin B	2007265A	A74		lysosome		degradation of proteins
cathepsin D	AAP35556	A91		lysosome		breaks down proteins
cathepsin H	CAA30428	A104		lysosome		degrades proteins in lysosomes
DJ-1 protein	NP_009193	A110		nucleus, cytoplasm	widely expressed	positive regulator of androgen receptor-dependent transcription and redox sensitive chaperone
enolase, gamma	AAA52388	A18, A46, A47, A48, 49		cytoplasm	most adult tissues	
filamin 1	NP_001447	A1, A2, A3, A4, A10, A11	actin-binding protein-280	cytoplasm	ubiquitous	promotes branching of actin filaments and links actin filaments to membrane glycoproteins
FK506-binding protein	AAC78853	A13	peptidyl-prolyl cis-trans isomerase	endoplasmic reticulum		accelerates protein folding during protein synthesis
glutathione S-transferase	CAA30894	A87				conjugates reduced glutathione to hydrophobic electrophiles
glyceraldehyde-3-phosphate dehydrogenase	CAA25833	A98		cytoplasm		catalyist for carbohydrate degradation and glycolysis
heat shock protein 27	AAA62175	A109, A111	p24k-1, estrogen	cytoplasm, nucleus		involved in stress resistance and actin

			receptor related protein			organization
lysyl hydroxylase isoform 2	AAB58363	A35		endoplasmic reticulum, peripheral membrane protein	majority of examined cell types	forms hydroxylysine residues in collagens for carbohydrate attachment
phosphoglycerate kinase 1	CAG32997	A85, A93, A102, A105	migration-inducing gene 10 protein	cytoplasm		glycolytic enzyme and primer recognition protein
ribonuclease/angiogenin inhibitor	AAH00677	A21				
thioredoxin domain containing 5	NP_110437	A29		endoplasmic reticulum		possesses thioredoxin activity; reduces insulin disulfide bonds
T-plastin polypeptide	AAB02844	A37	plastin-3	cytoplasm	variety of organs	actin bundling protein
transglutaminase	AAA63739	A54				
triosephosphate isomerase 1	AAH17947	A103				

Table 5-1F. Proteins identified from the soluble proteome of human RPE cells.

protein	NCBI asscession	spot	synonym	subcellular location	tissue specificity	function
14-3-3	AAD48408	K45, K46, K47		cytoplasm	widely expressed	adapter protein implicated in regulating signaling pathways
actin, beta	CAA45026	K61, K65, K66, K67, K68, K69, K70, K71, K95, K96		cytoplasm	ubiquitous	involved in cell motility
aldehyde dehydrogenase 1	AAC51652	K11		cytoplasm		binds free retinal and CRALBP-bound retinal; can oxidize retinaldehyde to retinoic acid
annexin A4	NP_001144	K16				promotes membrane fusion and is involved in exocytosis
annexin A5	AAH18671	K44		cytoplasm		involved in signal transduction and apoptosis
ATP synthase, H+ transporting, mitochondrial F1 complex, beta	NP_001677	K91, K92		Mito-chondrion		catalyzes ATP synthesis

subunit						
calnexin	AAB29309	K73				involved in calcium ion binding
calreticulin	AAP36116	K72		cytoplasm, nucleus, mitochondria	widely expressed	probable oxidoreductase and plays a role in apoptosis
cathepsin D	AAP35556	K19, K20, K30		lysosome		breaks down proteins
creatine kinase	AAC31758	K70, K71		cytoplasm		reversibly catalyzes the transfer of phosphate between ATP and various phosphogens
dihydropyrimidinase-like 2	AAH67109	K7		cytoplasm	ubiquitous	
dynactin 2	NP_006391	K93		cytoplasm, peripheral membrane protein		modulates cytoplasmic dynein binding to an organelle and plays a role in prometaphase chromosome alignment and spindle organization
enolase, gamma	AAA52388	K64		cytoplasm	most adult tissues	
glutathione S-transferase	CAA30894	K24, K25, K32, K34				conjugates reduced glutathione to hydrophobic electrophiles
glyceraldehyde-3-phosphate dehydrogenase	CAA25833	K52		cytoplasm		catalyist for carbohydrate degradation and glycolysis
guanine nucleotide-binding protein, beta 1	NP_002065	K18				modulator of various transmembrane signaling systems, required for GTPase activity
heat shock 70 protein 5	NP_005338	K83	glucose regulated protein, BiP, dnaK-type molecular chaperone			involved in folding and assembly of proteins in the ER
heat shock 70 protein 8	NP_694881	K97				involved in protein folding
heat shock 90 protein 1	CAI20097	K82				involved in protein folding
heat shock protein 27	AAA62175	K21, K31	p24k-1, estrogen receptor	cytoplasm, nucleus		involved in stress resistance and actin organization

			related protein			
heat shock protein gp96	AAK74072	K79	glucose-regulated protein 94, GRP94, tumor rejection antigen 1	endoplasmic reticulum		molecular chaperone that functions in the processing and transport of secreted proteins
interphotoreceptor matrix proteoglycan 1	CAI41298	K77				found between RPE and photoreceptor cells
interstitial retinol-binding protein	AAC18875	K78		Interphoto-receptor matrix		shuttles 11-cis and all trans retinoids between the RPE and photoreceptor cells
lactate dehydrogenase C	AAA59508	K15	Pro-liferation-inducing gene 19 protein	cytoplasm		catalytic enzyme in anaerobic glycolysis
peroxiredoxin 2	CAA80269	K26	thiol specific anti-oxidant protein	cytoplasm		involved in redox regulation; reduces peroxides
phosphoprotein phosphatase 2-beta	B34541	K84				
prolilferation inducing protein 15	AAP82230	K39	ferritin, heavy chain			stores iron in a soluble, nontoxic form
protein disulfide isomerase	BAA03759	K9, K81	Phosphor-lipase c alpha, glucose regulated protein	endoplasmic reticulum		catalyzes the rearrangement of disulfide bonds in proteins
protein kinase C substrate	AAA98668	K74				regulatory subunit of glucosidase II
retinaldehyde-binding protein	NP_000317	K42, K43	CRALBP	cytoplasm	retina and pineal gland	carries 11-cis retinol and 11-cis retinaldehyde as endogenous ligands
rho GDP dissociation inhibitor alpha	AAP35530	K35		cytoplasm		regulates GDP/GTP exchange reaction of Rho proteins
tat binding protein 1	AAB24840	K93	Pro-teasome 26S ATPase	cytoplasm		involved in the ATP-dependent degradation of ubiquitinated proteins
tat-associated	2110369A	K51				

protein						
tripeptidyl-peptidase I	NP_000382	K14	ceroid lipo-fuscinosis	lysosome	widely expressed	lysosomal serine protease
tropomyosin 1	A23562	K48, K56				binds to actin filaments
tropomyosin 4	NP_003281	K49, K53				binds to actin filaments
tubulin, alpha	CAA25855	K87, K88, K89, K91				major constituent of microtubules
tubulin, beta	0805287A	K89, K90				major constituent of microtubules
vimentin	NP_003371	K57, K58, K60, K61, K62			widely expressed	class three filaments found in various non-epithelial cells

Discussion

Proteomic Differences

There is a significant difference in the overall protein pattern observed on 2D gels of the proteomes of differentiated and undifferentiated ARPE-19. The large difference in protein patterns in these cells would seem to indicate that these cells are undergoing significant changes in their protein composition as they differentiate. It also appears from the protein pattern on 2D gels that UND and RPE cells have a more similar proteome than DIF and RPE cells. This is also confirmed by the Venn diagrams, which show there are indeed more proteins in common in the proteomes of UND and RPE cells than DIF and RPE. These results are surprising, as one would expect the differentiated state to be reflected in the morphology of the cells as well as in their proteomes. However, it would appear that the factors contributing to the morphology and proteome are independent. This may also suggest that the morphology of the cells is first affected upon differentiation followed by proteomic variations and that these cells have not reached a fully differentiated state. Another possibility is that the less abundant proteins in the cell,

which are not observable on a 2D gel, maybe be the proteins which are significant affected by the differentiation. To achieve a better understanding of the proteomic changes that may be occurring in these cells further analysis of individual subcellular fractionations would need to be examined.

Other Proteins of Interest

We examined the proteomes of these three cells for proteins that are vital to proper functioning of the RPE. As previously mentioned, RPE cells are the most active phagocytes in the body. To keep up with the phagocytosis and subsequent degradation of photoreceptor discs, RPE cells contain numerous proteases. While cathepsin D was identified in all three cell types, cathepsin B was only identified in UND and DIF. However, two of the four proteases identified in these cells were specific to DIF and RPE cells, cathepsin H and tripeptipdyl peptidase I, and the only cell type in which we identified all four proteases was DIF cells.

One protein that functions in the renewal of 11-cis retinal and therefore is crucial to proper functioning of the RPE is cellular retinaldehyde binding protein (CRALBP). CRALBP was only identified in RPE cells which would indicate that although DIF cells are undergoing significant changes, they have not achieved a fully differentiated state.

Phenotypic Differences

Of significant interest are the phenotypic characteristics of the differentiated (DIF) and undifferentiated (UND) ARPE-19 cells as viewed by electron microscopy. The UND ARPE-19 cells appear “flat” in comparison to the differentiated cells, which is

consistent with other reports of the morphology of UND cells. These cells were also void of microvilli on the apical surface. In contrast, microvilli are observable on the apical side of DIF ARPE-19 cells. These cells also appear more cuboidal and stand ~8 μm from the membrane. This is consistent with the report of Matsumoto, who observed differentiated feline, monkey and human RPE cells, and in all three species the apical surface of the cells was elevated 8-10μm above the substrate.[Matsumoto, 1990] These morphological features would suggest that the DIF cells have made significant progress towards achieving a differentiated state, although it would be difficult to assess the degree of differentiation. Additional experiments focused on examining the tight junctions and basal infoldings of these two cell types may provide further insight into the differentiated state of these cells.

Because the morphological specializations associated with the surfaces of RPE cells appear to be structural manifestations of functional requirements. We would therefore suggest that the state of differentiation of RPE cells *in vitro* is an important variable that needs to be considered when studying cellular events that depend on the presence of specialized structures.

LITERATURE CITED

Allikmets, R., Shroyer, N.F., Singh, N., Seddon, J.M., Lewis, R.A., Bernstein, P.S., Peiffer, A., Zabriskie, N.A., Li, Y., Hutchinson, A., Dean, M., Lupski, J.R. and M. Leppert (1997) Mutation of the Stargardt Disease Gene (ABCR) in Age-Related Macular Degeneration. *Science*, 277(19), 1805-7.

Azarian, S.M., McLeod, I., Lillo, C., Gibbs, D., Yates, J.R. and D.S. Williams (2006) Proteomic analysis of mature melanosomes from the retinal pigmented epithelium. *J Proteome Res*, 5(3), 521-9.

Attebo, K., Mitchell, P. and W. Smith (1996) Visual acuity and the causes of visual loss in Australia. The Blue Mountains Eye Study. *Ophthalmology,*103, 357-364.

Basrur, V., Yang, F., Kushimoto, T., Higashimoto, Y., Yasumoto, K., and J. Valencia (2003) Proteomic analysis of early melanosomes: identification of novel melanosomal proteins. *J Proteome Res,* 2(1), 69-79.

Beatty, S., Koh, H., Phil, M., Henson, D. and M. Boulton (2000) The role of oxidative stress in the pathogenesis of age-related macular degeneration. *Surv Ophthalmol*, 45, 115-34.

Berlett, B.S. and E.R. Stadtman (1997) Protein oxidation in aging, disease, and oxidative stress. *J Biol Chem,* 272, 20313-6.

Bird, A.C., Bressler, N.M., Bressler, S.B., Chisholm, I.H., Coscas, G., Davis, M.D., de Jong, P.T., Klaver, C.C., Klein, B.E. and R. Klein (1995) An international classification and grading system for age-related maculopathy and agerelated macular degeneration. *Surv Ophthalmol,* 39, 367-374.

Boulton, M., Marshall, J. and H.C. Wong (1986) The generation of dense granules within cultured human retinal pigment epithelial cells at senescence. *Graefes Arch Clin Exp Ophthalmol,* 224, 106-9.

Boulton, M., Docchio, F., Dayhaw-Barker, P., Ramponi, R. and R. Cubeddu (1990) Age-related changes in the morphology, absorption and fluorescence of melanosomes and lipofuscin granules of the retinal pigment epithelium. *Vision Res*, 30, 1291-303.

Boulton, M. (1991) Ageing of the retinal pigment epithelium. In: Osborne N, Chader G, (eds) Progress in retinal research. Pergamon, Oxford, pp 125–151.

Boulton, M., Dontsov, A., Jarvis-Evans, J., Ostrovsky, M. and D. Svistunenko (1993) Lipofuscin is a photoinducible free radical generator. *J Photochem Photobiol B,* 19, 201-4.

Boulton, M., Rozanowska, M. and B. Rozanowski (2001) *J Photochem Photobiol B,* 64, 144–161.

Bressler, N.M., Bressler, S.B. and S.L. Fine (1988) Age related macular degeneration. *SurvOphthalmo,* 32, 375-413.

Brunet, S., Thibault, P., Gagnon, E., Kearney, P., Bergeron, J.J. and M. Desjardins (2003) Organelle proteomics: looking at less to see more. *Trends Cell Biol,* 13, 629-38.

Brunk, U.T. and A. Terman (2002) Lipofuscin: mechanisms of age-related accumulation and influence on cell function. *Free Radic Biol Med,* 33, 611-9.

Crabb, J.W., Miyagi, M., Gu, X., Shadrach, K., West, K., Sakaguchi, H., Kamei, M.,

Hasan, A., Yan, L., Rayborn, M.E., Salomon, R.G. and J.G. Hollyfield. (2002) Drusen proteome analysis: An approach to the etiology of age-related macular degeneration. *PNAS,* 99(23), 14682–14687.

Davies, S., Elliott, M.H., Floor, E., Truscott, T.G., Zareba, M., Sarna, T., Shamsi, F.A. and M.E. Boulton. (2001) Photocytotoxicity of lipofuscin in lipofuscin in human retinal epithelial cells. *Free Radic Biol Med,* 31(2), 256-265.

Dayhaw-Barker, P., Davies, S., Shamsi, F., Rożanowska, M., Rozanowski, B. and M. Boulton (2001) The phototoxicity of aged RPE melanosomes. *Invest Ophthalmol Vis Sci,* 42, S755.

Delori, F.C., Goger, D.G. and C.K. Dorey (2001) Age-related accumulation and spatial distribution of lipofuscin in RPE of normal subjects. *Invest Ophthalmol Vis Sci*, 42, 1855-66.

Dorey, C.K., Torres, X. and T. Swart (1990) Evidence of melanogenesis in porcine retinal pigment epithelial cells in vitro. *Exp Eye Res*, 50(1), 1-10.

Dryja, T.P., Hahn, L.B., Kajiwara, K. and E.L. Berson (1997) Dominant and digenic mutations in the peripherin/RDS and ROM1 genes in retinitis pigmentosa. *Invest Ophthalmol Vis Sci*, 38(10), 1972-82.

Dunford, R., Land, E.J., Rozanowska, M., Sarna, T. and T. G. Truscott (1995) Interaction of melanin with carbon- and oxygen-centered radicals from methanol and ethanol. *Free Radic Biol Med*, 19, 735–740.

Edwards,R.B. and Szamier,R.B. (1977) Defective phagocytosis of isolated rod outer segments by RCS rat retinal pigment epithelium in culture. *Science*, 197, 1001-1003.

Eldred, G.E. and M.L. Katz (1988) Fluorophores of the human retinal pigment epithelium: separation and spectral characterization. *Exp Eye Res,* 47, 71-86.

Eldred, G.E. and M.R. Lasky (1993) Retinal age pigments generated by selfassembling lysosomotropic detergents. *Nature*, 361, 724-6.

Esterbauer, H., Schaur, R.J. and H. Zollner (1991) Chemistry and biochemistry of 4-hydroxynonenal, malonaldehyde and related aldehydes. *Free Radic Biol Med*, 11, 81-128.

Feeney-Burns, L. (1978) Lipofuscin and of human retinal pigment epithelium, fluorescence, enzyme cytochemical, and ultrastructural studies. *Invest Ophthalmol Vis Sci*, 17, 583–600.

Feeney-Burns, L. and G.E. Eldred (1983) The fate of the phagosome: conversion to 'age pigment' and impact in human retinal pigment epithelium. *Trans Ophthalmol Soc U K*, 103, 416-21.

Feeney-Burns, L., Hilderbrand, E.S. and S. Eldridge (1984) Aging human RPE: morphometric analysis of macular, equatorial, and peripheral cells. *Invest Ophthalmol Vis Sci*, 25, 195-200.

Feeney-Burns, L., Gao, C.L. and E.R. Berman (1988) The fate of immunoreactive opsin following phagocytosis by pigment epithelium in human and monkey retinas. *Invest Ophthalmol Vis Sci*, 29, 708-19.

Frennesson, C., Nilsson, U.L. and S.E. Nilsson (1995) Colour contrast sensitivity in patients with soft drusen, an early stage of ARM. *Doc Ophthalmol*, 90, 377-86.

Gaillard, E.R., Hill, C. and T.D. Griffiths (2003) UVC and visible light damage to re-pigmented RPE cells. *Invest Ophthalmol Vis Sci*, Abstract 377.

Garin, J., Diez, R., Kieffer, S., Dermine, J.F., Duclos, S., Gagnon, E., Sadoul, R., Rondeau, C. and M. Desjardins (2001) The phagosome proteome: insight into phagosome functions. *J Cell Biol,* 152, 165-80.

Group EDC-CS. (1993) Antioxidant status and neovascular age-related macular degeneration. *Arch Ophthalmol*, 111(1), 104-9.

Group. (1992) Risk factors for neovascular age-related macular degeneration. The Eye Disease Case-Control Study Group. *Arch Ophthalmol*, 110, 1701–8.

Gu, X., Meer, S.G., Miyagi, M., Rayborn, M.E., Hollygfield, J.G., Crabb, J.W. and R.G. Salomon (2003) Carboxyethylpyrrole protein adducts and autoantibodies, biomarkers for age-related macular degeneration. *J Biol Chem*, 278(43), 42027-35.

Hung, S. and J.M. Seddon (1997) The relationship between nutritional factors and age-related macular degeneration. In: Bendich A, Deckelbaum RJ, editors. Preventive nutrition: the comprehensive guide for health professionals. Totowa, NJ: Humana Press.

Johnson, P.T., Geller, S.F., Lewis, G.P. and B.E. Reese (1997) Cellular retinaldehyde binding protein in developing retinal astrocytes. *Exp Eye Res* 64, 759-66.

Jonas, J.B., Schneider, U. and G.O.H. Naumann (1992) Count and density of human retinal photoreceptors. *Graefes Arch Clin Exp Ophthalmol,* 230(6), 505-510.

Karan, G, Lillo, C., Yang, Z., Cameron, D.J., Locke, K.G., Zhao, Y., Thirumalaichary, S., Li, C., Birch, D.G., Vollmer-Snarr, H.R., Williams, D.S. and K. Zhang (2005) Lipofuscin accumulation, abnormal electrophysiology, and photoreceptor degeneration in mutant ELOVL4 transgenic mice: A model for macular degeneration. *PNAS*, 102(11), 4164-4169.

Kennedy, C.J., Rakoczy, P.E. and I.J. Constable (1995) Lipofuscin of the retinal pigment epithelium: a review. *Eye*, 9(6), 763-771.

Klein, R., Wang, Q., Klein, B.E., Moss, S.E. and S.M. Meuer (1995) The relationship of age-related maculopathy, cataract, and glaucoma to visual acuity. *Invest Ophthalmol Vis Sci,* 36, 182-191.

Kollias, N., Sayre, R.M., Zeise, L. and M.R. Chedekel (1991) New trends in photobiology. Photoprotection by melanin. *J. Photochem. Photobiol. B: Biol.*, 9, 135–160.

Korytowski, W., Kalyanaraman, B., Menon, I.A., Sarna, T. and R.C. Sealy (1986) Reaction of superoxide anions with melanins: electron spin resonance and spin trapping studies. *Biochim Biophys Acta,* 882**,** 145–153.

Landy, J. and G.C. Brown. (2003) Update on photodynamic therapy. *Curr Opin Ophthalmol,* 14, 163-168.

Mata, N.L., Weng, J. and G.H. Travis (2000) Biosynthesis of a major lipofuscin fluorophore in mice and humans with ABCR-mediated retinal and macular degeneration. *Proc Natl Acad Sci USA*, 97, 7154-9.

Matsumoto, B., Guerin, C.J. and D.H. Anderson (1990) Cytoskeletal redifferentiation of feline, monkey, and human RPE cells in culture. Inv Ophthalmol Vis Sci, 31, 879-889.

Midena, E., Segato, T., Blarzino, M.C. and C. Degli Angeli (1994) Macular drusen and the sensitivity of the central visual field. *Doc Ophthalmol*, 88, 179-85.

Midena, E., Degli Angeli, C., Blarzino, M.C., Valenti, M. and T. Segato (1997) Macular

function impairment in eyes with early age-related macular degeneration. *Invest Ophthalmol Vis Sci*, 38, 469-77.
Nilsson, S.E., Sundelin, S.P., Wihlmark, U. and U.T. Brunk (2003) Aging of cultured retinal pigment epithelial cells: oxidative reactions, lipofuscin formation and blue light damage. *Doc Ophthalmol*, 106, 13-6.
Old, W.M., Meyer-Arendt, K., Aveline-Wolf, L., Pierce, K.G., Mendoza, A. and J.R. Sevinsky (2005) Comparison of label-free methods for quantifying human proteins by shotgun proteomics. *Mol Cell Proteomics*, 4(10), 1487-502.
Orlow, S.J. (1995) Melanosomes are specialized members of the lysosomal lineage of organelles. *J Invest Dermatol*, 105(1), 3-7.
Pieramici, D.J. and S.B. Bressler (1998) Age-related macular degeneration and risk factors for the development of choroidal neovascularization in the fellow eye. *Curr Opin Ophthalmol*, 9, 38–46.
Raposo, G. and M.S. Marks (2002) The dark side of lysosome-related organelles: specialization of the endocytic pathway for melanosome biogenesis. *Traffic*, 3(4), 237-48.
Rones, B. (1937) Formation of drusen of the lamina vitrea. *Arch Ophthalmol*, 18, 388-402.
Rozanowska, M., Jarvis-Evans, J., Korytowski, W., Boulton, M.E., Burke, J.M. and T. Sarna (1995) Blue light-induced reactivity of retinal age pigment. In vitro generation of oxygen-reactive species. *J Biol Chem*, 270, 18825-30.
Rozanowska, M., Wessels, J., Boulton, M., Burke, J.M., Rodgers, M.A., Truscott, T.G. and T. Sarna (1998) Blue light-induced singlet oxygen generation by retinal lipofuscin in non-polar media. Free Radic Biol Med, 24, 1107-12.
Rozanowska, M., T. Sarna, E. J. Land and T. G. Truscott (1999) Free radical scavenging properties of melanin interaction of eu- and pheomelanin models with reducing and oxidizing radicals. *Free Radic Biol Med*, 26, 518–525.
Rożanowska, M., Korytowski, W., Rożanowski, B., Skumatz, C., Boulton, M., Burke, J. and T. Sarna (2002) Photoreactivity of aged human RPE melanosomes: a comparison with lipofuscin. *Invest Ophthalmol Vis Sci*, 43, 2088–2096
Ryan, E.M., Buzy, A., Griffiths, D.E., Jennings, K.R. and D.N. Palmer (1996) Electrospray ionisation mass spectrometry (ESI/MS) of ceroid lipofuscin protein; a model system for the study of F0 inhibitor interactions with mitochondrial subunit C. *Biochem Soc Trans*, 24, 289S.
Santoni, V., Vinh, J., Pflieger, D., Sommerer, N. and C. Maurel (2003) A proteomic study reveals novel insights into the diversity of aquaporin forms expressed in the plasma membrane of plant roots. *Biochem J*, 373, 289-96.
Sarna, T., I. A. Menon and R. C. Sealy (1985) Photosensitization of melanin: a comparative study. *Photochem Photobiol*, 42, 529–532.
Sarna, T. (1992) New trends in photobiology. Photoproperties and function of the ocular melanin—A photobiophysical view. *J Photochem Photobiol B: Biol*, 12, 216–258.
Sarna, T., Burke, J., Korytowski, W., Rozanowska, M., Skumatz, C., Zareba, A. and M. Zareba (2003) *Ex. Eye Res,* 76, 89–98.
Schlunck, G., Martin, G., Agostini, H.T., Camatta, G. and L.L. Hansen (2002)

Cultivation of retinal pigment epithelial cells from human choroidal neovascular membranes in age related macular degeneration. *Exp Eye Res*, 74, 571-6.

Schraermeyer, U. and H. Stieve (1994) A newly discovered pathway of melanin formation in cultured retinal pigment epithelium of cattle. *Cell Tissue Res*, 276(2), 273-9.

Schraermeyer, U. and K. Heimann (1999) Current understanding on the role of retinal pigment epithelium and its pigmentation. *Pigment Cell Res*, 12, 219–236.

Schraermeyer, U., Peters, S., Thumann, G., Kociok, N. and K. Heimann (1999) Melanin granules of retinal pigment epithelium are connected with the lysosomal degradation pathway. *Exp Eye Res*, 68(2), 237-45.

Schutt, F., Ueberle, B., Schnolzer, M., Holz, F.G. and J. Kopitz (2002) Proteome analysis of lipofuscin in human retinal pigment epithelial cells. *FEBS Lett*, 2002; 528, 217-21.

Schutt, F., Bergmann, M., Holz, F.G. and J. Kopitz (2003) Proteins modified by malondialdehyde, 4-hydroxynonenal, or advanced glycation end products in lipofuscin of human retinal pigment epithelium. *Invest Ophthalmol Vis Sci*, 44, 3663-8.

Seddon, J.M., Willett, W.C., Speizer, F.E. and S.E. Hankinson (1996) A prospective study of cigarette smoking and age-related macular degeneration in women. *JAMA*, 276, 1141–6.

Seddon, J.M., Ajani, U.A. and B.D. Mitchell (1997) Familial aggregation of age-related maculopathy. *Am J Ophthalmol*, 123, 199-206.

Shacter, E., Williams, J.A., Lim, M. and R.L. Levine (1994) Differential susceptibility of plasma proteins to oxidative modification: examination by western blot immunoassay. *Free Radic Biol Med*, 17, 429-37.

Shacter, E. (2000) Protein oxidative damage. *Methods Enzymol* 319, 428-36.

Shevchenko, A., Wilm, M., Vorm, O. and M. Mann (1996) Mass spectrometric sequencing of proteins silver-stained polyacrylamide gels. *Anal Chem*, 68, 850-8.

Sohal, R.S. and L.S. Wolfe (1986) Lipofuscin: characteristics and significance. *Prog Brain Res*, 70, 171-83.

Sparrow, J.R., Nakanishi, K. and C.A. Parish (2000) The lipofuscin fluorophore A2E mediates blue light-induced damage to retinal pigmented epithelial cells. *Invest Ophthalmol Vis Sci*, 41, 1981-1989

Sparrow, J.R. and B. Cai. (2001) Blue Light–Induced Apoptosis of A2E-Containing RPE: Involvement of Caspase-3 and Protection by *Bcl-2*. *Inv Ophthal Vis Sci*, 42(6), 1356-62.

Sparrow, J. R., Cai, B., Fishkin, N., Jang, Y. P., Krane, S., Vollmer, H., Zhou, J., and K. Nakanishi (2002) A2E, a fluorphore of RPE lipofuscin: Can it cause RPE degeneration? In: LaVail MM, Hollyfield JG, Anderson RE, editors. Retinal degenerations: mechanisms and experimental therapy. Proceedings of the 10th International Symposium on Retinal Degenerations; Sep 30-Oct 5; Burgenstock, Switzerland. New York: Kluwer Academic/Plenum; 2003. p. 205-11.

Takemoto, D.J., Spooner, B. and L.J. Takemoto (1985) Antisera to synthetic peptides of bovine rhodopsin: use as site-specific probes of disc membrane changes in retinal dystrophic dogs. *Biochem Biophys Res Commun*, 132, 438-44.

Tolentino, M.J., Miller, S., Gaudio, A.R. and M.A. Sandberg (1994) Visual field deficits

in early age-related macular degeneration. *Vision Res*, 34, 409-13.
Thulin, C.D., Howes, K., Driscoll, C.D., Savage, J.R., Rand, T.A., Baehr, W. and B.M. Willardson (1999) The immunolocalization and divergent roles of phosducin and phosducin-like protein in the retina. *Mol Vis*, 5, 40.
VanNewkirk, M.R., Weih, L., McCarty, C.A. and H.R. Taylor (2001) Cause-specific prevalence of bilateral visual impairment in Victoria, Australia: The Visual Impairment Project. *Ophthalmology,* 108, 960-967.
Verhaert, P., Uttenweiler-Joseph, S., de Vries, M., Loboda, A., Ens, W. and K.G. Standing (2001) Matrix-assisted laser desorption/ionization quadrupole time-of-flight mass spectrometry: an elegant tool for peptidomics. *Proteomics*, 1, 118-31.
Vollmer-Snarr, H.R., Cameron, D.J., Pew, M.R., Walker, G.L., Alvarez, M.L. and J.R. Swallow (2004) A2E and other Amino-Retinoid Compounds in Human Lipofuscin and Melanolipofuscin. In: XIth International Symposium on Retinal Degeneration; August 23-28; Perth, Western Australia.
Warburton, S., Southwick, K., Hardman, R.M., Secrest, A.M., Grow, R.K., Xin, H., Wolley, A.T., Burton, G.F. and C.D. Thulin (2005) Examining the proteins of functional retinal lipofuscin using proteomic analysis as a guide for understanding its origin. *Mol Vis*., 11, 1122-34.
Wassell, J., Davies, S., Bardsley, W. and M. Boulton (1999) The photoreactivity of the retinal age pigment lipofuscin. *J Biol Chem*, 274, 23828-32.
Winkler, B.S., Boulton, M.E., Gottsch, J.D. and P. Sternberg (1999) Oxidative damage and age-related macular degeneration. *Mol Vis*, 5, 32.
Yin, D. (1996) Biochemical basis of lipofuscin, ceroid, and age pigmentlike fluorophores. *Free Radic Biol Med*, 21, 871-88.
Zimmerman, W.F., Godchaux, W. and M. Belkin (1983) The relative proportions of lysosomal enzyme activities in bovine retinal pigment epithelium. *Exp Eye Res*, 36, 151-8.